EVALUATION OF PRECIPITATION PROCESSES FOR THE REMOVAL OF IRON FROM CHLORIDE-BASED COPPER AND NICKEL LEACH SOLUTIONS

by

Saviour Masambi

Thesis presented in partial fulfillment
of the requirements for the Degree

of

Master of Engineering
(Extractive Metallurgical Engineering)

in the Faculty of Engineering
at Stellenbosch University

Supervisor

Dr. Christie Dorfling

Co-Supervisor

Prof. Steven Bradshaw

December 2015

DECLARATION

By submitting this thesis electronically, I declare that the entirety of the work contained therein is my own, original work, that I am the sole author thereof (save to the extent explicitly otherwise stated), that reproduction and publication thereof by Stellenbosch University will not infringe any third party rights and that I have not previously in its entirety or in part submitted it for obtaining any qualification.

Date: 14 May 2015

ABSTRACT

A process route is being developed to recover nickel and copper from chloride leach solutions contaminated with iron. The concentrations of nickel and copper are approximately 3 g/L each, while that of iron is about 45 g/L. Iron contamination causes problems in processes typically used for the recovery of nickel and copper from leach solutions, such as solvent extraction or sulphide precipitation.

This study focused on the removal of iron from the chloride-based leach solution. Iron is commonly removed from hydrometallurgical solutions by the process of precipitation. In the leach solution under investigation, iron mainly exists as iron(II) chloride. Iron(II) generally precipitates at pH above 7 while iron(III) can be precipitated at pH above 0. In this study, it was desired to oxidize iron(II) to iron(III) using oxygen gas at a temperature below 100^{o}C and to subsequently precipitate iron(III). It was sought to produce an environmentally friendly precipitate, with minimal nickel and copper co-precipitation and easily separate the solids from the liquid.

The effect of hydrochloric acid and copper concentration on the rate of iron(II) oxidation were experimentally determined. Several concentrations of hydrochloric acid, ranging from about 0.7 M to 6.4 M, were investigated while the copper concentrations investigated were 0.3 g/L and 3 g/L. The effects of temperature (40^{o}C, 60^{o}C, 80^{o}C and 90^{o}C), pH (0, 1, 2 and 3) and 30 g/L seeding on the quality and extent of iron removal were experimentally determined. The conventional hematite precipitation process was compared to the iron phosphate process in terms of iron removal, nickel and copper co-precipitation, and solid-liquid separation. The experiments were conducted in a 1.6 L glass reactor using synthetic as well as plant solutions. Synthetic solutions contained about 45 g/L iron, 3 g/L nickel and copper. Plant solutions contained significantly higher iron and nickel, with traces of copper. The concentrations of iron and nickel in plant solutions were approximately 120 g/L and 12 g/L respectively.

The rate and extent of oxidation of iron(II) , using synthetic solutions, increased with both acid and copper concentrations. Experimental data and equilibrium calculations were used to prove that the mole ratio of associated acid to iron needed to be greater than or equal to 1 for rapid oxidation of iron(II) to occur. It was experimentally shown that oxidation in the presence of 3 g/L copper concentration yielded higher iron(III) compared to oxidation in the presence of 0.3 g/L copper concentration under uniform conditions.

Iron precipitation from synthetic solutions was complete at all pH points investigated (0, 1, 2, 3) in both iron phosphate and hematite precipitation processes. The co-precipitation of nickel and copper increased with pH for both precipitation processes. The co-precipitation of nickel and copper in the iron phosphate process increased with an increase in temperature from 40^{o}C while the co-precipitation of nickel and copper increased with reduction in temperature from 80^{o}C in the hematite precipitation process. Seeded iron phosphate precipitation at pH 1 and 40^{o}C resulted in over 99% iron removal with averages of 5% and 11% nickel and copper co-precipitation respectively. Increasing the pH to 3 resulted in complete iron removal at the expense of over 50% losses in nickel and copper. Seeded hematite precipitation at pH 1 and 80^{o}C yielded over 99% iron removal with averages of 6.5% nickel and 7% copper losses. Upon increasing the pH to 3, nickel and copper losses were above 35%. The iron phosphate precipitation was complete within 30 – 60 minutes while hematite precipitation was complete after 60 – 120 minutes.

All seeded precipitation experiments produced easily filterable precipitates. Attempts to precipitate unseeded hematite at 80^{o}C and pH 1 resulted in higher nickel and copper losses (about 16% and 27% respectively), with the precipitates practically impossible to filter. The unseeded iron phosphate precipitates produced at 40^{o}C and pH 1 were filterable however relatively higher losses of nickel and copper were observed (about 11% and 22% respectively). Settling experiments showed that iron phosphate precipitates completely settled within 26 minutes. Hematite precipitates did not settle after 8 h.

Plant solutions were tested to validate the direct applicability of the results obtained using synthetic solutions. It was observed that complete oxidation was achieved after 180 minutes. Iron phosphate precipitation at pH 1 and 40^{o}C achieved complete iron removal after 60 minutes and nickel losses of approximately 7.8% after 120 minutes. Hematite precipitation at pH 1 and 80^{o}C resulted in complete iron removal after 60 min and nickel co-precipitation of 12% after 120 minutes.

OPSOMMING

ʼn Prosesroete word tans ontwikkel om nikkel en koper te herwin vanuit chloried logingsoplossings wat met yster kontamineer is. Die konsentrasies van nikkel en koper is ongeveer 3 g/L elk, terwyl die konsentrasie van yster ongeveer 45 g/L is. Yster kontaminasie veroorsaak probleme in prosesse wat tipies gebruik word vir die herwinning van nikkel en koper van logingsoplossings, soos byvoorbeeld vloeistof-vloeistof ekstraksie of sulfied presipitasie.

Hierdie studie het op die verwydering van yster vanuit die chloried logingsoplossing gefokus. Yster word algemeen vanuit hidrometallurgiese oplossings verwyder met die proses van presipitasie. In die logingsoplossing relevant tot hierdie studie bestaan die yster hoofsaaklik as yster(II)chloried. Yster(II) sal gewoonlik by pH waardes bo 7 presipiteer, terwyl yster(III) by pH waardes groter as 0 presipiteer kan word. Die gewenste roete in hierdie studie was om die yster(II) te oksideer na yster(III) deur van suurstofgas by ʼn temperatuur onder 100°C gebruik te maak, en om daarna yster(III) te presipiteer. Die presipitaat moes omgewingsvriendelik wees met minimale nikkel en koper kopresipitasie, en moes maklik van die oplossing geskei kon word.

Die effek van soutsuur en koper konsentrasie op die tempo van yster(II) oksidasie is eksperimenteel bepaal. Verskeie konsentrasies soutsuur in die gebied van 0.7 M tot 6.4 M is ondersoek, terwyl koper konsentrasies van 0.3 g/L en 3 g/L ondersoek is. Die effekte van temperatuur (40°C, 60°C, 80°C en 90°C), pH (0, 1, 2 en 3), en 30 g/L saad byvoeging op die kwaliteit en mate van yster verwydering is eksperimenteel bepaal. Die konvensionele hematiet presipitasie proses is met die ysterfosfaat proses vergelyk in terme van ysterverwydering, nikkel en koper kopresipitasie, en vastestof-vloeistof skeiding. Die eksperimente is in ʼn 1.6 L glas reaktor met sintetiese sowel as aanleg logingsoplossings uitgevoer. Die sintetiese oplossing het ongeveer 45 g/L yster en 3 g/L nikkel en koper bevat. Aanleg oplossing het beduidend hoër konsentrasies yster en nikkel

bevat, met spore van koper teenwoordig. Die konsentrasies van yster en nikkel in die aanleg oplossing was ongeveer 120 g/L en 12 g/L, onderskeidelik.

Die tempo en mate van oksidasie van yster(II) in sintetiese oplossing het toegeneem met beide suur en koper konsentrasies. Eksperimentele data en ewewigsberekeninge is gebruik om te bewys dat die molêre verhouding van geassosieerde suur tot yster groter of gelyk aan een moet wees om vinnige oksidasie van yster(II) te laat plaasvind. Dit is eksperimenteel bewys dat, onder soortgelyke toestande, oksidasie in die teenwoordigheid van 3 g/L koper konsentrasie hoër yster(III) gelewer het as oksidasie in die teenwoordigheid van 0.3 g/L koper konsentrasie.

Yster presipitasie vanuit sintetiese oplossings was volledig by alle pH waardes wat ondersoek is (0, 1, 2, 3) in beide die ysterfosfaat en die hematiet presipitasie prosesse. Die kopresipitasie van nikkel en koper het toegeneem met pH vir beide presipitasie prosesse. Die kopresipitasie van nikkel en koper in die ysterfosfaat proses het toegeneem met ’n toename in temperatuur vanaf 40°C, terwyl die kopresipitasie van nikkel en koper toegeneem het met ’n verlaging in temperatuur vanaf 80°C in die hematiet proses. Ysterfosfaat presipitasie met sade wat by pH1 en 40°C uitgevoer is, het tot meer as 99% yster verwydering gelei, met gemiddelde nikkel en koper kopresipitasie van 5% en 11%, onderskeidelik. Volledige yster verwydering is behaal indien die pH tot 3 verhoog is, maar die nikkel en koper verliese het terselfdertyd tot meer as 50% verhoog. Hematiet presipitasie met sade by pH 1 en 80°C het meer as 99% yster verwydering behaal, met gemiddelde nikkel en koper verliese van 6.5% en 7%, onderskeidelik. Die nikkel en koper verliese het tot meer as 35% gestyg met ’n pH toename na 3. Die ysterfosfaat presipitasie is binne 30 – 60 minute voltooi, terwyl hematiet 60 – 120 minute geneem het om voltooiing te bereik.

Alle presipitasie eksperimente wat met sade uitgevoer is, het maklik filtreerbare presipitate produseer. Pogings om hematiet sonder sade te presipiteer by 80°C en pH 1 het aanleiding gegee tot hoër nikkel en koper verliese (ongeveer 16% en 27%, onderskeidelik) sowel as presipitaat wat basies onmoontlik was om te

filtreer. Die ysterfosfaat presipitaat wat sonder sade by 40°C en pH 1 produseer is was filtreerbaar maar relatiewe hoër verliese van nikkel en koper is waargeneem (ongeveer 11% en 22%, onderskeidelik). Uitsakking eksperimente het getoon dat ysterfosfaat presipitate volledig uitsak binne 26 minute. Hematiet presipitate het nie uitgesak na ag ure nie.

Aanleg oplossings is getoets om die toepaslikheid van die resultate wat met sintetiese oplossings verkry is te bevestig. Volledige oksidasie is na 180 minute behaal. Ysterfosfaat presipitasie by pH 1 en 40°C het volledige yster verwydering na 60 minute behaal met nikkel verliese van ongeveer 7.8% na 120 minute. Hematiet presipitasie by pH 1 en 80°C het volledige yster verwydering na 60 minute behaal met nikkel kopresipitasie van 12% na 120 minute.

ACKNOWLEDGEMENTS

I wish to thank my heavenly Father for giving me the strength and health to complete this project.

I would like to acknowledge the following:

- My supervisors, Dr. Christie Dorfling and Prof. Steven Bradshaw, for their guidance and technical advice.
- The Department of Process Engineering, Stellenbosch University, for the financial support.
- The technical and administrative staff at the Department of Process Engineering at Stellenbosch University, for their assistance.
- My wife and son, for their love and encouragement.

TABLE OF CONTENTS

LIST OF FIGURES

LIST OF TABLES

NOMENCLATURE

Symbol	Unit	Meaning
a	m^2/m^3	Specific interfacial area
C	mol/L	Concentration of a species
C_{eq}	mol/L	Solubility of a solute - equilibrium concentration
C_f	mol/L	Final concentration of the value metal in solution
C_i	mol/L	Initial concentration of the value metal in solution
C_{pi}	mol/L	Initial concentration of a primary ion
C_{pf}	mol/L	Final concentration of a primary ion
C_{O2}	mol/L	Dissolved oxygen concentration in the bulk liquid
C^*_{O2}	mol/L	Oxygen solubility in aqueous solution
C_{O2i}	mol/L	Oxygen concentration at the gas-liquid
$C^*_{O2,W}$	mol/L	Oxygen solubility in water
d	m	Diameter
D	m^2/s	Diffusivity
E_a	J/mol	Activation energy
F	coulombs/faraday	Faraday's constant
g	m/s^2	Gravitational acceleration
Gr	m/s	Growth rate
ΔG	J/mol	Gibbs free energy change
ΔG_r	J/mol	Gibbs free energy of a reaction
ΔG_{vol}	J/mol	Gibbs free energy - generation of embryo volume
ΔG_{surf}	J/mol	Gibbs free energy - generation of embryo surface
ΔG_{max}	J/mol	Maximum activation Gibbs free energy barrier
$\Delta H_{abs,\ O2}$	J/kg	Oxygen absorption heat
h_f	m	Bed height
J	$m^{-3}s^{-}$	Molar flux per volume
K		Equilibrium constant
k		Overall reaction rate constant

Symbol	Unit	Meaning
K_g	m^4/mol.s	Growth constant
k_L	m/s	Oxygen mass transfer coefficient
k_B	J/K	Boltzman constant
k_G	m/s	Apparent mass transfer coefficient of the gas phase
Kcα	L/mol	Setschenov coefficient
K_{sp}	mol/L	Solubility product
kw	mol^2/dm^6	Ionic product of water
m	kg	Mass
M	mol/L	Molarity
n		Number of moles
P	Pa	Pressure
ΔP	Pa	Change in pressure
pH		Negative log of H^+ activity
P_{O2}	Pa	Oxygen partial pressure
P_{O2i}	Pa	Oxygen partial pressure at the gas – liquid interface
Q		Ratio of activities of products to reactants
r_c	µm	Embryo critical size
r_f	m^-	Filtration resistance
R	J/mol·K	Ideal gas constant
S		Saturation ratio
s	m^2/kg	Specific surface of solids
T	°C or K	Temperature
t	min, h or s	Time
U_o	m/s	Superficial liquid velocity through the bed
$U\infty$	m/s	Settling velocity of the spherical particle
V	m^3	Volume
x	mol/L	Molarity change
%		Percentage

Greek letters	Units	Meaning
$f(\varepsilon_{av})$	Pa^{-}	Porosity function
ρ	kg/m^3	Density
δ	m	Effective film thickness
Φ	mV	Standard equilibrium potential
α		Activity
α_f	m/kg	Mass filtration resistance
η_f	kg/m.s	Dynamic viscosity of the fluid
λ		Logarithmic distribution coefficient

Acronym	Meaning
CAF	Central Analytical Facility
ICP	Inductively Coupled Plasma
ppm	Parts per million
rpm	Revolutions per minute
SEM	Scanning Electron Microscope
XRD	X-ray Diffraction
XRF	X-ray Fluorescence

1. INTRODUCTION

A project has been initiated to develop a hydrometallurgical process route for the recovery of nickel and copper from a chloride leach solution mainly contaminated with iron. The approximate concentrations of nickel, copper and iron are 3 g/L, 3 g/L and 45 g/L respectively. It is desired that nickel be produced as the primary product with copper as a by-product.

1.1. Background and problem statement

Nickel and its alloys are widely used in the steel making industry, aerospace industry, and in the rechargeable batteries and magnets industry. Copper is one of the best known metals used for electrical and thermal conduction. Copper coils are found in transformers, motors, dynamos and electromagnets (Mudd, 2009).

Nickel and copper can be recovered using hydrometallurgical methods that generally involve leaching of the nickel and copper containing material, followed by purification of the leach solution and recovery of nickel and copper. Chloride metallurgy has been reported to offer a number of advantages over sulphate metallurgy during leaching. One of the advantages of chloride leaching is that the association of the hydrogen ions with the chloride ions is weaker compared to the sulphate ions. This makes hydrochloric acid a more aggressive leaching reagent (Lu and Dreisinger, 2013; Park et al., 2006; Winand, 1991). It therefore follows that chloride leaching is associated with higher leach recoveries and inevitably higher impurities in the leach liquor compared to sulphate leaching. Iron is chief among these impurities.

The presence of iron in leach solutions causes significant challenges to the downstream processing of nickel and copper. In solvent extraction of nickel and copper, although significant progress has been made in designing highly selective extractants, iron still competes for extraction and generally encourages crud formation. If iron dissolves in the electrolyte and reports to electrowinning tank houses, it reduces the current efficiency by the cyclical oxidation of iron(II) to

iron(III). In sulphide precipitation of nickel and copper, iron poses the threat of co-precipitating with nickel and copper (Crundwell et al., 2011a; Hudson, 1982; Ritcey, 1980; Zhu et al., 2012).

Although iron removal methods such as solvent extraction and ion-exchange have been explored as possible iron removal alternatives, iron precipitation remains the dominant iron removal method (Demopoulos and Gefvert, 1984; Wang et al., 2011).

The leach solution under consideration in this project has a significantly high iron to nickel and copper ratio (approximately 15 gram Fe per gram Ni or Cu). This necessitates an iron removal step that involves oxidation of the iron(II) and subsequent precipitation of the iron(III), with minimal co-precipitation of nickel and copper. The extent of iron removal has to satisfy the iron tolerance demanded by the downstream processing options of nickel and copper. Furthermore, the precipitate has to be easily separable from the solution containing nickel and copper.

1.2. Research aim and objectives

The aim of this study was to investigate oxidation of iron(II) by molecular oxygen and the precipitation of iron(III) at atmospheric pressure, at a temperature below 100^{o}C. The specific objectives of the study were as follows:

- Investigate the effect of HCl concentration on the oxidation mechanism of iron(II) by dissolved oxygen.
- Determine the effect of copper concentration on the oxidation kinetics of iron(II) in chloride systems.
- Investigate the effect of operating variables such as pH, temperature, reaction time and seeding on the quantity and quality of iron precipitates produced.
- Compare appropriate iron precipitation processes in terms of the following: iron removal, nickel and copper losses, and solid-liquid separation.

1.3. Research limitations

In order to maintain focus and a reasonable scope, the following were the research limitations:

- Although the process development that provided the impetus to this study involves designing a process route to recover nickel and copper from a leach solution contaminated with iron, this study was limited to the iron removal step. An experimental verification of the downstream recovery of nickel and copper was not undertaken.
- During the investigation of oxidation of iron(II) by molecular oxygen, excess molecular oxygen was supplied to an agitated reactor. Based on previous work conducted, the chemical oxidation by dissolved oxygen was assumed to be the limiting step rather than the oxygen dissolution.
- Derivations of oxidation and precipitation rate expressions were outside the scope of this study.

1.4. Thesis structure

A literature survey covering the oxidation of iron(II) by molecular oxygen as well as the precipitation of iron at atmospheric conditions is presented in chapter 2. In each case, theoretical background is firstly reviewed before discussing the related applied research. Concepts related to solid-liquid separation and iron tolerance in downstream nickel and copper recovery processes are reviewed towards the end of chapter 2.

In chapter 3, the experimental materials and methodologies are discussed. Chapter 3 is divided into three main parts: oxidation, precipitation and solid-liquid separation experimental materials and methodologies.

Experimental results are presented and discussed in chapter 4. The first section of chapter 4 presents and discusses the results of the oxidation experiments. In the second part of chapter 4, precipitation results are presented and discussed. A

comparative summary of hematite and iron phosphate precipitation is then presented.

In chapter 5, results of experiments conducted using plant solutions are presented. Oxidation and precipitation flowsheets and high level mass balances for iron phosphate and hematite precipitation are proposed.

The main conclusions are presented in chapter 6. Recommendations for future work are then outlined.

2. LITERATURE REVIEW

2.1. Overview of iron control in hydrometallurgy

Iron is one of the major impurities in hydrometallurgical solutions. It exists as iron(II) and as iron(III) compounds. Iron(II) can be precipitated out of solution at pH around 7 and above while iron(III) can be precipitated at a pH above 0 (the equilibrium pH varies depending on the iron concentration). It is desirable to precipitate iron from solution as iron(III) rather than iron(II) to avoid operating at relatively higher pH. Precipitation of iron(II) is more likely to cause higher co-precipitation of value metals and inevitably increased cost of neutralization compared with precipitation of iron(III) (Crundwell et al., 2011b; Schwertmann and Cornell, 2000).

In most cases, iron(II) is oxidized to iron(III) and then iron(III) is precipitated. Precipitation of the iron can be carried out at the leaching stage or downstream, as long as the oxidation equilibrium pH is suitable for that particular stage (Claassen et al., 2002; Harris and White, 2008).

The removal of iron is commonly achieved by the precipitation of iron oxides or hydroxides and involves the co-precipitation of both divalent and trivalent elements (Loan et al., 2006). Significant progress has been made in the zinc industry regarding the removal of iron during zinc purification processes in sulphate systems. This could also be applied to the copper and nickel purification processes in sulphate systems (Wang et al., 2011). It remains to be seen whether the iron removal principles in sulphate systems can be directly applied in chloride systems.

2.2. Oxidation of iron(II) chloride by molecular oxygen

As mentioned in Section 2.1, oxidation of iron(II) to iron(III) precedes precipitation in many iron removal processes. This study focuses on oxidation by molecular oxygen.

Oxidation of iron(II) by molecular oxygen involves the dissolution of oxygen and the oxidation of iron(II) by the dissolved oxygen. The dissolution and oxidation reactions are shown in Equation 2.1and Equation 2.2 respectively.

$$O_{2(g)} \rightarrow O_{2(aq)} \qquad 2.1$$

$$4Fe^{2+} + O_{2\ (aq)} + 4H^{+} \rightarrow 4Fe^{3+} + 2H_2O \qquad 2.2$$

The dissolution and oxidation processes are discussed in Section 2.2.1 and Section 2.2.2 respectively.

2.2.1. Oxygen mass transfer

The two critical parameters in the transfer of oxygen from the gas phase to the liquid phase are the volumetric mass transfer coefficient (k_La) and the oxygen solubility (C^*_{O2}) (Filippou et al., 2000).

2.2.1.1. Oxygen mass transfer coefficient (k_La)

The difference in the chemical potential between two phases provides the driving force for the mass transfer of any substance to another phase. Filippou et al. (2000) suggested that the difference in the partial pressures of the O_2 in the bulk gas (P_{O2}) and the O_2 at the gas – liquid interface (P_{O2i}) defines the rate of oxygen mass-transfer across the gas phase (J_G).

$$J_G = k_G(P_{O2} - P_{O2i}) \qquad 2.3$$

k_G is the apparent mass transfer coefficient of the gas phase.

It then follows that the difference in O_2 concentrations at the gas – liquid interface (C_{O2i}) and the bulk liquid (C_{O2}) also defines the oxygen mass transfer across the liquid phase (J_L).

$$J_L = k_L(C_{O2i} - C_{O2}) \qquad 2.4$$

k_L is the apparent mass transfer coefficient of the liquid phase.

Filippou et al. (2000) suggested that Equation 2.3 and Equation 2.4 are equal at steady state.

$$k_G(P_{O2} - P_{O2i}) = k_L(C_{O2i} - C_{O2}) \qquad 2.5$$

Figure 2.1 shows the variation of partial pressure and concentration across the gas–liquid interface. Instead of considering k_G and k_L, the overall mass transfer coefficients (k'_G and k'_L) are considered because it is not practically feasible to determine the gas–liquid interface oxygen concentration and partial pressure.

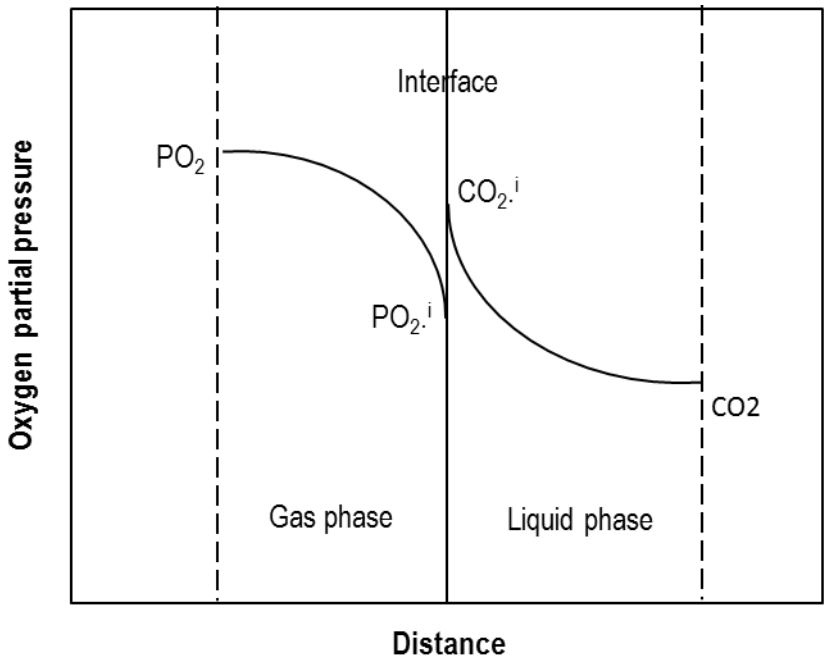

Figure 2.1. Gas – liquid interface variation of oxygen partial pressure and concentration (after Filippou et al., 2000)

In the case of oxygen, the distribution coefficient (Henry's constant, He_c) is high enough to ensure $k_L \approx k'_L$. It therefore follows that the per volume molar flux (J) in a gas – liquid mixture is given by Equation 2.6.

$$J = k_L a\left(C^*_{O2} - C_{O2}\right) \qquad 2.6$$

Where,

k_La is the volumetric mass transfer coefficient (t^{-1}), 'a' is the interfacial area

C^*_{O2} is the solubility of oxygen ($mol \cdot m^{-3}$)

C_{O2} is the concentration of oxygen in the bulk liquid ($mol \cdot m^{-3}$)

2.2.1.2. Oxygen solubility

Tromans (1998) investigated oxygen solubility in pure water at varying temperatures and pressure. He suggested that Equation 2.7 can be computed to deduce a specific concentration of dissolved oxygen (C_{O2}) at a given pressure (P_{O2}) and temperature (T). Equation 2.7 is valid for temperature between 273K and 616K and up to 60 atm oxygen partial pressure (Tromans, 1998).

$$C_{O2} = P_{O2}\left(\frac{0.046T^2 + 203.357T^2 \ln\left(\frac{T}{298}\right) - \left(299.378 + 0.092T\right)\left(T - 298\right) - 20.591\times10^3}{\left(8.314T\right)}\right) \qquad 2.7$$

A plot of the solubility of oxygen in pure water as a mole fraction $\frac{n(O_2)}{n(O_2)+n(H_2O)}$ is shown in Figure 2.2. Where $n(O_2)$ and $n(H_2O)$ is the number of moles of oxygen and water, respectively.

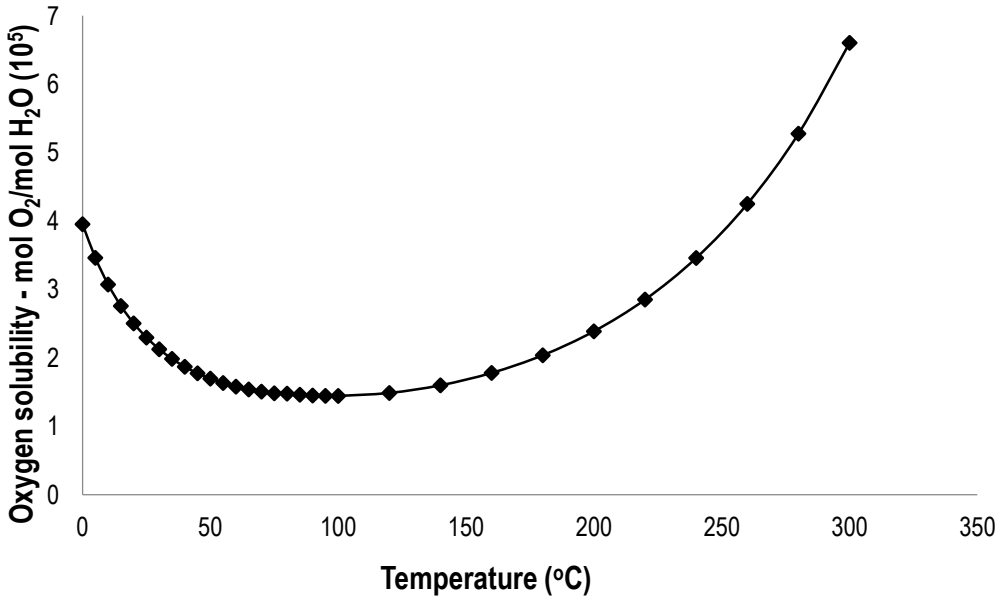

Figure 2.2. Solubility of oxygen in water at 1atm oxygen partial pressure (after Tromans, 1998)

Filippou et al. (2000) reported that the addition of various salts to a solution causes a reduction in oxygen solubility. The reduction in oxygen solubility is generally referred to as the salting effect. The salting effect is unique for a particular salt (and the quantities involved) with respect to oxygen solubility. The salting effect is quantified by the Setschenov coefficient (Kcα), as shown in Equation 2.8.

$$K_c\alpha = \left(\frac{1}{C}\right)\log\left(\frac{C^*_{O2,w}}{C^*_{O2}}\right) \qquad 2.8$$

Kcα is the Setschenov coefficient ($L.mol^{-1}$)

C is the concentration of electrolyte ($mol.L^{-1}$)

$C^*_{O2,w}$ is the solubility of oxygen in pure water ($mol.L^{-1}$)

C^*_{O2} is the solubility of oxygen in a particular electrolyte ($mol.L^{-1}$)

A number of researchers have reported that the dissolution of molecular oxygen in agitated systems is not the limiting step during iron(II) oxidation at low pH and atmospheric conditions, but rather the process is chemically controlled (Awakura et al., 1986; Georges et al., 1987; Iwai et al., 1979; Lamb and Elder, 1931; Posner, 1953; Stumm and Lee, 1961).

2.2.2. Chemical oxidation by dissolved oxygen

2.2.2.1. Rate expressions

There is no general agreement on the rate expressions for the oxidation of iron(II) by dissolved oxygen. The rate expressions generally vary depending on the concentration of iron(II), hydrochloric acid concentration and the presence of any form of catalyst (McBain, 1901).

According to Awakura et al. (1986), the oxidation of iron(II) in hydrochloric systems by dissolved molecular oxygen is proportional to the concentration of iron(II), oxygen partial pressure and strongly linked to the concentration of hydrochloric acid. It was suggested that the rate expressions differed with different $[Fe^{2+}]$ / [HCl] ratios. They reported that the rate expression moved from first order to second order with respect to ferrous concentration as the ratio $[Fe^{2+}]$ / [HCl] increased. It was further reported that oxidation of iron(II), at initial concentration of 0.716 M, occurred rapidly for solutions with over 4M HCl while for solutions with free acid lower than 4M the rate of oxidation was relatively slower. Although experiments were not performed to determine which component of the HCl influenced the kinetics of oxidation (besides the stoichiometric requirement of H^+), it was proposed that the Cl^- ions may have been the species responsible for the increase in the rate of oxidation as a result of its tendency to form complexes with Fe^{2+} and Fe^{3+} compounds. Further, it was suggested that both cupric ions and chloride ions played a catalytic role on the oxidation kinetics (Awakura et al., 1986).

Colborn and Nicol (1973) conducted research into the kinetics and mechanism of iron(II) chloride oxidation by oxygen in aqueous chloride media and reported that

the rate was second order with respect to ferrous chloride concentration and first order with respect to oxygen partial pressure. The rate of oxidation was not affected by the amount of nickel ions or zinc ions, but cupric ions were reported to have significant catalytic effect even in trace amounts. It was suggested that the cupric ion accepts an electron from the ferrous ion to form cuprous ion and ferric ion (Colborn and Nicol, 1973).

The fundamental difference in the work of Awakura et al. (1986) and that of Colborn and Nicol (1973) was the $[Fe^{2+}]$ / [HCl] ratios considered in their experimental work. Awakura et al. (1986) considered HCl concentration in the range of 2 – 6 M while Colborn and Nicol (1973) investigated the rate expressions in HCl concentration range of 1 – 3.9 M. The fundamental reasons for the difference in the rate expressions as the H^+ and Cl^- ion concentrations differ are discussed in detail in Section 2.2.2.2.

Table 2.1 shows a summary of rate expressions proposed by a number of researchers for the oxidation of iron(II) in HCl medium at various HCl and iron(II) concentrations. Table 2.1 also clearly highlights the difference in the proposed rate expressions by various researchers with different HCl and iron(II) concentrations considered in their work.

Table 2.1. Rate expressions for iron(II) oxidation by dissolved oxygen in hydrochloric medium (source: Lowson, 1982)

Rate Equation	**$[Fe^{2+}]$**	**[HCl]**	**Reference**
$k1+k2\ [Cl^-]$	0.2 M	0 - 3 M	Matseevskii, 1980
$k[Fe^{2+}]^2 P_{O2}$	0.01 - 0.3 M	1 M	McBain, 1901
$k[Fe^{2+}]^2 P_{O2}$	0.01 - 0.3 M	1 M	George, 1954
$k[Fe^{2+}]^2 P_{O2}$	0.01 - 0.3 M	1 M	Chernaya, 1980
$k[Fe^{2+}] P_{O2}\{HCl\}$	0.055 N	8 M	Posner, 1953
$k[Fe^{2+}] P_{O2}\{HCl\}$	0.2 M	6 M	Iwai et al, 1979
$k[Fe^{2+}] P_{O2}\{HCl\}$	0.72M	2 - 6 M	Awakura et al, 1986
$k[Fe^{2+}]^2 P_{O2}$	0.48 - 0.97 M	1 - 3.9 M	Colborn and Nicol 1973

2.2.2.2. Mechanism of oxidation

Posner (1953) reported rapid oxidation of iron(II) ions at HCl concentrations in the range 4 – 8 M. He reported that the reaction was first order with regards to iron(II) concentration and oxygen concentration; however, the role of HCl concentration in the oxidation mechanism was more complex. The role of the HCl concentration was explained by modifying the Haber-Weiss mechanism (Posner, 1953).

Weiss (1951) suggested that oxidation of iron(II) by dissolved oxygen in dilute acids is slow due to the need for the formation of superoxide (O_2^-), a thermodynamically unfavorable reaction (George, 1954; Weiss, 1935).

$$Fe^{2+} + O_2 \leftrightarrow O_2^- + Fe^{3+} \qquad 2.9$$

The formation of superoxide, as shown in Equation 2.9, requires +30 kcal/mole.

$$O_2^- + H^+ \leftrightarrow HO_2 \qquad 2.10$$

Equation 2.10 follows Equation 2.9 and requires –10 kcal / mole.

$$Fe^{2+} + O_2 + H^+ \leftrightarrow Fe^{3+} + HO_2 \qquad 2.11$$

Combining Equation 2.9 and Equation 2.10, Equation 2.11 is derived.

The mechanism of oxidation described in Equation 2.9, Equation 2.10 and Equation 2.11 is known as the Haber- Weiss mechanism. This mechanism leads to the derivation of the Haber- Weiss rate expression indicated in Equation 2.12 (Posner, 1953; Stumm and Lee, 1961).

$$\frac{d\,[Fe^{3+}]}{dt} = 4k_1[Fe^{2+}][O_2]\frac{[Fe^{2+}][H^+]}{k_2[Fe^{2+}][H+] + k_1'K_{HO_2}[Fe^{3+}]} \qquad 2.12$$

Posner (1953) suggested that in HCl systems, the formation of superoxide is bypassed due to the complexation of iron(II) with HCl according to Equation 2.13.

$$(Fe^{2+}.HCl\,complex) + O_2 \rightarrow HO_2 + Fe^{3+} + Cl^- \qquad 2.13$$

When the HCl is dissociated, the complexation can be represented by the equilibrium Equation 2.14.

$$H^+Cl^- + Fe^{2+} \leftrightarrow HFe^{2+}Cl \qquad 2.14$$

Considering Equation 2.13 and Equation 2.14, it can be observed that if dissociated HCl was the reactive species in the oxidation process, then the rate of oxidation must be proportional to the concentration of hydrogen and chloride ions, $[H^+]$ $[Cl^-]$ at any given acid concentration, unlike the reported various rate expressions owing to the difference in the acid concentrations (Astanina and Rudenko, 1971).

Posner (1953) suggested that associated HCl, rather than dissociated HCl, was responsible for the rapid oxidation of iron(II) chloride. A step by step series of equations were proposed. These equations have come to be known as the modified Haber-Weiss mechanism for the oxidation of iron(II) in HCl systems. The steps of the modified mechanism are shown in Equation 2.15 to Equation 2.19. Equation 2.15 shows the oxidation of Fe^{2+} - HCl (associated) complex by oxygen. Equation 2.15 is effectively the same as Equation 2.13. The HO_2 produced in Equation 2.15 then reacts with the Fe^{2+} present in solution to produce Fe^{3+} and HO_2^- according to Equation 2.16. The HO_2^- produced reacts with H^+ to produce H_2O_2 according to Equation 2.17. The H_2O_2 oxidizes the Fe^{2+} present in solution, producing OH according to Equation 2.18. The OH produced then further oxidizes the remaining Fe^{2+} according to Equation 2.19. The overall reaction is identical to Equation 2.2.

$$[HCl]Fe^{2+} + O_2 \rightarrow HO_2 + Fe^{3+} + Cl^- \qquad 2.15$$

$$HO_2 + Fe^{2+} \rightarrow Fe^{3+} + HO_2^- \quad 2.16$$

$$HO_2^- + H^+ \leftrightarrow H_2O_2 \quad 2.17$$

$$H_2O_2 + Fe^{2+} \rightarrow OH + OH^- + Fe^{3+} \quad 2.18$$

$$OH + Fe^{2+} \rightarrow OH^- + Fe^{3+} \quad 2.19$$

Equation 2.20 was the proposed rate expression for the oxidation of iron(II) in HCl systems at 5.5 M and below.

$$\frac{d\,[Fe^{3+}]}{dt} = k[O_2][HFe^{2+}Cl] \quad 2.20$$

Equation 2.21 was the suggested rate expression for the oxidation of iron(II) in HCl systems above 5.5 to 14 M.

$$\frac{d\,[Fe^{3+}]}{dt} = k[O_2][Fe^{2+}][HCl - 5.5] \quad 2.21$$

It can therefore be noted that bypassing the thermodynamically unfavorable formation of superoxide in HCl systems by the complexation of iron(II) with associated HCl is a possible mechanism of iron(II) oxidation (Astanina and Rudenko, 1971; Posner, 1953).

2.2.3. Catalytic effect of copper

The catalytic effect of copper has been reported by Stumm and Lee (1961) and a number of other researchers. The specific mechanism by which copper catalyzes the oxidation of iron(II) is not entirely known. Stumm and Lee (1961) reported that cupric ions were efficient catalysts in the oxidation of iron(II) in acidic solutions. They reported that low concentrations of cupric copper, as low as 3×10^{-7} M, are needed to catalyze the oxidation process. Several researchers have reported that the mechanism by which copper catalyzes the oxidation process

could be that cupric ions oxidize the ferrous ions while they are reduced to cuprous ions. The cuprous ions are then oxidized by dissolved oxygen back to cupric ions and the formation of perhydroxyl radical. This mechanism is highlighted in Equation 2.22 and Equation 2.23 (Awakura et al., 1986; Colborn and Nicol, 1973; Dreisinger and Peters, 1989; Georges et al., 1987; Posner, 1953; Stumm and Lee, 1961). Furthermore, copper ions have been reported to catalytically aid the decomposition of hydrogen peroxide in the presence of ferrous salts (see Equation 2.18). The catalytic decomposition of hydrogen peroxide by intermediate complexes of copper(II) is said to be that of a free radical mechanism that involves reversible oxidation–reduction of the cupric–cuprous couple. It is therefore possible that the mechanism by which copper catalyses ferrous ions may also include a radical pathway (Haber and Weiss, 1934).

$$Cu^{2+} + Fe^{2+} \rightarrow Cu^{+} + Fe^{3+} \qquad 2.22$$

$$Cu^{+} + O_2 \rightarrow Cu^{2+} + O_2^{-} \qquad 2.23$$

2.3. Precipitation of iron(III)

2.3.1. Theory of precipitation

Precipitation is defined as reactive crystallization. Both crystallization and precipitation involves two steps: nucleation and growth. Figure 2.3 shows the possible channels of precipitation. Nucleation and growth is as a result of supersaturation in a solution (Sohnel and Garside, 1992). The definition of supersaturation and its influence on precipitation is discussed in Section 2.3.1.4.

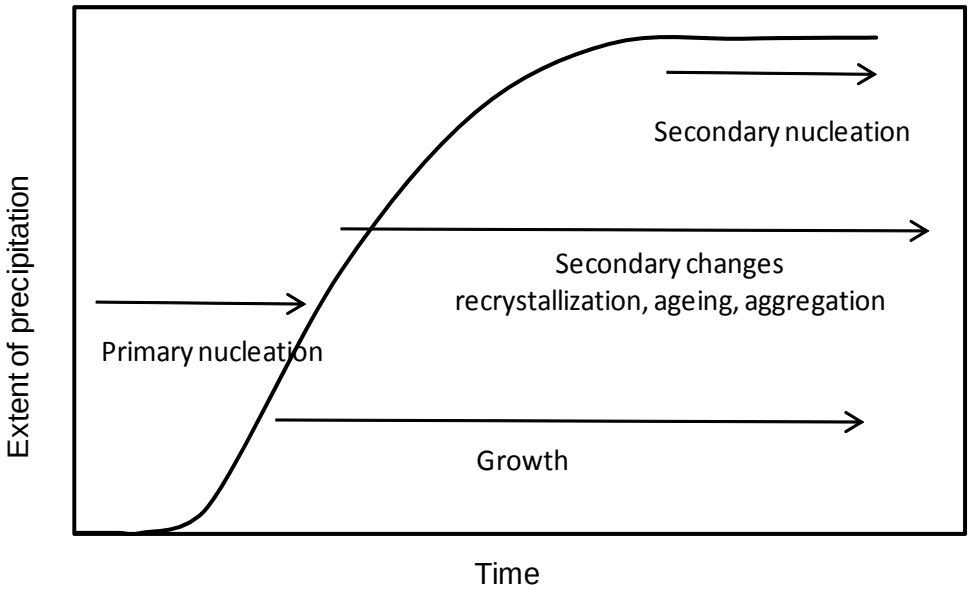

Figure 2.3. Precipitation kinetic processes (after Sohnel and Garside, 1992)

2.3.1.1. Nucleation

The formation of a solid from a supersaturated solution involves nucleation and growth. There are three main types of nucleation processes: homogeneous nucleation, heterogeneous nucleation and surface nucleation (also known as secondary nucleation). Homogeneous nucleation is the production of nuclei in the absence of a solid phase while heterogeneous nucleation involves production of nuclei on a foreign surface. Surface nucleation is the mechanism of formation of solid phase initiated by the presence of a surface of the crystallizing precipitate itself (Dirksen and Ring, 1991).

Homogeneous nucleation

Homogenous nucleation will proceed by the coming together of molecules in a supersaturated solution to form embryos consisting of 10 to 1000 molecules per embryo. The embryos keep on forming and disappearing until they attain a critical size (r_c). Beyond this size (r_c), the embryos stabilise. The free energy associated with the formation of the embryo is shown in Equation 2.24.

$$\Delta G_{(r)} = \Delta G_{vol} - \Delta G_{surf} \qquad 2.24$$

Where,

ΔG (r) is the free energy for the formation of an embryo

ΔG_{vol} is the free energy associated with the generation of embryo volume

ΔG_{surf} is the free energy associated with the generation of the embryo surface

The rate of homogeneous nucleation, as shown in Equation 2.25, can take the form of Arrhenius equation (Demopoulos, 2009).

$$J = \left(\frac{2D}{d^5}\right) exp\left(\frac{\Delta G_{max}}{k_B T}\right) \qquad 2.25$$

Where,

J is the number of nuclei per unit volume (m^3) per unit time (s)

D is the diffusivity of solute (m^2/s)

d is the molecular diameter of the solute species (m)

k_B is the Boltzman constant; 1.38 x 10^{-23} $J.K^{-1}$

ΔG_{max} is the maximum activation Gibbs free energy barrier (J)

T is the temperature (K)

A graphical representation of ΔG (r) is shown in Figure 2.4.

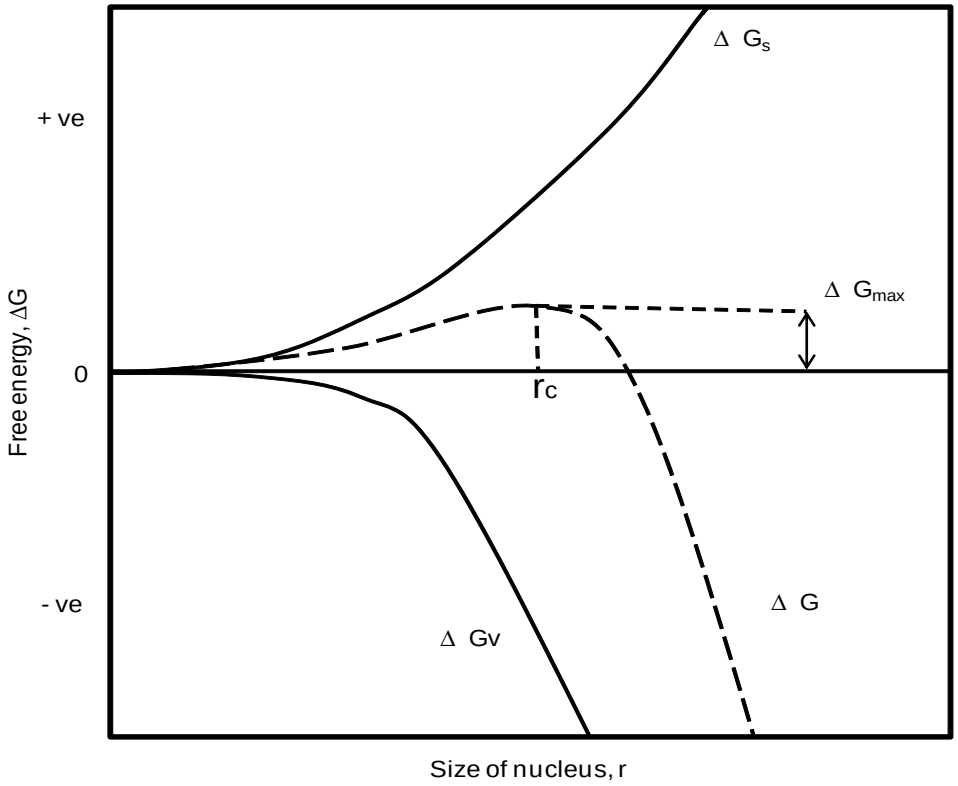

Figure 2.4. Crystallization free energy vs. nuclei size (after Demopoulos, 2009)

Heterogeneous nucleation

Precipitates have unique critical saturation values (S_c). From the definition of saturation ratio ($S=\alpha/\alpha_o$), critical saturation values varies from 1.1 to as high as over 10,000. Critical saturation is said to be an intrinsic kinetic property of individual precipitates. Heterogeneous and surface nucleation demand less surface energy, ΔG_{surf}, than homogeneous nucleation thus the critical saturation ratio is also lower for heterogeneous and surface nucleation as compared to homogeneous nucleation. The magnitude of critical saturation ratio, S_c, follows the order of the magnitude of activation energy which controls the rate of nucleation (Dirksen and Ring, 1991; Sohnel and Garside, 1992).

$$1 < S_{C,Surface} < S_{C,Hetero} < S_{C,Homo}$$

Surface nucleation (Seeding)

The formation of a solid phase in a supersaturated solution, in the presence of the very solid phase being synthesised, is called surface nucleation or secondary nucleation. Surface nucleation can be divided into two categories:

- Apparent secondary nucleation – a solid phase, similar to that desired to nucleate, is introduced into the system as seed.
- True secondary nucleation – the nuclei is formed due to crystal and solution interactions; this is typical of a system that later engages in Ostwald ripening growth.

Ostwald (1896) further proposed that during phase transformation, it is not the thermodynamically stable phase that will preferentially be formed, but rather the phase that is nearest to the original phase in terms of stability. With time, the metastable phase transforms to the stable phase which is more pure due to the cycle of crystallization, dissolution and recrystallization (Ostwald, 1896).

2.3.1.2. Growth

Growth can be said to be controlled by mass transfer rather than heat transfer. Two types of growth sites have been described to accommodate atoms or growth units: the step site, where two nearest bonds are made between the growth unit and the crystal, and the kink site, where three nearest bonds are made between the growth units and crystal. The steps that lead to growth can be summarized as follows (Dirksen and Ring, 1991):

- Interfacial transport of solute from the bulk solution to the crystal surface
- Adsorption of the solute on the surface of the particle
- Diffusion of solute onto a step or kink site
- Surface reaction or integration of the solute into the crystal lattice
- Heat of crystallization liberation and transfer away from the crystals

At molecular level, growth units diffuse towards the surface of the crystals and attach themselves. One of the important parameters during molecular level

growth is the crystal-solution interface. The manner in which the crystals interact with the solution determines the binding energy. Microscopic level growth involves growth that results from hundreds of molecular layers that have reduced diffusive flux. The trapping of impurities inside the crystal structure can be attributed to microscopic level growth. Macroscopic growth is attributed to the binding together of microscopic particles. The concentration gradient at macroscopic level will influence the surface concentration profile which results in instabilities at surface level. These instabilities can result in the formation of dendrite (Sohnel and Garside, 1992).

The growth rate of a particle is mathematically defined as shown in Equation 2.26.

$$Gr = K_g C_{eq}(S-1) \qquad 2.26$$

Where,

Gr is the crystal growth rate (m s^{-1})

K_g is the growth constant (m^4 mol^{-1} s^{-1})

C_{eq} is the solubility of the solute (mol m^{-3})

S is the saturation ratio

If a number of mechanisms take place in parallel, the faster mechanism controls the overall rate. However, if the process is taking place in series (bulk diffusion and surface reaction or integration), the slower mechanism controls the growth rate (Dirksen and Ring, 1991).

2.3.1.3. Solubility product

Precipitation occurs only when the reactant activities exceeds the solubility product K_{sp}. The equilibrium constant (K) of a dissociation reaction (reverse precipitation reaction) is inversely correlated to the solubility product (see Equation 2.27) (Habashi, 1999).

$$\frac{1}{K_{sp}} = K \qquad 2.27$$

The change in free energy of a reaction (ΔG_r) can be expressed as shown in Equation 2.28.

$$\Delta G_r = \Delta G_r^o + RT\ln Q \qquad 2.28$$

ΔG_r^o is the standard free energy change, R is the gas constant (8.3144 J/mol.K) and Q is ratio of activities of products to reactants. At equilibrium, Q is equal to the equilibrium constant, K, and ΔG_r is equal to zero. Therefore the free energy equation at equilibrium can be expressed as shown in Equation 2.29.

$$\Delta G_r^o = -RT\ln K \qquad 2.29$$

Therefore,

$$K = \exp\left(\frac{-\Delta G_r^o}{RT}\right) \qquad 2.30$$

From the standard free energy change data, we can therefore determine the solubility product K_{sp} as shown in Equation 2.31.

$$K_{sp} = \frac{1}{\exp\left(\frac{-\Delta G_r^o}{RT}\right)} \qquad 2.31$$

K_{sp} for a metal sulphide containing z M^{n+} and m S^{2-} ions is expressed as indicated in Equation 2.32.

$$K_{sp} = [M^{n+}]^z.[S^{2-}]^m \qquad 2.32$$

$$z\log[M^{n+}] = \log K_{sp} - m\log[S^{2-}] \quad 2.33$$

For hydroxide precipitation of metal M^{n+} and m OH^-, Equation 2.33 can be rewritten as shown in Equation 2.34.

$$\log[M^{n+}] = \log K_{sp} - m\log[OH^-] \quad 2.34$$

$$pH + pOH = \log k_W \quad 2.35$$

k_W is the ionic product of water.

$$\log[M^{n+}] = \log K_{sp} + m\log k_W - m\,pH \quad 2.36$$

Equation 2.36 gives the basis for the theoretical estimation of pH values at which metal values will precipitate depending on their activities (concentrations) in the solutions (Free, 2013; Gupta, 2003; Habashi, 1999)

2.3.1.4. Supersaturation control

Definition of supersaturation

Thermodynamics dictates that a solid phase will be formed out of solution if the molar Gibbs free energy is less than zero.

$$\Delta G = -RT\ln(S) < 0 \quad 2.37$$

Where ΔG is the molar Gibbs free energy, R is the universal gas constant, T is the absolute temperature and S is the saturation ratio.

The saturation ratio, S, is defined as the ratio of activity, α, of the solute in the solution at time zero to the activity, $\alpha_{f,}$ of the solute in the final solution. This ratio is equal to the ratio of the initial concentration of the solute in solution, C, to the equilibrium concentration, C_{eq}, for a system whose activities are equal to concentrations.

$$S = \frac{\alpha}{\alpha_f} = \frac{C}{C_{eq}} \qquad 2.38$$

It follows that when S > 1, then $\Delta G < 0$.

The statement above defines supersaturation. It can therefore be deduced that supersaturation is the driving force for precipitation.

At low supersaturation, the dominant nucleation mechanism is heterogeneous and therefore the number of crystals formed is dependent on the availability of heteronuclei in the solution. At high supersaturation, crystals grow so fast such that the heat of crystallization cannot be transferred quickly enough away from the crystals to the surrounding solution. The depleted solution surrounds the crystal face because diffusion cannot provide the solute at the demanded rate. This causes elongation and crystal surface extensions as the crystal attempts to aid the transfer of crystallization heat (Demopoulos, 2009; Sohnel and Garside, 1992). Table 2.2 shows the effect of initial saturation ratio on the nucleation and growth mechanism and the particle morphology.

Table 2.2. Effect of initial supersaturation on crystal growth (after Sohnel and Garside, 1992)

Initial S_o	Nucleation Mechanism	Growth Mechanism	Particle Morphology
< 2	Heterogeneous	Surface reaction	Compact crystal shape and well defined
2 to 10	Heterogeneous	Surface reaction	Compact crystal shape and well defined
10 to 50	Heterogeneous	Compound	3/4 - developed crystals - dendrites
> 100	Homogeneous	Diffusion or compound	Small, isometric, agglomerated crystalline partices
> 1000	Homogeneous	Diffusion	Very small, colloids and often amorphous agglomerates

Advantages of low supersaturation

It is clear from the theoretical point of view that supersaturation has a significant influence on the precipitate quality. As discussed, higher supersaturation tends to produce poor quality crystals that inevitably gives rise to challenges during solid-liquid separation. Low supersaturation has the following advantages:

- Immobile and large polymeric species are avoided.
- Homogeneous nucleation and therefore amorphous crystal production is avoided.
- Surface integration proceeds undisturbed because of reduced external transfers.

  (Dirksen and Ring, 1991)

pH and temperature supersaturation control

A number of measures can be taken to control supersaturation: pH control, temperature control, dilution of solute and metal complexation. However, pH control and temperature control are the most suitable supersaturation control parameters during the iron precipitation in order to ensure that the process is as simple as possible (Claassen and Sandenbergh, 2007a; Demopoulos, 2009; Dirksen and Ring, 1991).

Slow neutralization may lead to supersaturation control. The solution pH can be raised by weak bases such as urea or a low molar strong base. The equilibrium pH of metal precipitates increases with decrease in the solute activity up to a certain pH, beyond which the shape of the equilibrium pH reverses direction. Step-wise neutralization has the advantage of controlling nucleation rates by operating near equilibrium pH for a given band solute activity. Step-wise neutralization is shown in Figure 2.5.

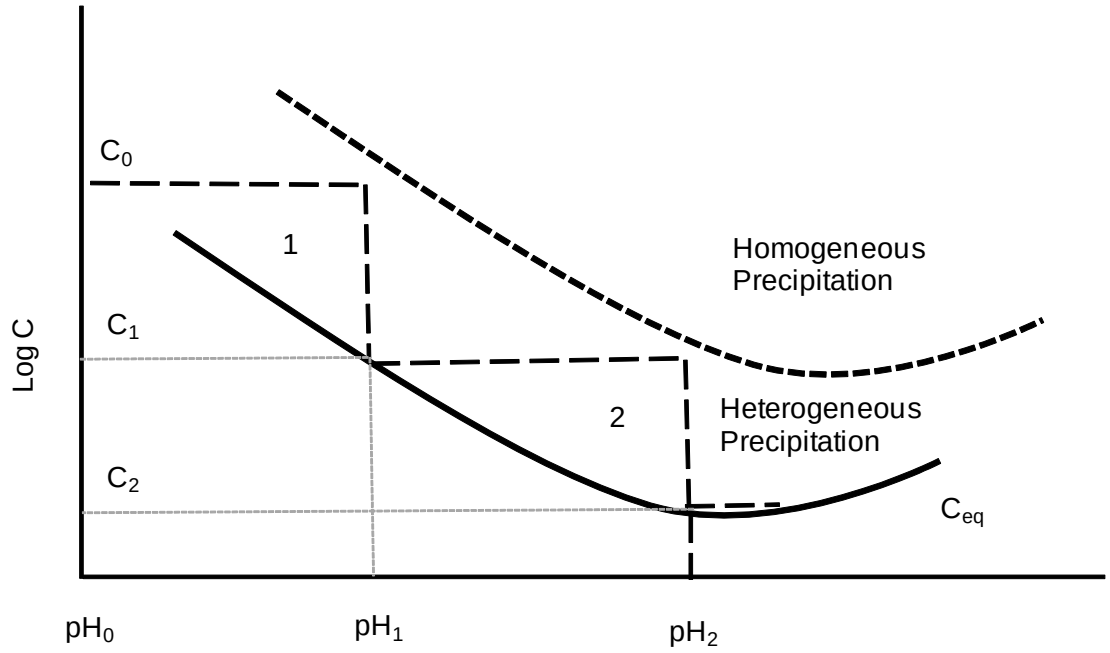

Figure 2.5. Stage-wise pH control (after Demopoulos, 2009)

Generally, lower supersaturation is attained at lower pH and higher temperature. A combination of low pH and high temperature ensures control of supersaturation and results in better quality precipitates (Claassen and Sandenbergh, 2007a).

Figure 2.6 shows the general effect of temperature on supersaturation at various pH points. As the temperature increases, relative supersaturation reduces. This is in line with the mathematical description of the solubility product and supersaturation ratio (see Equation 2.30 and Equation 2.37 respectively).

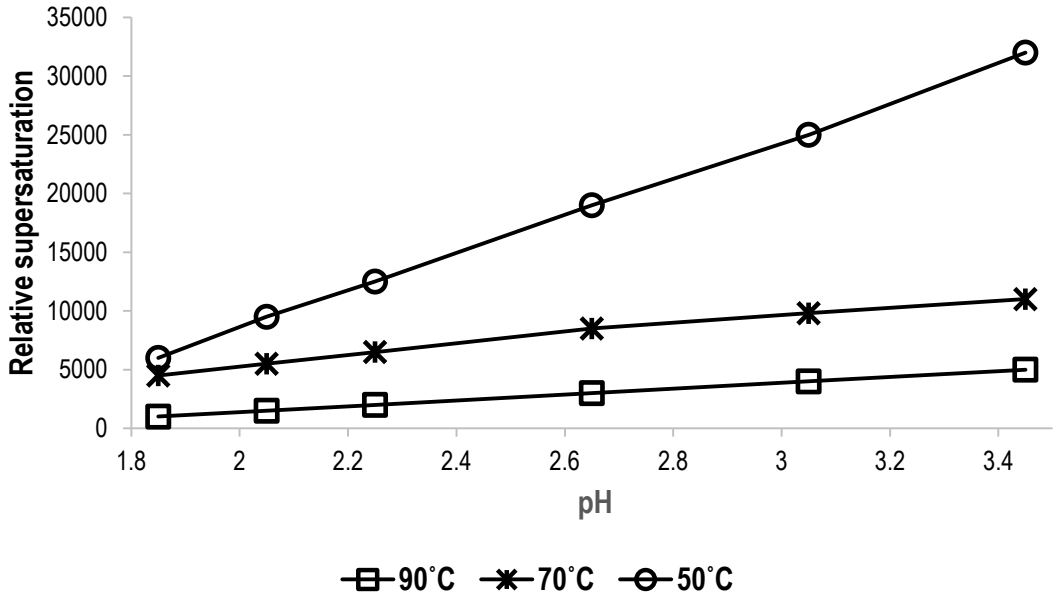

Figure 2.6. Relative supersaturation at various temperatures as a function of pH during precipitation of ferric iron with an initial concentration of 11.5 g/L (After Claassen, 2006)

2.3.1.5. Physical aspects of precipitation

Influence of mixing

Mixing influences the physical properties of precipitates because it directly influences the localized supersaturation. Nucleation and growth is influenced by the hydrodynamic conditions obtained during the crystallization process.

Mixing can be classified into three environments: macro-mixing, meso-mixing and micro-mixing. Macro-mixing endeavours to reduce the concentration difference across the reactor diameter. The reactor circulation time is the key performance indicator for this level of mixing.

Meso-mixing refers to the mixing level at reactant injection tubes. The injection tube diameter and reactant flow rate influences the mixing at meso-mixing level.

Micro-mixing refers to the segregation of fluid elements where mixing occurs at molecular level. The energy involved in the system and the fluid properties dictates the micro-mixing timescale. These three environments occur

simultaneously, making it challenging to have a decent investigation of their individual influence (Claassen and Sandenbergh, 2007b).

The difference in the three mixing environments as related to the process of nucleation and growth is shown in Figure 2.7.

Generally, rapid mixing results in higher rates of nucleation compared to growth and therefore precipitation tends to be nucleation dominant. This leads to the production of smaller sized crystals and narrower size distribution (Sohnel and Garside, 1992).

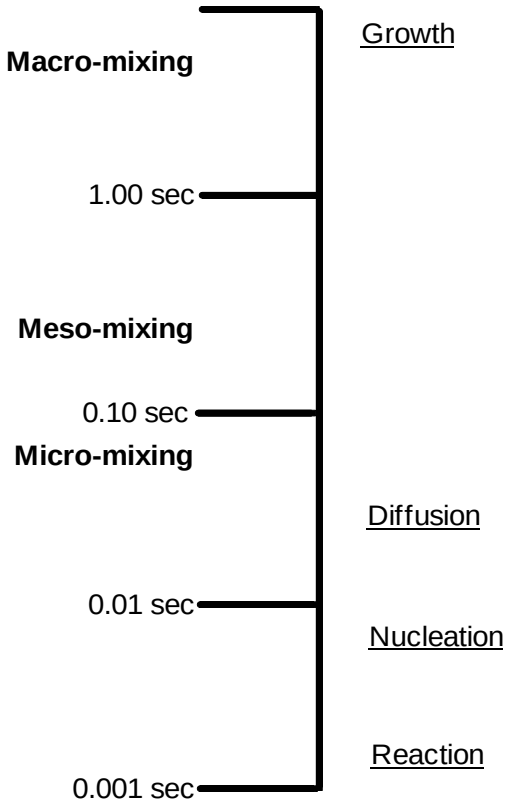

Figure 2.7. Difference between mixing times and nucleation and growth (after Claassen and Sandenbergh, 2007b)

Secondary precipitation

The following processes are able to make changes to the physical and chemical properties of precipitates: recrystallization, ripening, ageing, aggregation, agglomeration and coagulation.

Recrystallization is a process that changes the size and the shape of the crystal by surface integration or mass transfer through the liquid phase. It can be categorized as either isothermal or non-isothermal recrystallization.

Isothermal recrystallization is also known as Oswald ripening. It involves the shift of crystal distribution towards large ones as a result of smaller crystals redissolution.

Ageing is a slow process that changes the microscopic and at times macroscopic solid phase by contacting of the solid phase with the mother solution. Ageing causes recrystallization of needles, dendrites and plates to produce compact shapes. Amorphous solids can be transformed into stable and crystalline phases by the process of ageing.

Aggregation is the coming together of smaller particles to produce larger particles. Aggregation can either be in the form of agglomeration or coagulation. Agglomeration involves clustering of particles earlier formed to form secondary particles that are stronger and held together by crystalline bridges and physical forces. When the clusters are held by physical forces, it is called coagulation. Flocculation is a practice that encourages aggregation (Sohnel and Garside, 1992).

2.3.1.6. Co-precipitation mechanisms

Co-precipitation, in the context of this research, can be defined as the contamination of the intended precipitate by ions that were not intended to be precipitated. Co-precipitation has two interrelated main disadvantages;

- Loss of value metals to the precipitate
- Contamination of the precipitate by the value metals. This applies if the precipitate is needed as pure as possible

It is therefore critical to understand the mechanisms that promote co-precipitation. There are three mechanisms by which co-precipitation can occur;

- Inclusion
- Occlusion and
- Surface adsorption

Inclusion is a mechanism of co-precipitation that is as a result of homogeneous precipitation. In inclusion co-precipitation, the logarithmic distribution of ions applies according to Equation 2.39 (Habashi, 1999).

$$\log\left(\frac{C_i}{C_f}\right) = \lambda \log\left(\frac{C_{Pi}}{C_{Pf}}\right) \qquad 2.39$$

Where,

C_i is the initial concentration of the value metal in solution

C_f is the final concentration of the value metal in solution

C_{Pi} is the initial concentration of the primary ion, to be precipitated, in solution

C_{Pf} is the final concentration of the primary ion, to be precipitated, in solution

λ is the logarithmic distribution coefficient

Lambda, λ, decreases with increase in temperature therefore, *inclusion* co-precipitation is pronounced at lower temperatures. Homogeneous nucleation is also pronounced at lower temperatures (see Equation 2.25, which describes the rate of homogeneous nucleation in relation to temperature).

Occlusion is the mechanism of co-precipitation that occurs when the unintended ions are mechanically trapped, either as solids or liquids, in the crystal layers of the parent precipitate. Therefore, it follows that these unintended ions cannot be washed off the precipitate in an attempt to free them.

It has been suggested that *occlusion* is the main mechanism of co-precipitation in many freshly prepared oxides and hydroxides. This is because of high supersaturation that leads to higher nucleation rates and lower growth rates

thereby trapping unintended ions between ‘rushed’ crystal layers (Claassen and Sandenbergh, 2006; Habashi, 1999; Sohnel and Garside, 1992).

Surface adsorption is the mechanism of co-precipitation that occurs as a result of precipitate impurities being introduced through the surfaces of the precipitate itself. This mechanism occurs only when the precipitate surface ions are not completely coordinated and therefore able to attract oppositely charged ions that are still in solution.

When surface adsorption is the main mechanism of co-precipitation, higher co-precipitation is experienced when larger crystals are precipitated and when there is prolonged contact with solution (Demopoulos, 2009).

2.3.2. Iron precipitation processes

Conventional iron precipitation processes in hydrometallurgical solutions include jarosite precipitation, goethite precipitation and hematite precipitation (Ismael and Carvalho, 2003). The stability fields for jarosite, goethite and hematite as a function of pH and temperature are shown in Figure 2.8.

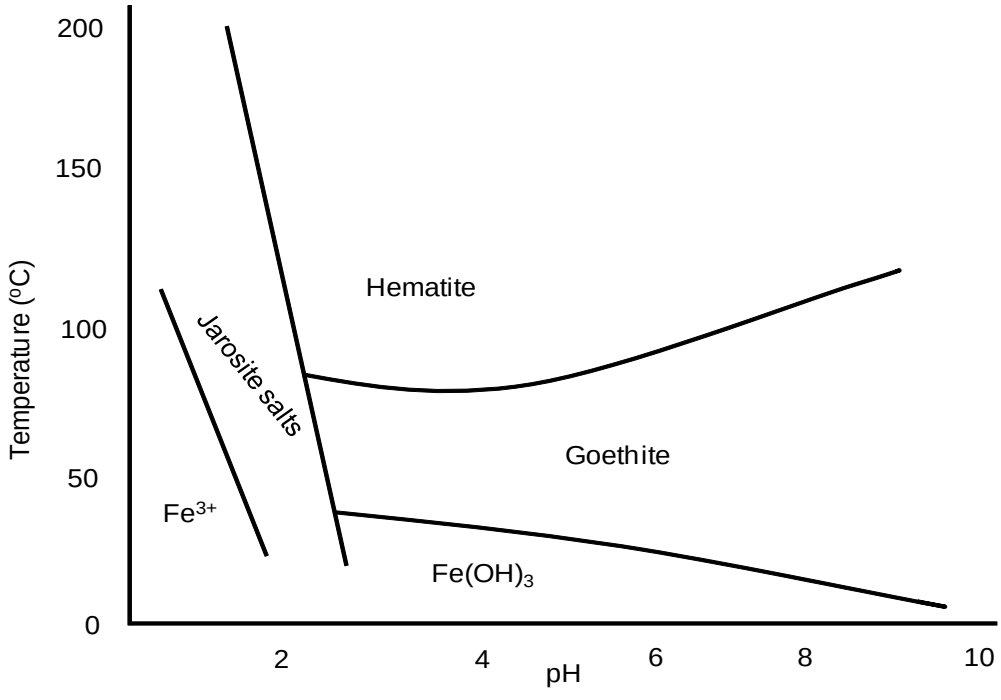

Figure 2.8. Equilibrium condition for iron oxides (after Claassen et al., 2002)

2.3.2.1. Jarosite precipitation

The jarosite process is the most commonly used process in sulphate systems. Jarosite is a complex basic iron sulphate of the form $2MFe_3(SO_4)_2(OH)_6$, where *M* represents one of the ions Na^+, NH_4^+ , H_3O^+, Li^+, K^+, or $1/2Pb_2^+$ The jarosite precipitation reaction is shown in Equation 2.40 (Schwertmann and Cornell, 2000).

$$3Fe_2(SO_4)_3 + M_2SO_4 + 12H_2O \leftrightarrow 2MFe_3(SO_4)_2(OH)_6 + 6H_2SO_4 \qquad 2.40$$

Babcan (1971) reported that the jarosite stability zone is between pH 1 to 3 and temperature is between 20°C and 200°C (Babcan, 1971; Ismael and Carvalho, 2003).

The jarosite process is extensively used during iron removal in zinc hydrometallurgy. Generally, iron is precipitated from the hot leach solution at temperatures around 95 – 100^{o}C in the presence of sodium, potassium or ammonium ions. Zinc calcine is used to control the precipitation pH around 1.5 – 1.8. Depending on the precipitation pH, less than 1% iron is left in the solution after precipitation. The co-precipitation of metal ions (Zn, Cu, Ni, Mn, Al, Ga and Ge) was cited as one of the major weaknesses of the jarosite process however typical losses were not reported (Claassen et al., 2002; Wang et al., 2011).

Dutrizac (1991) investigated the formation of jarosite compounds in chloride systems. Experiments were conducted at 98^{o}C in a glass reactor customized with titanium baffles. HCl and Li_2CO_3 were used to adjust the solution pH while Li_2SO_4 was added as the sulphate source because it does not participate in the formation of jarosite compound end-members. Upon precipitation, the precipitates were easily filtered and washed with hot water to remove mechanically trapped solution. Before precipitation could occur, a minimum of 0.1 M sulphate concentration was needed. It was reported that the precipitate yield increased linearly with the sulphate concentration above 0.1 M. For experiments conducted at room temperature, precipitation did not occur at pH below 0. At pH

above 0.8, amorphous precipitates were produced. These precipitates were identified as ferric hydroxides, $Fe(OH)_3$. Further experiments were conducted at temperatures above 100^{o}C in a Parr 2 L titanium autoclave. It was observed that the product yield and filterability increased with temperature. This increase in filterability was attributed to the transformation of jarosite to hematite (Dutrizac, 1991).

Jarosite compounds are thermodynamically unstable and tend to decompose over time releasing sulphuric acid and heavy metals. Jarosite compounds are universally classified as hazardous waste because of the adverse effects to the environment and the human health (Asokan et al., 2006). The Basel Convention, ratified in 1992 throughout Europe and by 148 other countries worldwide, regulates the movement and management of hazardous waste (Hsing et al., 2004; Leclerc et al., 2003). The accumulation of hazardous waste, such as jarosite compounds, implies significant challenges in waste management.

2.3.2.2. Goethite (akaganeite) precipitation

The essential feature of goethite (FeO.OH) precipitation is that the iron(III) concentration of the parent solution should be maintained at about 1 g/L. The removal of iron as goethite is mainly achieved by the Vieille Montgane (V.M.) technique. In the V.M. technique, the iron bearing solution is initially reduced to iron(II), such that only about 1 g/L iron(III) is present in the solution. Controlled oxidation of iron(II) is then employed by bubbling molecular oxygen in an agitated reactor at a controlled rate to limit the concentration of iron(III) to about 1 g/L (Allen et al., 1970; Davey and Scott, 1975).

In the case of laterite ore and most chloride systems, iron ions are usually in the state of iron(II) and therefore conveniently do not need to be reduced but only have to be oxidized at a controlled rate (Chang et al., 2010).

The goethite precipitation reaction is shown in Equation 2.41. The reaction takes place at 70^{o}C – 90^{o}C at pH 2 – 3 (Posnjak and Merwin, 1922).

$$2Fe^{2+} + 0.5O_2 + 3H_2O \leftrightarrow 2FeO.OH + 4H^+ \qquad 2.41$$

Goethite has been reported to be formed as either α-goethite in sulphate systems or β-goethite (akaganeite) in chloride systems. Akaganeite is said to be practically impossible to filter (as low as 2 mL/min) (Cohen et al., 2005; Dutrizac and Riveros, 1999). However, controlled precipitation of α-goethite in sulphate systems ensures filterable precipitates (Ismael and Carvalho, 2003).

Depending on the operating pH, the initial goethite patented process was designed to reduce iron from solution by at least 98%. However, the incorporation of the V.M. techniques has led to almost complete removal of iron (above 99%) at pH 2 and temperature around 90^{o}C (Davey and Scott, 1975).

Production of large volumes of goethite has been reported to be an environmental concern even though it is presently stored in secure impoundments (Dutrizac and Riveros, 1999).

Goethite and akaganeite are both made up of double bands of edge sharing $FeO_3(OH)_3$ octahedra structures. The double bands in goethite are connected by corner sharing in a way that forms 2 by 1 octahedra tunnels that are crossed by hydrogen bridges. The tunnels in goethite are only large enough to accommodate the passage of protons. The structure of akaganeite has squared molecular channels connected by 4 by 2 rows of octahedral. The channels in the akaganeite structure are large enough to permit the passage of anions and other impurities. It is thought that the structural difference of goethite and akaganeite gives raise to the differences in the purity and filterability of the two compounds (Schwertmann and Cornell, 2000).

Davey and Scott (1975) investigated the removal of iron from chloride and sulphate leach solutions containing about 30 g/L iron and cations (mainly nickel and copper) amounting to 15 g/L. The V.M. goethite precipitation technique was employed. 3% hydrogen peroxide was added at a controlled rate to maintain the concentration of iron(III) at about 1 g/L. The precipitation pH was varied at two

points, 2 and 3.5. The temperature points investigated were 65^{o}C, 75^{o}C, 85 ^{o}C and 95^{o}C. The precipitation reaction was deemed complete after 3 to 3.5 h. In the sulphate system, α-FeOOH (goethite) precipitates were generated while in the chloride system, β-FeOOH (akaganeite) precipitates were produced. Goethite precipitates produced at all temperatures investigated were reported to be filterable; however, akaganeite precipitates caused peptization (dispersion of colloid particles) upon washing with water. Precipitates produced were reported to have been contaminated with at least 0.4% and 0.3% nickel in chloride and sulphate systems respectively. The equivalent percentage nickel losses were however not reported.

2.3.2.3. Hematite precipitation

Hematite (Fe_2O_3) is the preferred iron oxide / hydroxide precipitate because it is a stable, high density and more pure form of iron. These properties of hematite make it easier for disposal and offer the potential for it to qualify as a byproduct. Hematite is used as starting material in the production of iron and steel, pigments and ferrites (Riveros and Dutrizac, 1997).

The hematite structure is made of layers of FeO_6 octahedra. The octahedra are stacked perpendicular to the c-direction. Iron(III) occupies 2/3 of the octahedral interstices. The lack of hydrogen-bonds results in a compact structure, yielding a relatively high density of 5.26 g/cm^3. Compared to other iron precipitates in hydrometallurgy, hematite is less voluminous for the same quantity of iron. This is because of its relatively high density compared to other iron precipitates (Schwertmann and Cornell, 2000).

The hydrolysis of ferric ions can be represented by Equation 2.42. Traditionally, hematite precipitation has been reported to be possible at a temperature greater than 100^{o}C, under pressure oxidation of greater than 5 bar and at a pH as low as 1 (Dutrizac and Monhemius, 1986).

$$2Fe^{3+} + 3H_2O \leftrightarrow Fe_2O_3 + 6H^{+} \qquad 2.42$$

It can be seen from Equation 2.42 that hematite precipitation is a reversible reaction. Increasing the acid concentration tends to cause dissolution of the hematite according to the reverse reaction of Equation 2.42. At the same time, an increase in acid concentration lowers the supersaturation of the system, as discussed in Section 2.3.1.4.

Another pathway by which hematite can be prepared, besides the one highlighted in Equation 2.42, is the pre-neutralization of acidic ferric solutions at a temperature below 100^{o}C. The neutralized solution is then heated to about 150^{o}C.

Equation 2.43 shows the hydrolysis of ferric ions after pre-neutralization. Over an extended period of time, the iron-hydroxyl complex formed as shown in Equation 2.43 undergoes further hydrolysis (see Equation 2.44). It is possible that the hydroxyl component of the iron-hydroxyl complexes produced, as highlighted in Equation 2.43 and Equation 2.44, can take part in the neutralization of acid as shown in Equation 2.45. Upon pre-neutralization and hydrolysis, if the solution is then heated to about 150^{o}C, hematite is precipitated according to Equation 2.46.

$$Fe^{3+} + H_2O \rightarrow Fe(OH)^{2+} + H^{+} \qquad 2.43$$

$$Fe(OH)^{2+} + H_2O \rightarrow Fe(OH)_2^{+} + H^{+} \qquad 2.44$$

$$H^{+} + OH^{-} \rightarrow H_2O \qquad 2.45$$

$$2Fe(OH)^{2+} + 4Cl^{-} + H_2O \rightarrow Fe_2O_3 + 4HCl \qquad 2.46$$

Significant research on the precipitation of hematite in chloride media has been conducted by Riveros and Dutrizac (1997) and Dutrizac and Riveros (1999).

Riveros and Dutrizac (1997) conducted a series of experiments in a 2 L Parr titanium autoclave. A liter of $FeCl_3$ prepared from reagent grade chemicals was used for each experimental run. Some of the prepared solutions contained reagent grade HCl, $FeCl_2$, NaCl, $CaCl_2$, $PbCl_2$ and $ZnCl_2$. The solutions were

placed in an autoclave and rapidly heated to the desired reaction temperature. The retention times were measured from the moment the operating temperature was attained. In the absence of hematite seed, 0.3 M $FeCl_3$ solutions were heated for 3 h at various temperatures. The precipitates produced at temperatures below 120°C contained approximately 53% Fe and 8% Cl while those produced at temperatures above 130°C contained approximately 65% Fe and less than 1% Cl. It was reported that the presence of Cl in the precipitates was due to the entrainment of parent solutions. It was observed that the precipitates produced in the absence of seeding and at temperatures below 120^{o}C were fine grained, and difficult to filter and wash. These precipitates were identified to be akaganeite.

To investigate the effect of seeding, Riveros and Dutrizac (1997) conducted a series of experiments using 0.3 M $FeCl_3$ solutions. The solutions were heated for 3 h at various temperatures (100^{o}C being the lowest temperature investigated) in the presence of 50 g/L of initial seeds. It was reported that the precipitates obtained at all temperatures investigated contained over 65% Fe and less than 0.5% CI. The 5% Fe discrepancy with the theoretical Fe composition in hematite was accounted for by hydration of hematite. The amount of iron left in the parent solution was however not reported. When 0.6 M of $ZnCl_2$ and 1 M of NaCl were added to the $FeCl_3$ solutions, the precipitates produced contained less than 0.03% and 0.02% Zn and Na respectively.

Dutrizac and Riveros (1999), further to their earlier study, investigated the precipitation of hematite from ferric chloride at temperatures below 100^{o}C and ambient pressure mainly by employing seeding. The experiments were conducted in a 1 L reactor, placed in a temperature controlled oil bath. Chemical grade reagents were used to prepare desired solutions containing $FeCl_3$, $FeCl_2$, HCl, NaCl, $CaCl_2$ and $ZnCl_2$. Zinc oxide was used to control the solution pH. The unseeded experiments conducted at 100^{o}C required almost 100 h reaction time for akaganeite to initially precipitate and then completely transform to hematite. The seeded experiments (15 g/L of Fe_2O_3) conducted at 100^{o}C yielded hematite

after only 2 h of reaction time. It was reported that hematite precipitation occurred in two pathways; the precipitation of akaganeite (metastable phase) which with time transforms to hematite and the direct precipitation of hematite. A combination of both pathways was suggested to be possible. The direct formation of hematite was suggested to be the more likely pathway in seeded reactions while the akaganeite phase transformed to hematite with time. Further seeded experiments were conducted in a bid to investigate the lowest temperature at which hematite precipitation was possible. It was reported that at temperatures as low as 60^{o}C, for a reaction time of 2 h, hematite was precipitated in the presence of 15 g/L Fe_2O_3 seed. All precipitates identified as hematite contained less than 0.1% Zn and Ca regardless of the initial concentrations of Zn and Ca in solution. More than 99% of the initial solution iron was reported to be in the hematite precipitate.

Cohen et al. (2005) performed similar experiments to that performed by Riveros and Dutrizac (1997) and Dutrizac and Riveros (1999) to ascertain the direct applicability to the Intec zinc recovery process. The Intec zinc recovery process was reported to consist of a leaching circuit, leachate purification (removal of iron) and electrowinning. $BrCl_2^-$ anions were reported as the lixiviant. The concentration of zinc and iron in the leachate was 65 g/L and 15 g/L respectively. Traces of Cu, Cd, Pb, Mn and Mg were also present in the solution. The iron removal stage was investigated for the possible precipitation of hematite and the following factors were tested: pH, seeding, reaction time and temperature.

Cohen et al. (2005) reported that pH below 1 did not significantly affect filtration rates and ensured almost complete removal of iron, provided seeding levels were between 10 - 20 g/L. Further tests were thus conducted at pH 0.9 to minimize the composition of zinc in the precipitate to below 1%.

Cohen et al. (2005) observed that, for unseeded experiments conducted at temperatures below 100^{o}C, filtration was rendered practically impossible for reaction times of 4, 24 and 72 h. This was attributed to the formation akaganeite instead of hematite. When the reaction temperatures were increased to 100 and

110^{o}C, filtration rates were observed to take 10 to 40 minutes, for 500 mL of slurry. The improvement in the filtration rates was attributed to the formation of hematite. Seeding was reported to have a significant impact on the rate of filtration for all investigated temperatures (70, 100, and 110^{o}C) after 4h and 24h reaction times. Typical filtration rates were observed to be averaging 12 min/L and increased with increase in operating temperature and reaction time. Seeding beyond 20 g/L did not have any further impact on filtration rates.

Cohen et al. (2005) further reported that longer experiments, 24 to 72 h improved filtration rates with or without seeding. This was attributed for the transformation of akaganeite to hematite with time (Cohen et al., 2005).

2.3.2.4. Iron phosphate precipitation

Phosphate precipitation was earlier reported by Jenkins et al. (1970) as a process for removing phosphates from domestic water. This was achieved by introducing iron in the system. The iron would then precipitate with the phosphate in the water, followed by the removal of the solid phase from water stream (Jenkins et al., 1971). In hydrometallurgy, iron is the impurity that is to be precipitated out of solution by the introduction of a suitable phosphate; however, the principal remains the same as in the water system.

Cruz et al. (1980) investigated the removal of iron from electrowinning solutions. It was reported that iron(III) phosphate was precipitated at pH 2 and at a temperature of about 50°C. Compared to jarosite compounds precipitated at higher temperatures, the morphology of the iron phosphate was spherites and agglomerates of spherites and therefore easier to filter. Redissolution of the phosphate precipitate was however observed at a ferric to phosphate ratio higher than 3.15 (Cruz et al., 1980).

Twidwell et al. (1987) reported the invention of a method for recovering metal values from mixed aqueous solutions by selective phosphate precipitation. The researchers claimed the invention produced superior precipitate crystals easily separated by conventional solid/liquid filtration techniques. This process was

reported to be applicable in most known systems at that time (sulphates, chlorides and mixtures of these lixiviants). Because of its distinctive selectivity of trivalent metals from divalent metals, phosphate precipitation was suggested to be a suitable iron removal method during the purification of divalent metals such as nickel and copper. In terms of operational optimization of iron phosphate precipitation, it was suggested that iron phosphate precipitation is possible at temperatures as low as 60°C and pH as low as 2. The regime of operation suggested in the invention was that the pH of the solution is firstly adjusted to below the predetermined pH level and then stoichiometric multiples of phosphates are added while maintaining the temperature at a constant level. The pH is then gradually increased to the predetermined value. Typical retention times recorded ranged from 0.5 – 1 h. Iron removal of over 99% was reported. Iron phosphate precipitation is shown in Equation 2.47 (Twidwell et al., 1987).

$$Fe^{3+} + PO_4^{3-} + 2H_2O \rightarrow FePO_4.2H_2O \qquad 2.47$$

Garole et al. (2012) reported the recovery of metal values from electroplating sludge. It was suggested that because of high temperature associated with hydroxide precipitation of iron and difficulties of separating the precipitate, the technology of the removal of iron as ferric phosphate was a more efficient and economic method. It was reported that phosphate iron solids had lesser tendency to adsorb contaminating ions because of its spherical and lower specific surface area (Garole et al., 2012).

Robins et al. (1991) reviewed literature on the solubility and speciation of iron(III) phosphate and concluded that the reported solubility of di-hydrate ferric phosphate, which is the more common kind of iron(III) phosphate, was different by significant orders. The dimorphic nature of iron phosphate (the fact that it can exist in an orthorhombic structure or monoclinic structure) was the proposed reason for the differences in solubility products obtaining in literature. Table 2.3 shows some of the solubility products obtained experimentally by a number of researchers (Robins et al., 1991).

Table 2.3. Iron phosphate solubility products obtained experimentally (after Robin et al., 1991)

Reference	log K_{sp}	ΔG_f (kcal / mol)
Zharovskii (1951)	-2.34	-390.76
Chang and Jackson (1957)	-5.61	-395.22
Lindsay and Moreno (1960)	-7.01	-397.13
Egan et al. (1961)	-6.51	-396.45
Galal - Gorchev and Stumm (1963)	-2.48	-390.95
Nriagu (1972)	-6.85	-396.91
Brown and Allison (1989)	-	-396.93
Kharaka and Barnes (1973)	-7.65	-398.01

It is expected that the solubility of iron phosphate will vary with varying pH. Twidwell and Dahnke (2001) reported the simulations of Huang (2001) during the precipitation of iron phosphate at 50°C with varying pH (see Figure 2.9). The solubility data obtained with OLI chemical modeling software are shown in APPENDIX A: OLI SIMULATIONS. In both instances, less than 0.6 g/L iron is left in solution. This would represent close to 99% iron removal, if the initial iron concentration was about 45 g/L.

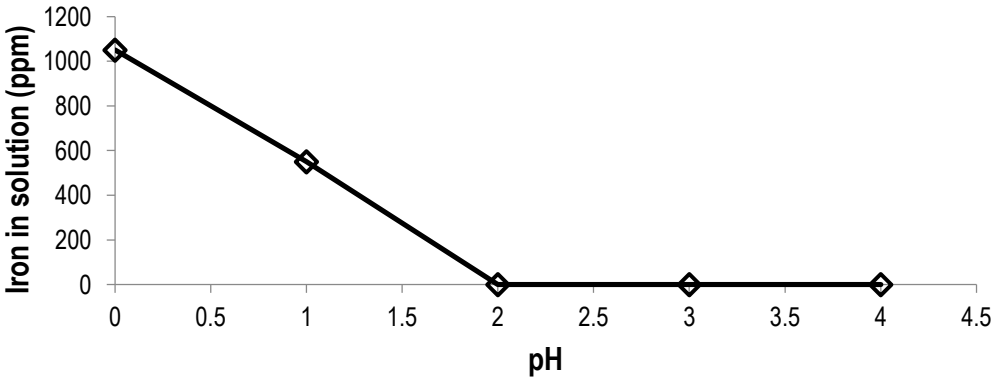

Figure 2.9. $FePO_4$ solubility as a function of pH at 50°C (Source: Huang, 2001)

Phosphate reagent regeneration

Twidwell et al. (1986) reported that complete conversion of ferric phosphate to ferric hydroxide (and therefore regeneration of the phosphate) was observed at moderate temperature and high pH. Unlike the precipitates produced in a conventional hydroxide precipitation process, the ferric hydroxide precipitates produced by the conversion of ferric phosphate filter as easily as ferric phosphate. Furthermore, the precipitates produced in this manner do not contain heavy metals, which present environmental challenges, because of the purity and morphology inherited from the ferric phosphate precipitates (Twidwell et al., 1986).

Twidwell and Dahnke (2001) confirmed the work of Twidwell et al. (1986) and Nordwick (1987) that ferric phosphate could be leached with caustic soda at pH 12 and at a temperature of 50^{o}C (Twidwell and Dahnke, 2001). The conversion of ferric phosphate to ferric hydroxide can be shown in Equation 2.48.

$$FePO_4 + 3NaOH \leftrightarrow Fe(OH)_3 + Na_3PO_4 \qquad 2.48$$

A summary of the rate of conversion of iron phosphate to ferric phosphate at specific pH and temperature is shown in Figure 2.10.

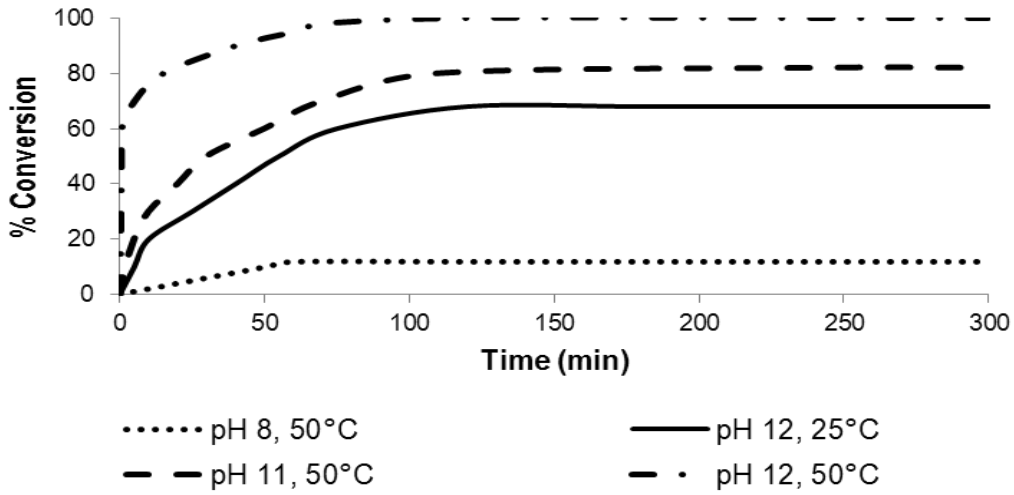

Figure 2.10. Conversion of ferric phosphate to ferric hydroxide at various pH and temperature (after Twidwell et al., 1986)

Preparation of crystalline ferric phosphate

Beck et al. (2011) patented a process for the production of a more pure and crystalline ferric phosphate dihydrate precipitate from an amorphous ferric phosphate dihydrate precipitate. Amorphous ferric phosphate precipitate is reported to be produced when ferric is precipitated in the presence of a phosphate source (Beck et al., 2011).

It should be pointed out that the production of crystalline ferric phosphate dihydrate is specifically intended to be used in the production of lithium batteries and in the field of catalysis. Whether this approach can be used in the removal of iron as a pure iron phosphate in hydrometallurgy processes is a matter of economics (Scaccia et al., 2003).

A two-step crystalline ferric phosphate preparation method was reported by Beck et al. (2011). Step one involved the oxidation of a ferrous salt by a powerful oxidizing agent, such as hydrogen peroxide, in the presence of a soluble phosphate salt at 65^{o}C to form a yellow to white amorphous ferric phosphate precipitate. The amorphous ferric phosphate is then filtered and washed to remove any surface impurities. The second step involved suspending the amorphous ferric phosphate in phosphoric acid at a pH less than 1 and the slurry temperature is adjusted between 80^{o}C to 100^{o}C in order to now crystallize the crystalline ferric phosphate dihydrate.

2.4. Solid-liquid separation

Solid-liquid separation cannot be over emphasised. Three operations typically follow precipitation: solid-liquid separation, washing and at times drying. The amount of mother solution trapped in the filter cake will inevitably affect the precipitate purity and the cake moisture content will affect the dryer load.

2.4.1. Filtration

Filtration of precipitate slurry can be defined in terms of specific volume filtration resistance (r_f) and mass filtration resistance (α_f). In order to get a clear

understanding of the parameters that influence the resistance to filtration, the specific volume filtration resistance and the mass filtration resistance can be defined from the Carman – Kozeny equation (Equation 2.49).

$$\frac{\Delta P}{h_f} = f(\varepsilon_{av})\, s^2 \eta_f U_O \qquad 2.49$$

Where

ΔP is the pressure drop

h_f is the bed height

$f(\varepsilon_{av})$ is the porosity function

s is the specific surface of solids

η_f is the liquid viscosity

U_o is the superficial liquid velocity through the bed

The specific surface of solids, s, is a function of particle size distribution. The specific volume and mass filtration resistance, r_f and α_f, can be defined in terms of average cake porosity, ε_{av}, and effective specific surface, s_{eff}, as shown in Equation 2.50 and Equation 2.51.

$$r_f = \frac{(5(1-\varepsilon_{av})^2 s_{eff}^2)}{\varepsilon_{av}^3} \qquad 2.50$$

$$\alpha_f = \frac{r_f}{(\rho_s(1-\varepsilon_{av}))} \qquad 2.51$$

Since the specific surface area, s, is inversely proportional to the average particle size, d_p, Equation 2.50 can be expressed as shown in Equation 2.52, where k is a constant.

$$r_f = \frac{5(1-\varepsilon_{av})^2}{k d_p^2 \varepsilon_{av}^3} \qquad 2.52$$

If we define $k_f = \frac{5(1-\varepsilon_{av})^2}{k\varepsilon_{av}^3}$

$$r_f = \frac{k_f}{d_p^2} \qquad 2.53$$

(Sohnel and Garside, 1992)

It is therefore mathematically clear that smaller particles will have higher filtration resistance than larger particles. Smaller particles are synonymous with high supersaturation as a result of fast nucleation rates as discussed in Section 2.3.1.4.

2.4.2. Sedimentation

Sedimentation is one of the widely used methods of solid-liquid separation in hydrometallurgical processes. Sedimentation is the separation of liquid and solids by gravitational settling of solids for the purposes of either *clarification* or *thickening*. It is ideally desired that the solid particles settle to the bottom as fast as possible, making a clear interface between the solid and the liquid phase (Koo, 2009).

Sedimentation is affected by a number of suspension and emulsion properties and chief among them are particle size and shape, particle surface characteristics, permeability and porosity of the suspension (Burger and Wendland, 2001). The key performance indicator for a settling unit is the settling velocity of the solid phase (Salas et al., 1993).

According to Kynch (1952), neglecting the effect of the wall and the variations in the horizontal distribution of particles, it can be assumed that the settling velocity of particles is mainly dependent on the localized properties of the suspension (Kynch, 1952).

According to Stokes formula, the settling velocity of a particle in an unbounded fluid is given by Equation 2.54 (Richardson et al., 2002).

$$U_\infty = \frac{(\rho_S - \rho_f)gd^2}{(18\eta_f)} \qquad 2.54$$

Where,

U_∞ is the settling velocity of the spherical particle

d^2 is the sphere diameter

ρ_S is the sphere density

ρ_f is the unbounded fluid density

η_f is the dynamic viscosity of the fluid

g is the acceleration of gravity

From Equation 2.54, it can be deduced that smaller particles will settle slower than larger ones. The magnitude of the particle size distribution will therefore determine the clarity of the liquid phase with respect to time. This is the case because if the particle size distribution is too large, the range of individual particle velocities will also be large such that a cloudy suspension is likely to be obtained (Betancourt et al., 2013).

A method of improving the settling rate of particles is known as flocculation. Betancourt et al. (2013) reported that flocculation aggregates smaller particles into larger ones (flocs) and thereby, according to Stokes Equation 2.54, increasing the particle settling velocity.

2.5. Iron tolerance in downstream processes

The choice of copper and nickel purification process largely depends on the final product desired. In this section, copper and nickel purification processes are discussed in relation to typical iron tolerance for these processes

2.5.1. Solvent extraction and electrowinning

Iron is generally detrimental to the solvent extraction process of nickel and copper because it causes operational challenges such as the formation of crud and the cyclic oxidation and reduction of iron(II) and iron(III). The effective organic extractant in the solvent extraction circuit is lost to the crud. This then leads to frequent topping-up of the organic inventory to avoid poor metal extraction. Cyclic oxidation and reduction of iron causes drops in the tankhouse current efficiency by consuming some of the electric current intended for the cathode growth. Furthermore, iron causes corrosion of the cathode loops giving rise to significant cathode drops during harvesting. This may lead to serious cell furniture damages and cathode physical defects (Crundwell et al., 2011a; Cruz et al., 1980; Hudson, 1982; Ritcey, 1980).

Complete elimination of iron from leach solutions is a challenging matter. Solvent extraction has been reported to selectively extract value metals over iron. The selectivity of value metal(s) over iron(III) is dependent on the choice of the extractant, the extraction pH and organic to aqueous ratio and contact time. Equilibrium discrimination is achieved by control of the extraction pH and the organic to aqueous ratio. Kinetic discrimination is achieved by controlling the organic to aqueous contact time. Iron(III), rather than iron(II), is the concern when it comes to co-extraction during the extraction of copper and nickel (Lu and Dreisinger, 2013; Ritcey, 2006).

Lu and Dreisinger (2013) reported successful extraction of copper from a high chloride media at a pH of 0.5, by solvent extraction. The objective of the study was to build equilibrium data for chloride media solvent extraction of copper from a solution contaminated with iron (as much as 9 g/L). Copper was extracted in the chloride media and stripped with sulphuric acid in order to conduct electrowinning in the conventional sulphate media. Four extractants were tested: LIX84-1, LIX612N-LV, XI-04003, LIX984N. The aqueous-organic ratios (A/O) investigated included; 2:1, 1:1, 1:2, 1:4 and 1:8. The Cu/Fe increased with

increase in A/O ratio for all extractants investigated. At pH 0.5, 40^{o}C and A/O ratio of 2:1, XI-04003 resulted in the highest Cu/Fe of 295 in the loaded organic.

Nickel solvent extraction is normally conducted within pH range of 5 – 6.5. In this pH range, almost all of the iron(III) is expected to have been precipitated during neutralization stage. It is therefore common practice for solvent extraction plants to be incorporated with clarifier vessels just before extraction streams (Crundwell et al., 2011a).

Coll et al. (2012) investigated the extraction and separation of nickel and cobalt from a chloride solution using synergistic reagent. The synergistic reagent was a combination of ionic liquid extractant tertiary alkyl, primary ammonium and phosphinate. The equilibrium pH was reported to be 6.3. About 89% of nickel was extracted in a 4-stage extraction setup (Coll et al., 2012).

2.5.2. Cementation

In order to capture the iron that is introduced into the system during copper cementation using iron metal, the cementation process makes sense to be conducted prior to iron removal stage. This sequence is also likely to mitigate the impact of co-precipitation of copper during the precipitation of iron.

The cementation pH has been reported by several researchers to be optimized within the pH range of 1.5 – 2.5 and the operating temperature of 40^{o}C - 60°C. More than 98% copper recovery has been reported for a number of cementation processes (Amin et al., 2014; Djoudi et al., 2007; Guerra and Dreisinger, 1999; Habashi, 1999; Stefanowicz et al., 1997).

$$Cu^{2+} + Fe \rightarrow Fe^{2+} + Cu \qquad 2.55$$

Once Equation 2.55 is at equilibrium, the Nernst equation (Equation 2.56) is then satisfied.

$$\Phi_{Cu} + \left(\frac{2.303RT}{nF}\right)\log\alpha\left(Cu^{2+}\right) = \Phi_{Fe} + \left(\frac{2.303RT}{nF}\right)\log\alpha\left(Fe^{2+}\right) \qquad 2.56$$

Φ is the standard equilibrium potential and α is the activity for the respective cations (Shen et al., 2008).

2.5.3. Sulphide precipitation

Copper sulphide can be precipitated prior to the precipitation of nickel because of its lower solubility. The suggested precipitation temperature is around 60°C. The pressure is normally less than 0.1 bar. The pH range is 3 - 3.4. H_2S gas is generally the precipitating agent. Copper sulphide precipitation has been reported to achieve over 92% recovery of copper. The typical iron composition in the copper sulphide precipitation feed is about 0.6 g/L (Crundwell et al., 2011; Kyle, 2010; Lewis and van Hille, 2006).

Nickel sulphide precipitation is usually conducted at elevated temperature and pressure in autoclaves. The operating temperature has been reported around 100^oC - 120^oC. The H_2S gas pressure is said to be optimized between 2 and 10 bar, resulting in a recovery of about 99% nickel. The solution pH is reported in the range of 3 - 3.5. Kyle (2010) reported that one of the advantages of nickel sulphide precipitation is the selectivity of nickel over impurities such as iron, aluminium, chromium. Crundwell et al. (2011) suggested that aluminium, chromium, magnesium, calcium and manganese are not precipitated at the conditions at which nickel precipitates. Almost all the iron (together with aluminum, chromium and silicon) is precipitated out of solution by the addition of limestone during the neutralization process to raise the pH to 3 – 3.5. The typical composition of iron in the sulphide precipitation feed is about 0.6 g/L (Crundwell et al., 2011; Kyle, 2010; Lewis, 2010).

2.6. Chapter summary

Iron removal in hydrometallurgical solutions is mostly achieved by the precipitation of ferric iron. Oxidation of ferrous iron by molecular oxygen at atmospheric pressure involves the transfer of oxygen from gas to liquid phase and the chemical oxidation of iron(II) by dissolved oxygen. In chloride systems, it has been reported that acid concentration influences the rate of iron(II) oxidation.

The ratio of HCl to iron(II) has been said to affect the oxidation kinetics. Rapid oxidation of iron(II) has been reported at HCl to iron(II) ratio above 5.6. It has been suggested that iron(II) forms a complex with associated HCl which is more readily oxidized. This mechanism of iron(II) oxidation is referred to as the modified Haber-Weiss mechanism. The presence of copper catalyzes iron(II) oxidation. It has been suggested that cupric copper gains an electron from ferrous iron to produce ferric iron and cuprous copper. It was the objective of this study to determine the effect of HCl and copper concentration on iron(II) oxidation.

Precipitation involves 2 fundamental steps: nucleation and growth. Growth controlled precipitation results in better quality precipitates. Supersaturation is the driving force of precipitation. Lower supersaturation is desirable for the production of high quality precipitates (relatively pure and ease solid–liquid separation). In hydrometallurgical solutions, supersaturation can be mainly controlled by carefully controlling the solution pH and temperature.

A summary comparison of the iron precipitation processes is shown in Table 2.4. The traditional iron removal processes include: the jarosite process, the goethite process and the hematite process. Of these 3 processes, the hematite process has been reported to produce better quality precipitates. Hematite precipitates are easily filtered and its co-precipitation of other metals, such as nickel and copper, is lower than jarosite and goethite precipitates. It has been reported that seeded hematite precipitation is possible at a temperature below 100^{o}C. Unlike the environmental challenges that jarosite and goethite precipitates pose, hematite precipitates are useful in the iron and steel industry. Iron phosphate precipitation has been reported, in mostly patented literature, to produce high purity precipitates that are easily filterable. Phosphate precipitation has been suggested to be highly selective of trivalent metals from divalent metals rendering it less likely to co-precipitate nickel and copper during ferric phosphate precipitation. Iron phosphate can be precipitated in the presence of a phosphate

source at temperatures as low as 40^{o}C. Iron phosphate has been reported to be a useful precipitate in the agriculture industry as a source of phosphate.

It was therefore the objective of this study to experimentally compare the traditionally superior hematite precipitation with iron phosphate precipitation in terms of the extent of iron removal, the co-precipitation of nickel and copper and solid-liquid separation.

Table 2.4. Summary comparison of the various hydrometallurgical iron precipitation processes discussed in Section 2.3.2

	Iron precipitation processes			
	Jarosite	**Goethite (akaganeite)**	**Hematite (seeded)**	**Iron phosphate**
Filterability	Easily filterable	Poor - as low as 2 mL/min	Good - above 12.5 mL/min	Easily filterable
Operating temperature	95 - 100^{o}C	70 - 90^{o}C	60^{o}C and above	40 - 80^{o}C
Operating pH	about 1.5 - 2	about 2 - 3.5	about 1 and above	about 2
Iron removal from solution	pH 1.8 - close to 99%	pH 3 - almost complete	pH 1 - almost complete	pH 2 - 99%
Incorporation of Ni and Cu	Relatively medium	Relatively high	Relatively low	Relatively low
Precipitate handling	Environmental concern	Environmental concern	Useful in iron and steel industry	Useful as a source of phosphate
Required cations	Na^{+}, K^{+} or NH_4^{+}	Non	Non	Non
Required anions	SO_4^{2-}	Non	Non	PO_4^{3-}

3. EXPERIMENTAL

As discussed in Section 2, oxidation of iron(II) precedes precipitation of iron(III). Precipitation is then followed by solid-liquid separation. In this study, experiments were divided into 3 sets: oxidation experiments, precipitation experiments and solid-liquid separation experiments. Each of the 3 experimental sets was subdivided into a series of interactive experiments, with specific objectives.

3.1. Oxidation of iron(II) chloride

3.1.1. Materials

Synthetic leach solutions, containing about 45 g/L iron, 3 g/L nickel and 3 g/L (at instances 0.3 g/L) copper, were prepared from reagent grade chemicals and deionized water. The synthetic leach solution preparation calculations are documented in APPENDIX B: LEACH SOLUTION PREPARATION. A list of these chemicals is shown in Table 3.1.

Table 3.1. Reagent grade chemicals used in oxidation experiments

Name	Source	Physical form
Iron chloride tetra hydrate	Sigma Aldrich ™	Powder
Copper chloride	Sigma Aldrich ™	Powder
Nickel chloride hexa hydrate	Sigma Aldrich ™	Powder
Hydrochloric acid	Sigma Aldrich ™	Solution
Phosphoric acid	KIMIX	Solution
Potassium dichromate	KIMIX	Solution
Sodium diphenylamine	KIMIX	Solution
Sodium chloride	Merck .N.T	Powder

3.1.2. Methodology

The scope of the oxidation experiments was limited to the investigation of the chemical oxidation of iron(II) by dissolved oxygen in an agitated reactor. It has been suggested in Section 2.2 that the rate and mechanism of oxidation by dissolved oxygen is a strong function of the concentration of hydrogen and chloride ions. These ions can be associated or dissociated. This research therefore sought to experimentally investigate suitable concentrations of hydrogen and chloride ions, associated or dissociated, that could yield acceptable oxidation rates.

Section 2.2 also proposed that the presence of copper has a catalytic effect on the oxidation of iron(II). In the context of the study, it was important to investigate whether a lower copper concentration would have a detrimental effect on oxidation.

3.1.2.1. Experimental design

Oxidation experiments were conducted according to a full factorial experimental design. The oxidation experiments were divided into 5 categories: factor screening, optimization runs, confirmatory runs, discovery runs and robustness runs. The experimental categories and the independent variables investigated are shown in Table 3.2. As discussed in Section 2.2, the HCl and copper concentrations were reported to affect the rate of iron(II) oxidation. For a solution containing about 45 g/L iron(II), oxidation was reported to be rapid when the HCl concentration was above 4 M. It was desired to observe if a lower acid concentration would have a negative effect on the extent and rate on iron(II) oxidation. 2 M HCl concentration was thus included as a screening value. The copper concentrations of the leach solutions to be treated were about 3 g/L. It was decided to investigate whether a reduction in copper concentration would be detrimental to the oxidation rate. Copper concentration of 0.3 g/L was therefore adopted as a screening value. It was desired to investigate oxidation at a temperature below 100^{o}C; therefore 50^{o}C and 80^{o}C were adopted as screening values. Based on the results of screening experiments, optimization variable

values were selected. Based on optimization experiments and confirmatory runs, discovery experiments were conducted to investigate the individual effects of hydrogen and chloride ions at various concentrations. Robust experiments were designed on the basis of discovery experimental results.

Table 3.2. Experimental planning and variables investigated in the oxidation experiments

Category	Variables	Variable values
Screening	HCl molarity (M)	2, 4
	Cu concentration (g/L)	0.3, 3
	Solution temperature (^{o}C)	50, 80
Optimization	HCl molarity (M)	4, 4.6
	Cu concentration (g/L)	0.3, 3
	Solution temperature (^{o}C)	80
Confirmatory	HCl molarity (M)	2, 4, 4.6,
	Cu concentration (g/L)	3
	Solution temperature (^{o}C)	80
Discovery	H^{+} molarity (M)	1
	Cl^{-} molarity (M)	2, 3, 4, 4.6
	Cu concentration (g/L)	3
	Solution temperature (^{o}C)	80
Robustness	H^{+} molarity (M)	1
	Cl^{-} molarity (M)	4.6
	Cu concentration (g/L)	3
	Solution temperature (^{o}C)	80
	Semi continuous oxidation precipitation	-

3.1.2.2. Experimental setup

Figure 3.1 shows the diagram of the oxidation experimental setup. The setup consisted of a 1.6 L capacity custom made reactor. The reactor was equipped

with a reflux system to condense the vapours back into the reactor chamber. A heating plate, equipped with temperature feedback control, was used to maintain the desired reaction temperature within accuracy of ± 2°C.

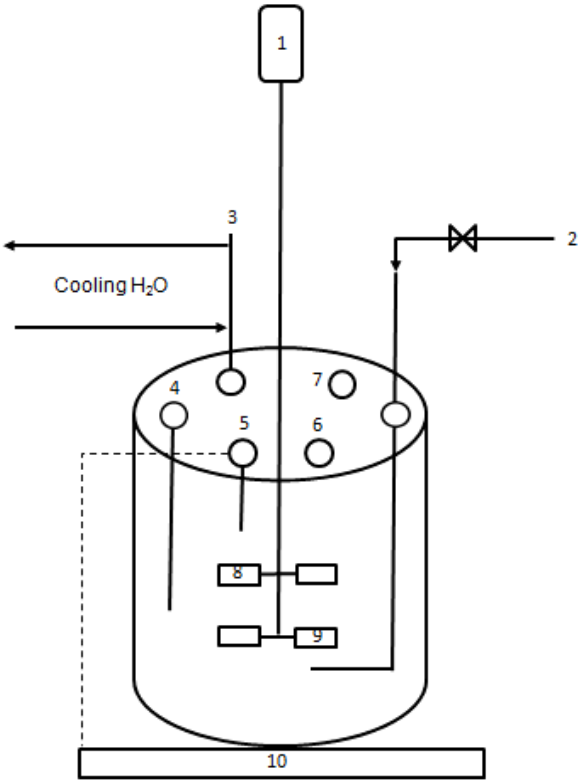

Number	Description
1	Mechanical agitation system
2	Oxygen flow meter
3	Reflux unit
4	pH meter
5	Thermometer
6	Reagent addition point
7	Sampling point
8	Radial impeller
9	Axial impeller
10	Heating plate

Figure 3.1. Diagram of the oxidation experimental setup

The reactor was fitted with an overhead mechanically stirred agitation system. The dimensions of the stirring shaft and gas sparger are shown in Figure 3.2. A custom made dual impeller stirring shaft, coated with Teflon, was used. The dual impellers were axial and radial impellers. The axial impeller was below the radial impeller. The distance between the impellers was 3.5 cm. The radial impeller was 2 cm away from the bottom of the reactor. The diameter of the impellers was 4.5 cm. The sparger was made of a Teflon hollow pipe. The Teflon pipe was positioned 0.5 cm below the axial impeller and 1.7 cm away from the axial impeller. The hollow gas sparger had an effective diameter of 0.5 cm. The sparger was connected to the oxygen cylinder, fitted with a pressure regulator and oxygen flow meter, via a flexible polycarbonate tube (Birch and Ahmed, 1995).

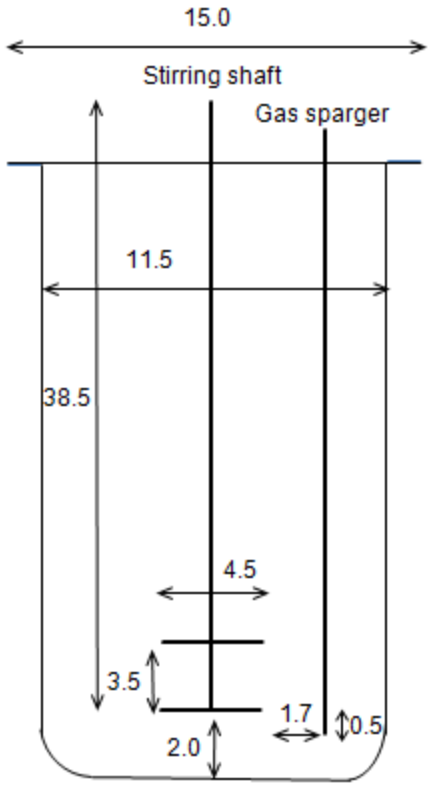

Figure 3.2. 1.6 L capacity reactor showing dimensions (in cm) of the stirring shaft and gas sparger

3.1.2.3. Experimental procedure

About 800 mL of synthetic leach solution, prepared as described in APPENDIX B: LEACH SOLUTION PREPARATION, was fed into the reactor chamber. The reactor was sealed and safely secured with a stainless steel safety clamp. The solution was then agitated at a rate of 600 rpm and heated to a desired temperature. It took about 25 minutes and 35 minutes to attain 50^{o}C and 80^{o}C respectively. At this point, about 5 mL of solution sample was obtained as the base line sample. To avoid evaporation and/or further oxidation, the sample was bottled in a carefully sealed 15 mL test tube bottle and analyzed within 5 h. After obtaining the base line sample, agitation was then increased to 1600 rpm. Almost immediately after increasing agitation, oxygen gas was introduced into the reactor at 2 L/min via the gas sparger. The oxygen pressure was maintained at 1 bar by the oxygen gas cylinder regulator. This point was noted as the starting time for the experimental run. The experimental duration was 300 minutes.

Samples were collected at the following time intervals: 10 minutes, 20 minutes, 30 minutes, 60 minutes, 120 minutes, 180 minutes, 240 minutes, and 300 minutes. The samples were bottled and sealed in 15 mL test tube bottles and analysed within 5 h.

3.1.2.4. Analytical methods

Riveros and Dutrizac (1997) determined the levels of oxidation in the study of iron oxy-hydrolysis by wet chemistry. The iron containing solution was titrated with 0.1 N dichromate and diphenylamine sulphonic acid as the indicator (Riveros and Dutrizac, 1997). Raos et al. (1995), in the study of ferrous oxidation in acidic mineral process effluents, determined the concentration of iron(II) by titration with standard potassium dichromate solution using phenathroline as an indicator (Raos et al., 1995).

In this study, wet chemistry was used to determine the iron(II) present in the solution. The titrant was a 0.0084 M potassium dichromate standard solution. 50 mL of deionized water was added into a 250 mL Erlenmeyer flask and about 5 mL of phosphoric acid was added to mask the iron(III) in solution. 1 mL of the solution sample was then added to the flask using a carefully calibrated standard adjustable pipette. Sodium diphenylamine was used as the indicator to make a purple titration end point. The redox titration equation and calculations are described in APPENDIX C: ANALYSIS OF IRON (II).

3.2. Precipitation from iron(III) chloride

3.2.1. Materials

The leach solutions used in precipitation experiments were prepared as described in APPENDIX B: LEACH SOLUTION PREPARATION and oxidized following the procedure described in Section 3.1.2.3. The conditions at which iron(II) chloride was oxidized are described in Section 4.1. The chemicals used during precipitation experiments are shown in Table 3.3.

.

Table 3.3. Reagent grade chemicals used in precipitation experiments

Name	Source	Physical form
Iron chloride tetra hydrate	Sigma Aldrich ™	Powder
Copper chloride	Sigma Aldrich ™	Powder
Nickel chloride hexa hydrate	Sigma Aldrich ™	Powder
Hydrochloric acid	Sigma Aldrich ™	Solution
Sodium hydroxide	Sigma Aldrich ™	Pellets
Sodium phosphate	Sigma Aldrich ™	Powder
Iron (III) phosphate seed	Sigma Aldrich ™	Powder
Iron (III) oxide seed	Sigma Aldrich ™	Powder

3.2.2. Methodology

It has been proposed in Section 2.3.2 that seeded hematite and iron phosphate precipitation are the most competitive methods of iron removal. These two processes were therefore compared experimentally with the response variables being the degree of iron removal, co-precipitation of nickel and copper and solid liquid separation.

In Section 2.3.1.4, it was suggested that the degree of supersaturation determines the quality of precipitate, i.e. the filterability and purity of precipitate. Precipitation pH, temperature and the manner neutralization is conducted were identified as the preferred methods of controlling supersaturation. In Section 2.3.1.1, it was proposed that metastable phases will precipitate first before stable phases due to the lesser energy needed for metastable phases to be precipitated. This study implicitly investigated suitable reaction times at which more pure and stable phases may be produced.

3.2.2.1. Experimental design

The hematite process and the iron phosphate process were compared at different levels of pH and temperature with and without seeding. Further

experiments that involved the simultaneous oxidation and precipitation were conducted, for both the iron phosphate process and the hematite process.

Statistically designed experiments were conducted to validate the effect of the solution pH, the solution temperature, seeding and retention time on the precipitation of iron(III) and the resulting losses of nickel and copper. Similar to the design of experiments discussed in Section 3.1.2.1, a sequential set of experiments, with specific objectives, was adopted. A summary of the sets of experiments and independent variable levels investigated for both, the hematite process and the iron phosphate process is shown in Table 3.4 and Table 3.5 respectively.

Table 3.4. Experimental planning and variables investigated in the Hematite precipitation experiments

Category	**Variable**	**Variable values**
Screening	Solution pH	1, 2, 3
	Solution temperature (^{o}C)	60, 80, 90
	Seeding (g)	30
Optimization	Solution pH	0, 1
	Solution temperature (^{o}C)	80
	Seeding (g)	0, 30
Confirmatory	Solution pH	1
	Solution temperature (^{o}C)	80
	Seeding (g)	30
Robustness	Solution pH	0
	Solution temperature (^{o}C)	80
	Seeding (g)	30
	Simultaneous oxidation and precipitation	-

Table 3.5. Experimental planning and variables investigated in the iron phosphate precipitation experiments

Category	Variable	Variable values
Screening	Solution pH	1, 2, 3
	Solution temperature (^{o}C)	40, 60, 80
	Seeding (g)	30
Optimization	Solution pH	0, 1
	Solution temperature (^{o}C)	40
	Seeding (g)	0, 30
Confirmatory	Solution pH	1
	Solution temperature (^{o}C)	40
	Seeding (g)	0
Robustness	Solution pH	0
	Solution temperature (^{o}C)	80
	Seeding (g)	30
	Simultaneous oxidation and precipitation	-

Hematite precipitation has been reported to occur at pH 1 and above. The extent of iron removal increases with increase in pH. It is expected that the co-precipitation of nickel and copper would increase with increase in pH, due to relatively higher supersaturation at higher pH values. pH points of 1, 2 and 3 were therefore adopted to be screened. Dutrizac and Riveros (1999) reported precipitation of hematite at temperatures as low as 60^{o}C by seeding (30 g/L hematite seed). The concentration of the hematite phase in the precipitates produced generally increased with increase in temperature. The experimental plan was interactive. Optimization and confirmatory variables were selected based on screening results. While optimization results led to the selection of robust experimental variable points.

Iron phosphate has been reported to precipitate at pH about 2 and temperature around 40^{o}C – 80^{o}C. Similar to hematite precipitation, the extent of iron removal and the co-precipitation of nickel and copper were expected to increase with increase in pH. Although no reports of seeded iron phosphate precipitation were found in literature surveyed during this study, seeding has been reported to generally improve the purity of precipitates produced (Hove et al., 2009). Similar to hematite experiments, iron phosphate series of experiments were interactive and therefore optimization and confirmatory variable points depended on screening results while robust variable points depended on optimization results.

3.2.2.2. Experimental setup

The experimental setup used during precipitation experiments was the same as that described in Section 3.1.2.2, but with the inclusion of an automatic titration system (Thermo Scientific alpha pH 560 controller). Figure 3.3 shows the diagram of the precipitation experimental setup.

The Thermo Scientific alpha pH 560 controller had an auto temperature compensation unit that accounted for the temperature fluctuations in reading the solution pH. A desired pH set point controlled the relay contacts that in turn controlled the valve to the vessel holding the base, sodium hydroxide. The unit had provisions to control the hysteresis pH values to prevent rapid relay contact switching if the pH reading was fluctuating near the pH set point. Hysteresis pH value of 0.05 was configured.

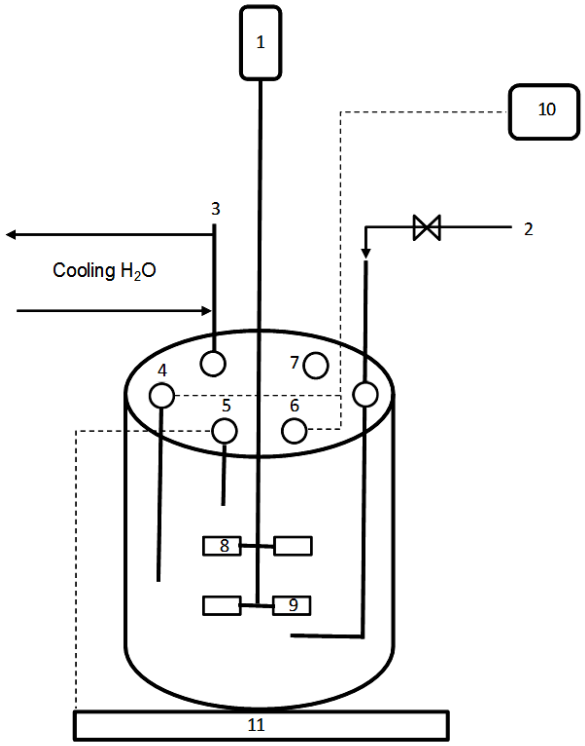

Number	Description
1	Mechanical agitation system
2	Oxygen flow meter
3	Reflux unit
4	pH meter
5	Thermometer
6	Reagent addition point
7	Sampling point
8	Radial impeller
9	Axial impeller
10	pH controller
11	Heating plate

Figure 3.3. Diagram of the precipitation experimental setup

3.2.2.3. Experimental procedure

Upon oxidation of over 98% iron(II) chloride, and verified by titration analysis of iron(II), the solution in the reactor was left to cool to about 40^{o}C. Cooling took approximately 60 minutes. As the solution was cooling, the pH meter and the auto titrator were calibrated at 2 points; pH 4 and pH 7. A buffer solution, pH 1.68, was then read to ensure accuracy of pH meter at lower values. After cooling and calibration of the pH meter, the solution was then agitated at 600 rpm using the mechanically stirred agitation system. The solution acidity was neutralized with 15.5 M sodium hydroxide by means of auto titration to a pH of 0. To raise the pH from 0 to the desired pH, a 1 M sodium hydroxide standard solution was used. The solution temperature was maintained by a temperature controlled heating plate fitted with a temperature probe. A mercury thermometer was placed in the bath occasionally to verify the heating plate temperature probe reading. The temperature readings were within a difference of $\pm 2^{o}$C. For seeded experimental runs conducted at pH 1 and above, 30 g/L seeds were added at pH

0.5. For seeded experimental runs conducted at pH below 1, 30 g/L seeds were added when the pH was just above 0. Stoichiometric amounts of sodium phosphate were then added in the case of the iron phosphate precipitation experiments. This point was noted as the starting time of the experimental run. The total volume of the slurry in the reactor was measure at the end of each experimental run for the purposes of mass balance calculations. Solution samples were obtained every 10 minutes for the first 30 minutes and then at 30 minutes intervals for the other duration of the experimental run. The solution samples were obtained by filtering about 10 mL of slurry using 0.45 µm syringe filters. The samples were then carefully sealed and stored in 15 mL test tube bottles.

3.2.2.4. Solid sampling

About 200 mL of slurry was filtered on a 0.45 µm filter paper under vacuum pressure of about -55 kPa. During filtration, the precipitates were washed with about 200 mL of deionised water and then left to dry in a laboratory scale oven at 40^{o}C for a duration of 20 h. The precipitates were then sampled using the Coning and Quartering method.

The dry precipitates were placed on a clean filter paper such that they formed a cone pile. The cone piles were then flattened to about a quarter of the original height and then divided into 4 quarters. Two of the opposite quarters were then mixed together, repeating the described procedure. From the second mixing, samples were collected and stored in sample containers.

3.2.2.5. Analytical methods

The solution samples were analyzed using inductively coupled plasma optical emission spectrometry (ICP-OES). The concentrations of nickel, copper, iron, sodium and phosphorus were analyzed by this method.

X-ray fluorescence (XRF) analysis was used to determine the chemical composition of the precipitates. XRF was able to detect minor elements in the precipitates to a detection limit of 1 ppm.

X-ray powder diffraction (XRD) can conclusively be used to qualitatively and quantitatively identify the crystalline phases present in a material and also give an indication of the degree of amorphousness of the material (Schwertmann and Cornell, 2000). In this study, XRD analyses of the precipitates produced was used to identify and quantify the crystalline phases. XRD analyses also gave a qualitative indication of the degree of amorphousness of some of the precipitates produced.

Scanning electron microscopy (SEM) can be singularly used as an effective tool to study and deduce hydrometallurgical reaction products. This is made possible by utilizing its energy dispersive X-ray, backscattered electron imaging and X-ray mapping. Specifically, X-ray mapping can give clear and exact positions of elemental composition of the material and thereby suggesting the compounds present at specific sites on the sample (Chen and Dutrizac, 1990). In this study, to determine the possible compounds produced during precipitation, X-ray mapping were used. The X-ray maps were also used to get an indication of the distribution of the nickel and copper loses in the precipitate samples.

In order to understand the distribution of primary particles, aggregates and agglomerates, and therefore get a better understanding of solid–liquid separation (as discussed in Section 2.4), particle size distribution (PSD) was conducted using the Saturn DigiSizer 5200. Saturn DigiSizer 5200 uses a laser with more than a million detector elements that measures primary particle sizes, de-agglomerated and suspended in water. The detectors measure the intensity of light scattered by the particles in a pattern depending on the particle sizes.

3.3. Solid–liquid separation

Solid-liquid separation experiments were performed on ‘as received’ slurries in order to relate the precipitation conditions to the solid-liquid separation rates.

3.3.1. Filtration tests

At the end of each precipitation experiment, the slurry was filtered under a vacuum pressure of -55 to -60kPa. The experimental setup is shown in Figure 3.4.

A Buchner flask was fitted with a 0.45 µm filter paper on which, 200 mL of slurry was poured and simultaneously the stopwatch was started. The stopwatch was stopped when no solution drops were visible inside the flask. The filtration rate was recorded as L/min.

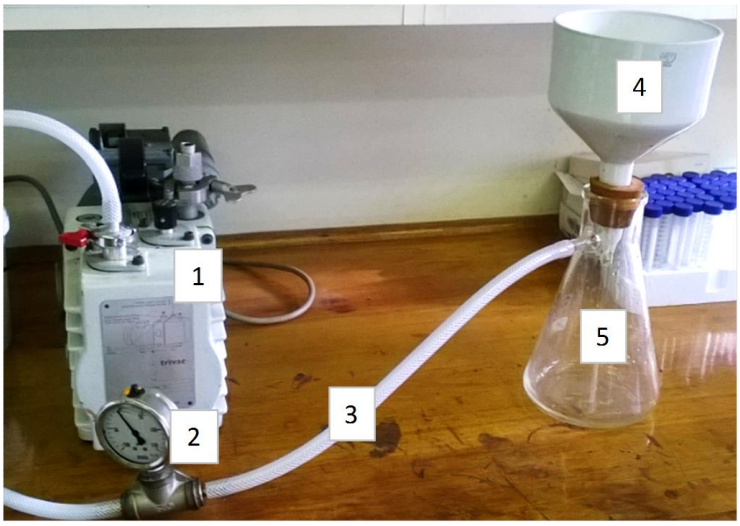

Number	Description
1	Vacuum pump
2	Vacuum meter
3	Vacuum line
4	Buckner funnel
5	Filtration flask

Figure 3.4. Picture of the filtration experimental setup

3.3.2. Sedimentation tests

Clearly marked, filtered and dried precipitates were mixed with deionized water to prepare suspensions that contained approximately 45 g/L iron in solids. For flocculated experiments, a dosage of 2 mL/L of 0.014 M aluminium sulphate (alum) was used at respective precipitation pH points.

The slurries were placed in 1 L glass cylinders. To investigate hindered settling rate of the suspended solids by gravity, a video camera was used to record the solid-liquid interface change with time. At the start of each experiment, the suspension was well mixed to attain homogeneity and then placed on a flat surface against a black background. At this point, the video camera was set to record. Pictures of settling experimental setup are shown in Figure 3.5.

The settling video was converted to multiple split second images and processed in MATLAB interface tracking tool to obtain the graphs depicting solid-liquid interface changes with time.

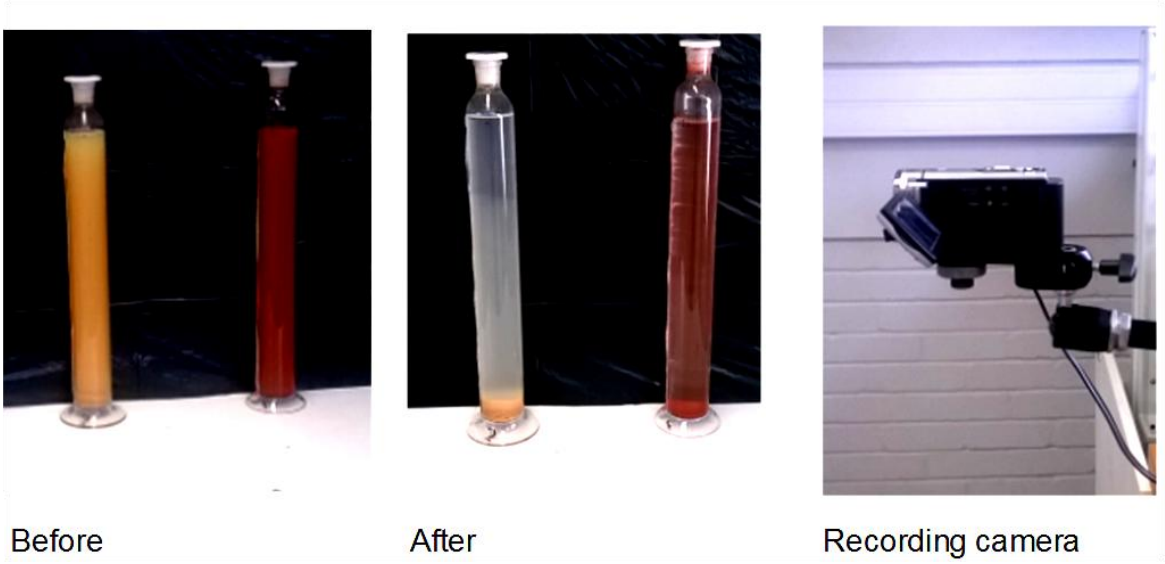

Figure 3.5. Pictures of the sedimentation experimental setup

4. RESULTS AND DISCUSSION

4.1. Oxidation of iron(II) chloride

4.1.1. Screening of [HCl], [Cu] and temperature

Figure 4.1 displays average results obtained during the experimental screening of the effect of [HCl], temperature and Cu concentration. The base solution contained about 45 g/L iron(II) and 3 g/L nickel. The [HCl] was varied at 4 M and 2 M, temperature at 80^{o}C and 50^{o}C while Cu concentration was varied at 3 g/L and 0.3 g/L. Experimental results, and repeat results, are documented in APPENDIX E: EXPERIMENTAL DATA, Figure E 13. The error bars represents the deviation of experimental data points from the calculated average points. The deviation of experimental data points from the calculated average points are within the range of ±2%.

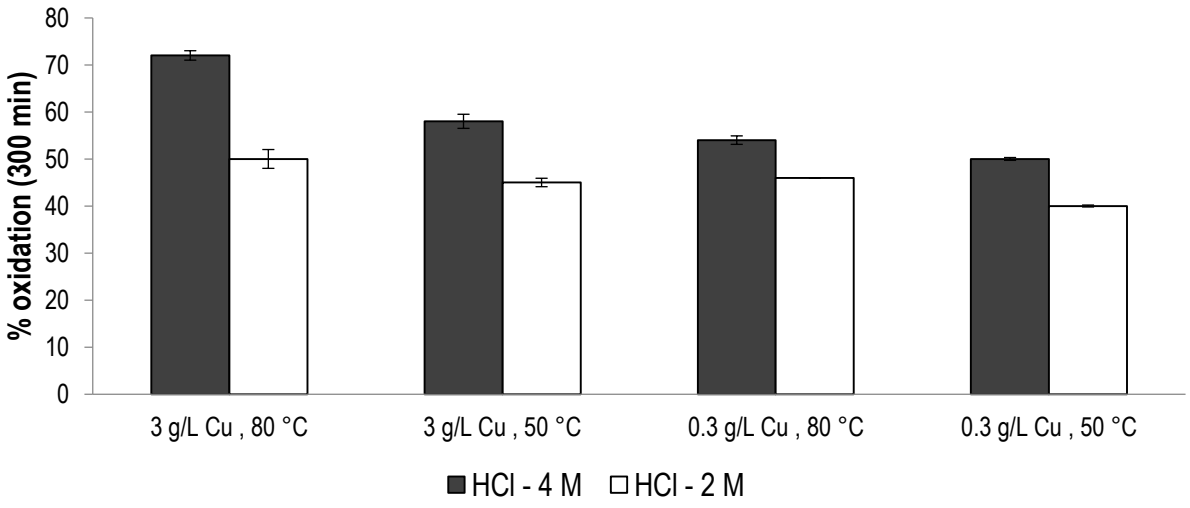

Figure 4.1. Oxidation of iron(II) after 300 minutes at 4M and 2 M [HCl] with varying Cu concentration and temperature

The iron(III) yield increased with increase in [HCl], temperature and Cu concentration at all points investigated. Although it was known from literature that oxidation would increase with increase in all the 3 factors investigated, the extent of oxidation for a given combination of variables was not known prior to the

screening tests. Analysis of variance (ANOVA) was conducted to quantify the effect of variables on the extent of oxidation after 300 minutes of reaction time. Table 4.1 shows the analysis of variance. It can be noted, from the p-values and sum of squares, that the order of significance of the variables was; HCl, Cu and temperature. The Model F-value of 18.23 suggests that the model is significant. There is only 0.01% chance that the F-value is due to noise.

Table 4.1. Analysis of variance (ANOVA) table

	p-value	**F-value**	**Sum of Squares**
Model	0.0001	35.39	1232.60
HCl	0.0001	61.40	712.89
Cu	0.0002	26.53	308.00
Temperature	0.0011	18.23	211.70
Residual			139.32

Iwai et al. (1975) investigated the effect of HCl during the oxidation of iron(II) chloride in concentrated HCl solutions (6 M) and reported that the rate of iron(II) oxidation increased with increase in [HCl] and had a complex relationship with the concentration of chloride ions. According to Filippou et al. (2000), although temperature increase from 25^{o}C to 100^{o}C reduces the solubility of oxygen, increase in temperature improves the kinetics of the chemical oxidation with dissolved oxygen. It is not clear at this point why the effect of temperature was more significant at higher copper concentrations than at lower copper concentrations. Stumm and Fred (1961) suggested that copper catalyses the iron oxidation process by itself gaining an electron in the presence of iron(II) and easily losing the electron in the presence of oxygen.

Figure 4.2 shows the average oxidation rate of experiments conducted at 4 M [HCl], 80^{o}C and 3 g/L Cu concentration. About 72% oxidation was achieved after 300 minutes.

Rapid oxidation was observed during the first 10 minutes of the oxidation process; however, the process appeared to slow down with time. A similar oxidation profile was observed for the 2 M [HCl] runs, as will be seen in Figure 4.4.

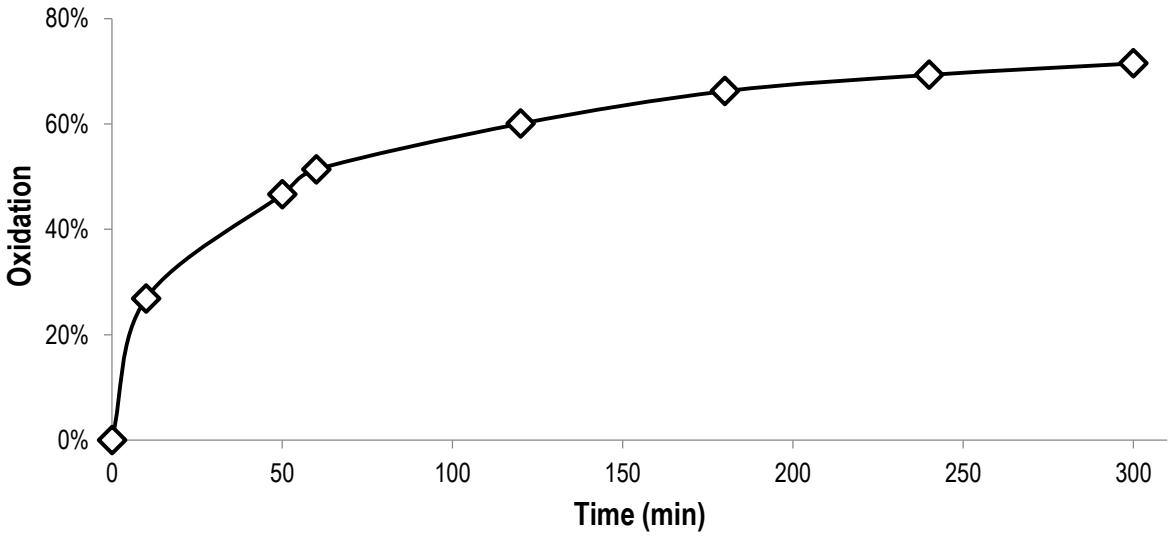

Figure 4.2. Oxidation rate of iron(II) at 80°C, 3 g/L Cu concentration and 4 M [HCl]

4.1.2. Optimization of [HCl] and [Cu]

Based on screening results summarized in Section 4.1.1, further tests were conducted in an attempt to completely oxidize the iron(II) within the shortest feasible time frame. The objective of the project was to investigate oxidation at a temperature below 100°C. Therefore, for further experiments the temperature was maintained at about 80°C, even though screening results suggested increase in oxidation with temperature.

Based on Equation 2.2, about 0.6 to 0.9 moles of HCl per liter of a solution containing about 35 g/L to 50 g/L of iron(II) would be consumed when iron(II) is completely oxidized to iron(III). The free acid in the system was expected to be less than the initial acid concentration by a magnitude equal to the iron(II) oxidized. As can be observed in Figure 4.2, experiments conducted at 4 M HCl, 80°C and 3 g/L copper concentration, the oxidation rate was rapid for the first 10 minutes and there after appeared to slowdown. It was assumed that the

slowdown in oxidation was due to the reduction in HCl concentration as the oxidation process proceeded according to Equation 2.2. It was therefore decided to include 4.6 M [HCl] as a test point so that the acid concentration can be maintained above 4 M during the oxidation process.

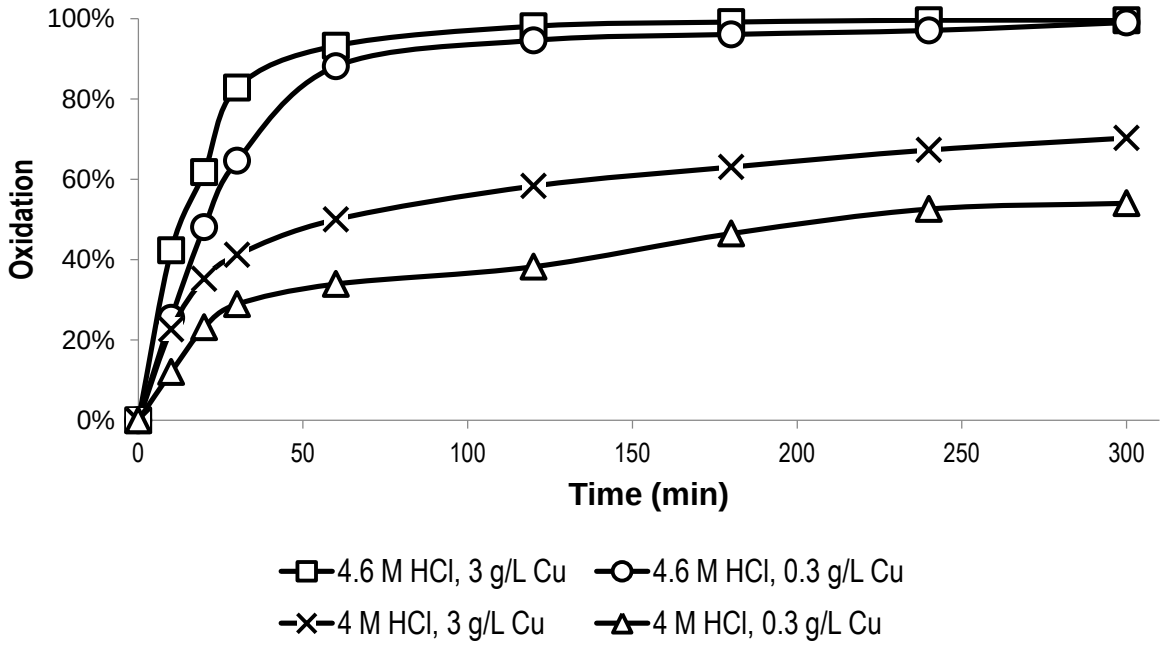

Figure 4.3. Oxidation rate of iron(II) at 80^{o}C as a function of [HCl] and Cu concentration

Figure 4.3 shows results of experiments conducted at 80^{o}C. The Cu concentration was varied at 3 g/L and 0.3 g/L while [HCl] was varied at 4 M and 4.6 M. Repeat experimental results are recorded in APPENDIX E: EXPERIMENTAL DATA, Figure E 14. It was observed that for runs conducted at 4.6 M [HCl] and 3 g/L Cu concentration, oxidation was rapid. Over 98% oxidation was achieved within 120 minutes of the oxidation process. This observation is in line with the results obtained by Awakura et al. (1986), Posner (1953) and Astanina and Rudenko (1971).

Reducing the Cu concentration to 0.3 g/L while maintaining 4.6 M [HCl] yielded only about 94% iron(III) for the same period of time. The catalytic effect of copper has been reported by several other researchers (Awakura and Majima (1986), Colborn and Nicol (1973), George (1954), Posner (1953) and Stumm and

Lee (1961)). Apart from the suggestion that cupric copper accepts an electron from ferrous iron to form cuprous copper and ferric iron, the mechanism by which copper catalyses ferrous oxidation remains unclear. The oxidation of iron(II) by copper(II) is electrochemically favored as shown by the standard reduction potentials ($Cu^{2+} + e \leftrightarrow Cu^{+}$, 0.158 V; $Fe^{3+} + e \leftrightarrow Fe^{2+}$, 0.770 V). It is not clear at this point why the effect of copper concentration appeared to be more significant at lower acid concentrations.

4.1.3. Confirmatory tests - proposed oxidation mechanism

As discussed in Section 2.2.2, Awakura et al. (1986) reported rapid oxidation of 0.72 M iron(II) in [HCl] above 4 M. It was suggested that the oxidation rate increased with a decrease in the $[Fe^{2+}]$ / [HCl] ratio. Posner (1953) suggested the complexation of iron with associated HCl was a key step in the rapid oxidation of iron(II). It was reported that unless iron formed an active complex with the acid, any oxidized iron(II) would easily be reduced back to iron(II).The modified Haber-Weiss mechanism, Equation 2.15 to Equation 2.19, was the proposed mechanism of oxidation.

Confirmatory experiments were conducted at 80^{o}C and 3 g/L Cu concentration with varying [HCl]: 2 M, 4 M and 4.6 M. Figure 4.4 shows the oxidation rates obtained from these runs. Repeat experimental results are documented in APPENDIX E: EXPERIMENTAL DATA, Figure E 15. As expected, the rate of oxidation increased with increase in the [HCl].

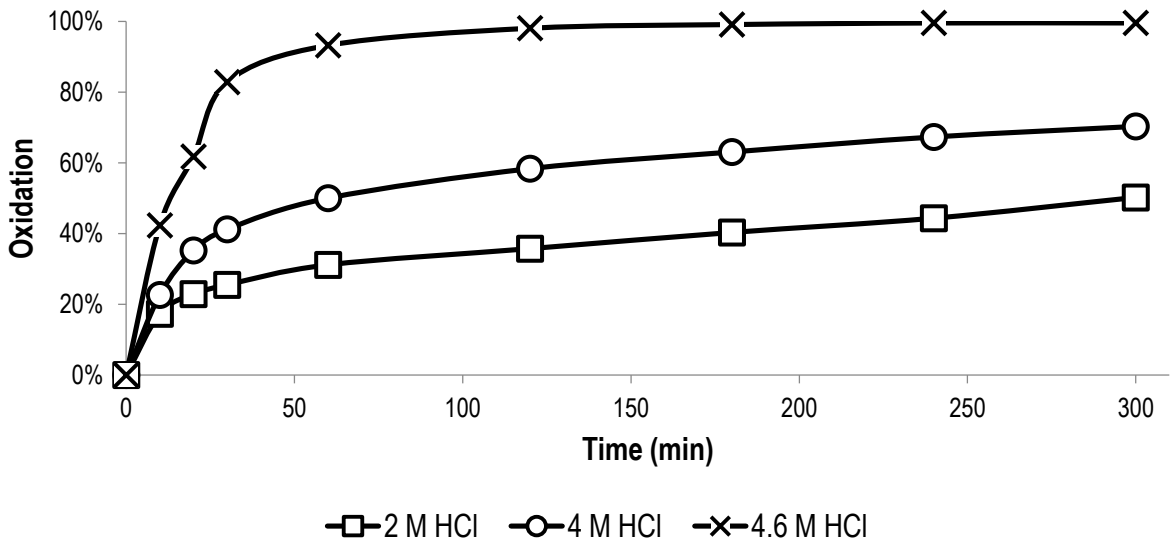

Figure 4.4. Oxidation rate of iron(II) at 80^{o}C and 3 g/L Cu concentration as a function of [HCl]

Based on the respective [HCl], equilibrium associated and dissociated [HCl] were calculated. The calculations are documented in APPENDIX D: ASSOCIATED AND DISSOCIATED [HCl]. Tagirov et al. (1997), in their study of the thermodynamic properties of HCl, documented dissociation constants of HCl as a function of temperature and pressure (Tagirov et al., 1997). The logarithms of HCl dissociated constants at atmospheric pressure as a function of temperature are shown in Figure 4.5. Table 4.2 shows the calculated associated and dissociated [HCl] at equilibrium.

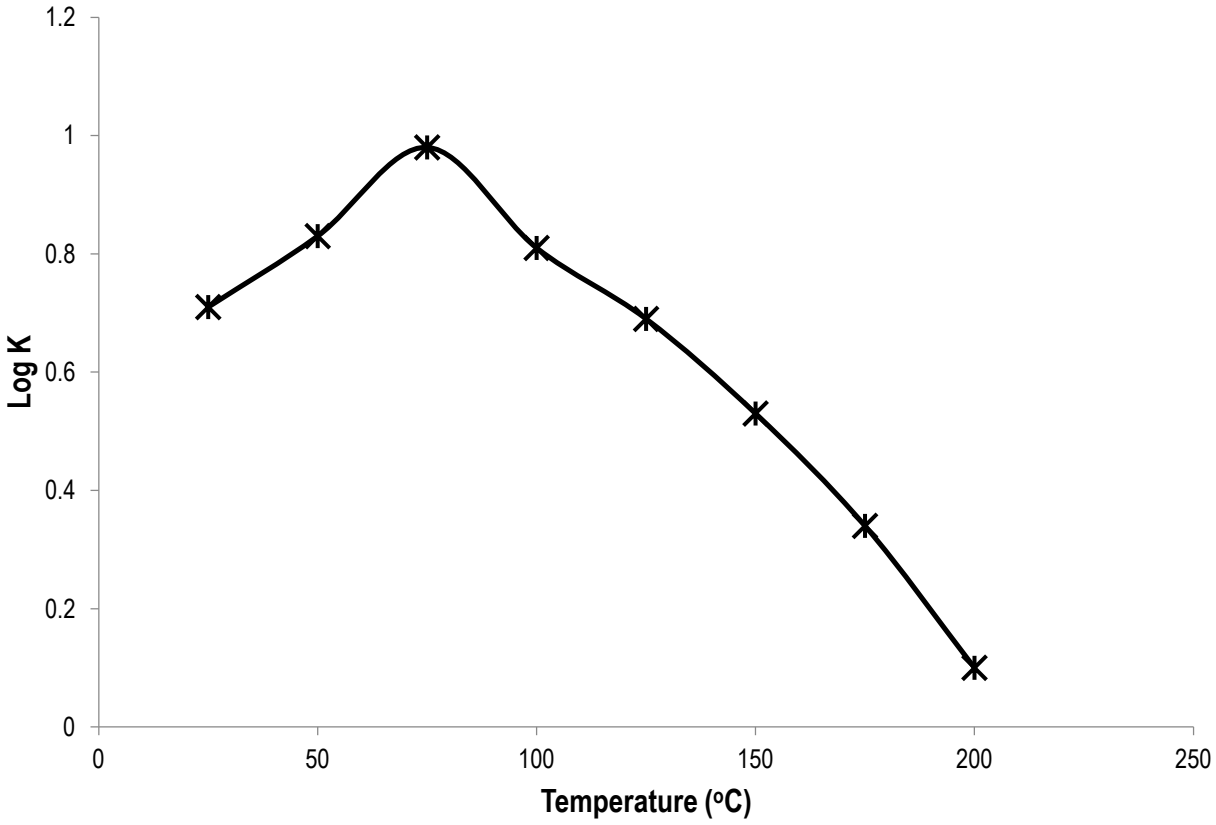

Figure 4.5. Plot of HCl Logarithm dissociation constants (K), at atmospheric pressure, as a function of temperature (after Tagirov et al., 1997)

Table 4.2. Calculated equilibrium associated and dissociated [HCl] with respective contained [HCl]

HCl (M)	Associated HCl (M) at equilibrium	Dissociated HCl (M) at equilibrium
2	0.35	1.65
3	0.67	2.33
4	1.08	2.92
4.6	1.34	3.26

Figure 4.6 shows a plot of associated [HCl] as a function of the [HCl]. On the same plot, oxidation of iron(II), at 80^{o}C and 3 g/L Cu, after 120 minutes is plotted as a function of the [HCl].

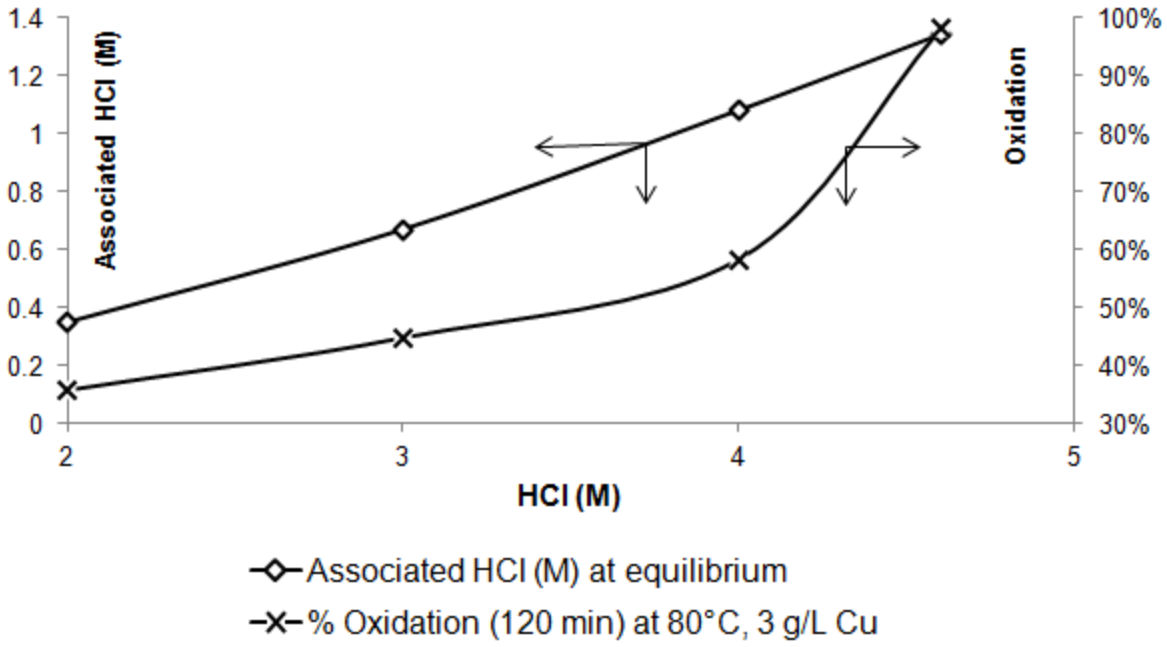

Figure 4.6. Plots of associated [HCl] and oxidation of iron(II) after 120 min, as a function of total [HCl]

Both associated [HCl] and iron(II) oxidation increased with increase in [HCl]. It can be noted that above 4 M [HCl], oxidation appears rapid. The amount of associated [HCl] above 4 M [HCl] is above 1 M. For a solution containing about 0.9 M iron, the stoichiometric requirement of associated [HCl] for complete complexation is above 0.9 M. It was observed from this study that for rapid oxidation of about 0.9 M iron(II), the ratio of associated [HCl] to $[Fe^{2+}]$ should be above 1.08. Equation 2.20 further implies that the rate of oxidation of iron(II) increases with increase in the $HFe^{2+}Cl$ complex.

4.1.4. Discovery tests - effect of chloride ion addition

Awakura (1984) suggested that chloride ions may have been the significant species in the oxidation of iron(II) in HCl systems as chlorine is a well established oxidizing agent.

Experiments were conducted at 80^{o}C, 3 g/L Cu concentration and 1 M [HCl] with the addition of various amounts of chloride ions in the form of NaCl. The concentrations of chloride ions added to the 1 M [HCl] solutions were 3.6 M, 3 M,

2 M and 1 M. Figure 4.7 shows results obtained from the experiments conducted at specified conditions. When the total chloride ion concentrations are considered, the oxidation profiles obtained were almost similar to those obtained when only HCl was used (see Figure 4.4 and Figure 4.7). It was thought that thermodynamic equilibrium would govern the extent of HCl association (and dissociation) regardless of how the hydrogen and the chloride ions entered the solution. Although equilibrium calculations for the dissociation of sodium chloride were not performed, it was assumed that the minor difference in the extent of oxidation in Figure 4.4 and Figure 4.7 may be attributed to the incomplete dissociation of sodium chloride in the case of Figure 4.7. Posner (1953) investigated the addition of common ions to a solution containing [HCl] below that required for rapid oxidation. LiCl and $CaCl_2$ were used to provide the additional chloride ions in a solution containing less than 4 M HCl. The results of this study are in line with the observations made by Posner (1953).

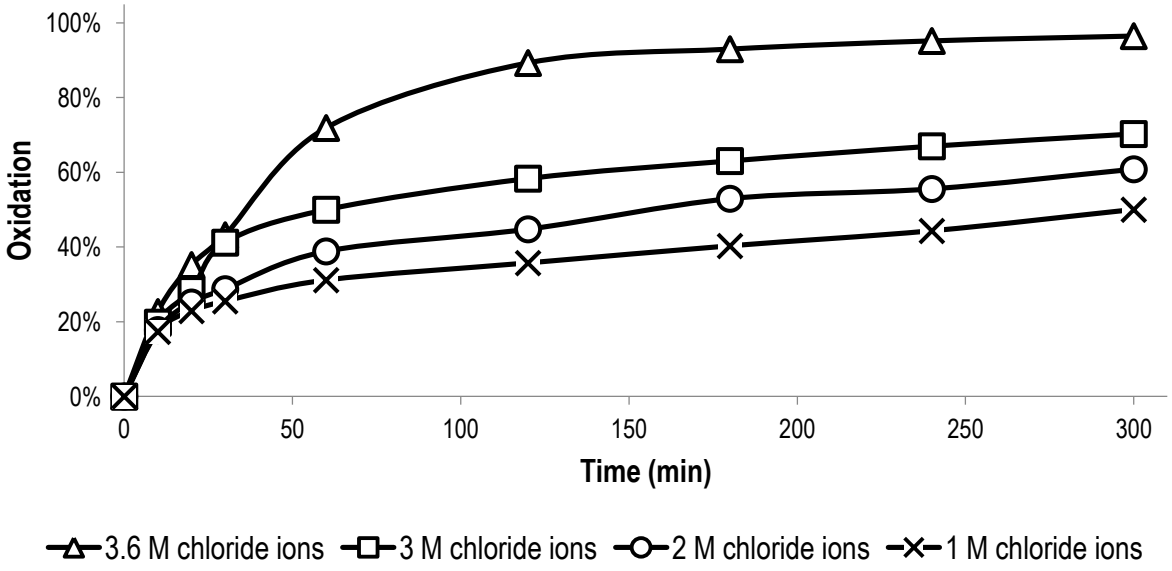

Figure 4.7. Oxidation rate of iron(II) at 80°C, 3 g/L Cu concentration and 1 M [HCl] at different additional chloride ions

4.1.5. Robustness tests - effect of simultaneous oxidation and precipitation

Experiments that involved simultaneous oxidation and precipitation were conducted with a view of improving the oxidation rate and limiting the

concentration of iron(III) available for precipitation (hence controlling supersaturation during precipitation). These experiments were conducted at 80^{o}C, 3 g/L Cu concentration, 1 M [HCl] and an additional 3.6 M NaCl.

It was assumed that the iron precipitated only upon oxidation to iron(III), considering that the solution pH was about 0. Generally, iron(III) begins to precipitate at pH 0 while iron(II) precipitates at pH 7 and above. Equation 2.36 shows the basis for the estimation of pH values at which metals precipitate, depending on their concentrations in solutions. It was thus assumed that iron(II) in solution dropped only on account of oxidation rather than precipitation. The iron(II) in solution was analysed as described in APPENDIX C: ANALYSIS OF IRON (II).

From Figure 4.8, it can be shown that precipitating iron(III) during oxidation yielded higher conversion of iron(II) to iron(III). This is what was expected and indeed in line with literature (Habashi, 1999). The precipitate quality obtained when precipitated during oxidation of iron(II) will be discussed in Section 4.2.3 and Section 4.3.3.

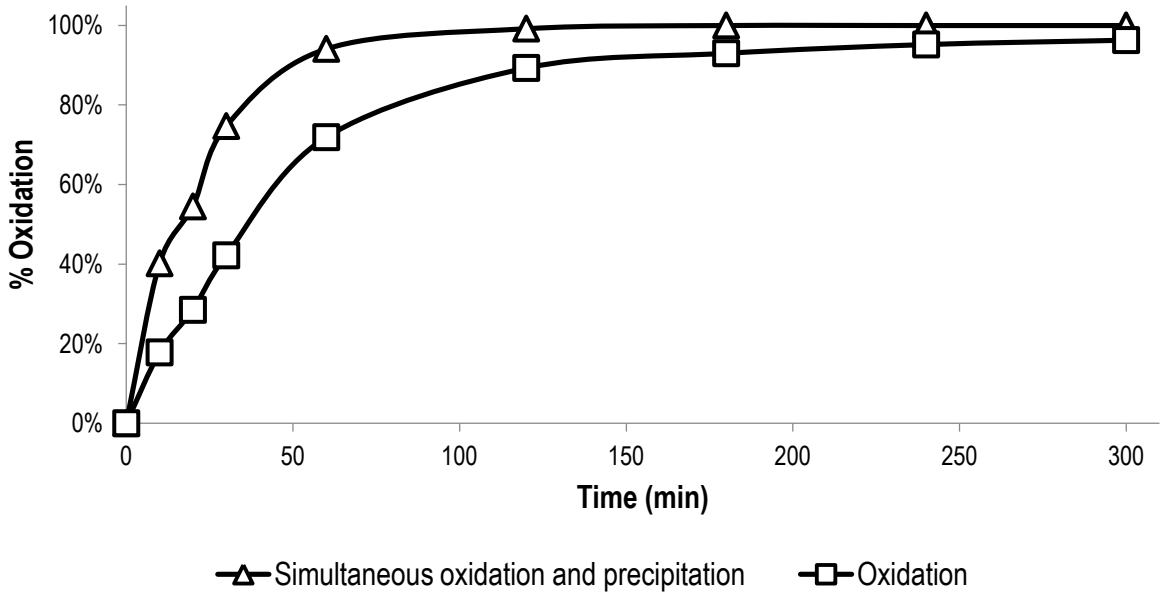

Figure 4.8. Oxidation rate of iron(II) at 80^{o}C, 3 g/L Cu concentration, 1 M [HCl] and additional 3.6 M chloride ions

4.2. Iron phosphate precipitation

4.2.1. Effect of pH and temperature on the precipitate purity

As discussed in Section 2.3.1.4, pH and temperature are the main variables that influence supersaturation. Supersaturation plays a major role in the primary crystallization process, which then determines the purity of precipitates formed. This study involved investigating the effect of pH and temperature on iron precipitation and co-precipitation of nickel and copper. Experiments were conducted as discussed in Section 3.2 and results are presented and discussed in this section.

Figure 4.9 [A] to [D] shows some of the results of seeded precipitation experiments conducted at varying pH and temperature. The base solution contained about 45 g/L iron(III), 3 g/L nickel and 3 g/L copper. Iron was almost completely precipitated out of solution at all pH points investigated (1, 2 and 3) and all temperature points investigated (40^{o}C, 60^{o}C and 80^{o}C) after about 20 minutes of reaction time. However, nickel and copper losses varied with varying pH and temperature. At pH below 1, almost complete precipitation of iron phosphate was observed but no further benefits in terms of minimization of nickel and copper losses was observed (see Table E.33 in APPENDIX E: EXPERIMENTAL DATA).

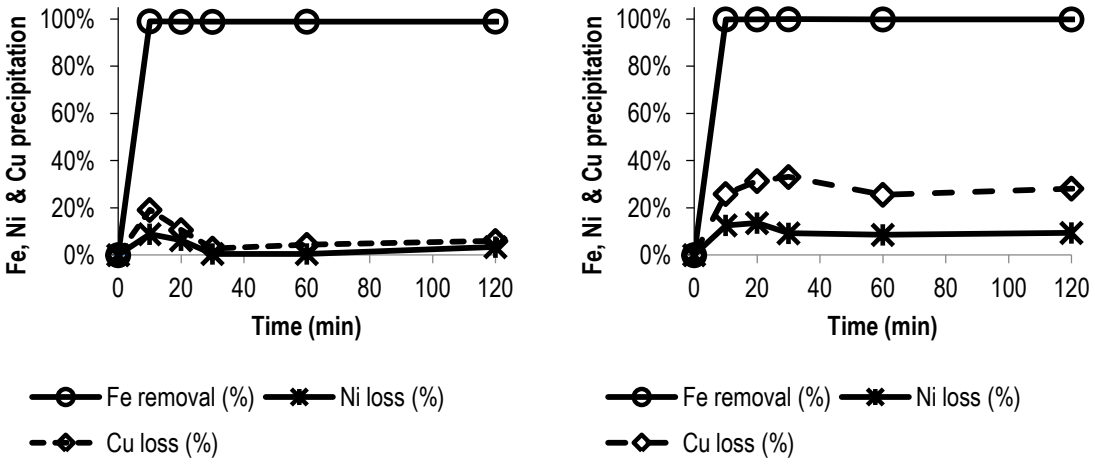

[A] [B]

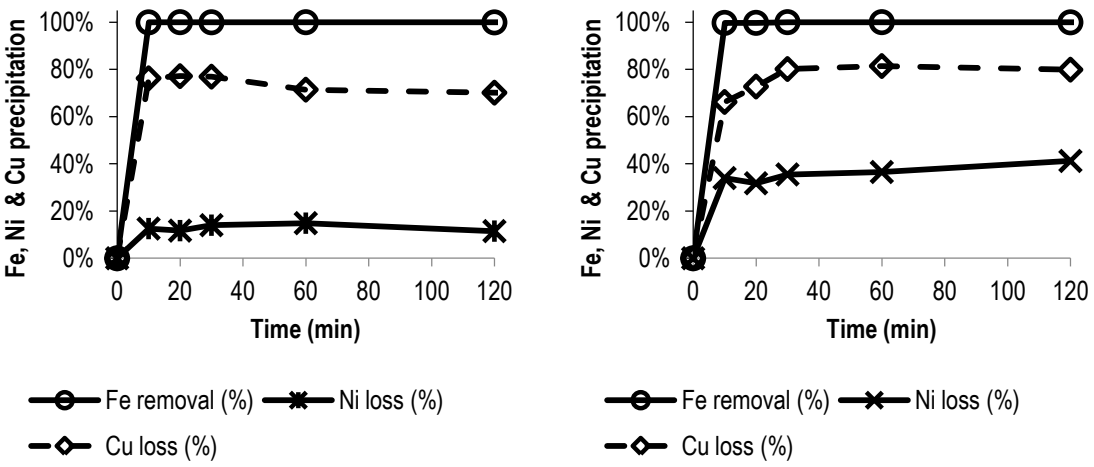

[C] [D]

Figure 4.9. Seeded precipitation of iron phosphate depicting losses of nickel and copper at varying pH and temperature: [A] pH 1 at 40°C, [B] pH 1 at 60°C, [C] pH 2 at 40°C, [D] pH 3 at 40°C

From Figure 4.9, it can be observed that nickel and copper losses increased with increase in pH from 1 to 3. At pH 1 and 40°C, the nickel loss was less than 2% for a reaction time of about 30 minutes. At this pH, temperature and reaction time, the copper loss was less than 5%. Increasing the pH to 2 resulted in nickel losses above 8% and copper losses above 20%, for the same reaction time and temperature. The nickel and copper losses were even higher for tests conducted at pH 3, regardless of the temperature and reaction time. As discussed in Section 2.3.1.4, the purity of precipitates can be controlled by lowering supersaturation. Lower pH results in lower supersaturation and therefore more pure precipitates are produced. At lower supersaturation levels, heterogeneous precipitation dominates. As opposed to homogenous precipitation, heterogeneous precipitation is growth controlled rather than nucleation controlled. As discussed in Section 2.3.1.6, the main mechanism by which co-precipitation occurs during the precipitation of iron is occlusion. Occlusion mainly occur when the precipitation process is nucleation controlled rather than growth controlled.

It can be seen from Figure 4.9 [A] that during the first 10 minutes, the losses of nickel and copper increased with time and after that nickel and copper losses

appeared to start reducing and attained equilibrium after about 30 minutes. Repeat experimental results are recorded in APPENDIX E: EXPERIMENTAL DATA, Table E 31. It is proposed that this is due to Ostwald's ripening. Ostwald's ripening involves the crystallization of larger crystals at the expense of smaller impure crystals. It is suggested that nickel and copper losses, during the first 10 minutes, were due to occlusion of nickel and copper liquid within the iron phosphate structure. As the smaller crystals of iron phosphate re-dissolved to form larger crystals, the trapped liquid was released back into solution (Ostwald, 1896; Threlfall, 2003).

Even though increasing the temperature from 40^{o}C to 60^{o}C and 80^{o}C did not have as large an impact as increasing the pH, it can be seen from Figure 4.9 [A] and [B] that lower temperature precipitation resulted in lower losses of nickel and copper for the same pH and retention time.

The iron/phosphorous ratio in reagent grade iron phosphate is about 1.8.

Table 4.3 shows the iron/phosphorous ratio of precipitates produced at various operating pH and temperature as obtained from X-ray fluorescence (XRF) analysis. Freshly prepared precipitates were filtered using 0.45 µm filter paper and washed with 200 mL of deionised water. The ratio of slurry to deionised water was 1 to 1, to ensure complete wash-off of the nickel and copper that was not mechanically trapped in the precipitate. It can be observed from

Table 4.3 that as the pH and temperature increased, the iron/phosphorous ratio also increased. Twidwell et al. (1986) reported the formation of iron compounds, other than iron phosphate, such as goethite and jarosites, when attempting to precipitate iron phosphate at temperatures above 50^{o}C. It is proposed that the

increase in nickel and copper losses, with temperature, was mainly due to the formation of additional iron species besides iron phosphate.

Table 4.3. Iron/phosphorous ratio for seeded precipitates produced at various pH and temperature conditions

Operating condition	40°C	60°C	80°C
pH1	1.76	2.20	2.29
pH2	1.94	2.30	2.33
pH3	2.24	2.34	2.44

Seeded precipitates produced at varying pH, 40^{o}C and retention time of 3 h were analyzed using XRF. Figure 4.10 shows results of solid analysis, with regards to nickel and copper losses. Solid sample results were in line with the solution sample results that suggested that higher pH resulted in higher nickel and copper losses. It can be seen in Figure 4.10 that at pH 1, nickel and copper in solids was below 0.2%. As the pH was increased to 3, nickel in solids was found to be above 0.6% while copper was almost 1% in solids.

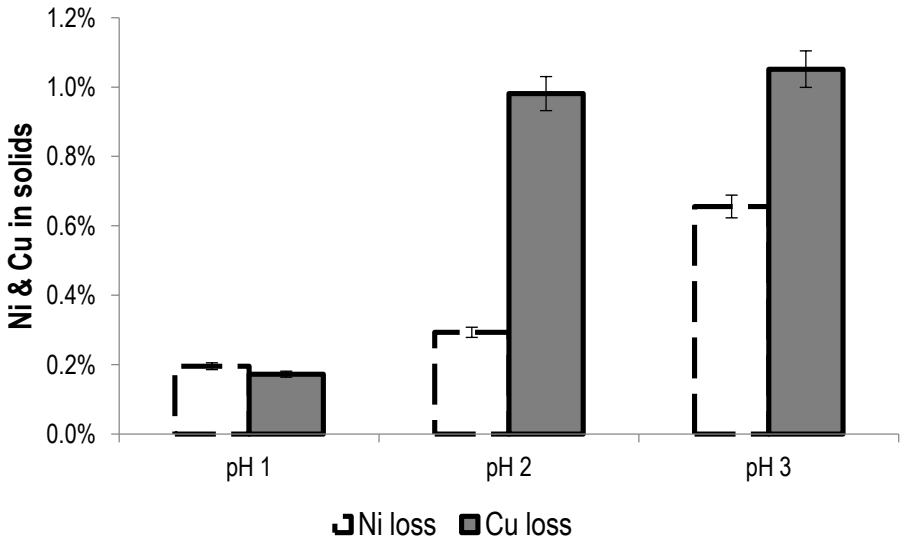

Figure 4.10. Nickel and copper % composition by weight in the iron phosphate precipitate as a function of pH for seeded precipitation tests conducted at 40°C, including 5% deviation error bars

Figure 4.11 shows average results of stepwise pH control experiments. The pH was kept at 0 for 10 minutes, and then increased to about 0.2, held there for 20 minutes and then again increased to about 0.5 and held there for a further 30 minutes. Even though there was almost no nickel and copper loss for the first 10 minutes, at pH 0, almost 3% iron was still in solution. Further increase in pH to 0.5, after 60 minutes, did not result in further significant reduction of iron in solution. From the data obtained, stepwise pH control appears ideal in terms of minimizing nickel and copper loses, although the iron removal data indicated that there was still room for further improvement.

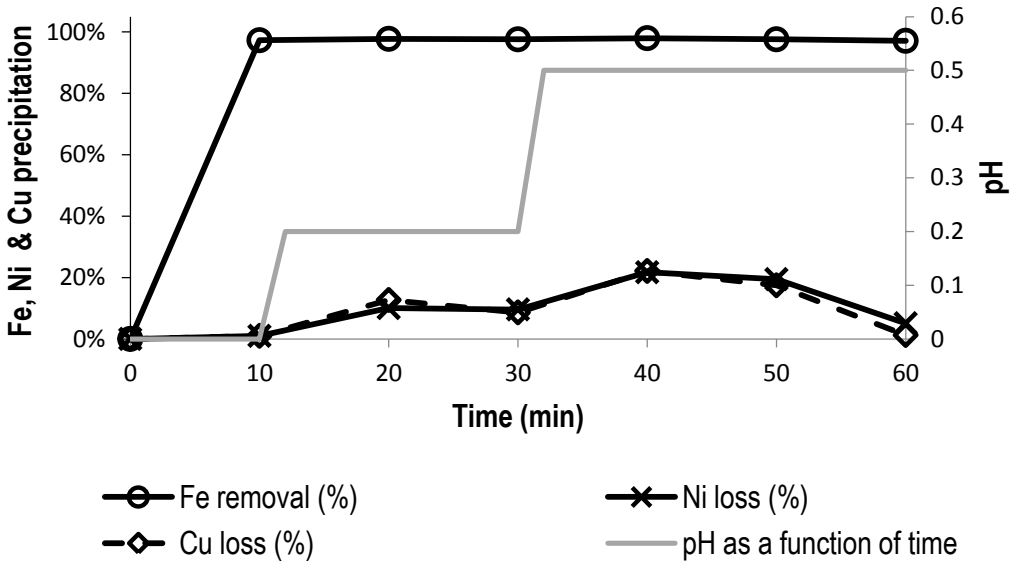

Figure 4.11. Stepwise pH control and the response of iron phosphate precipitation, nickel and copper losses for seeded precipitation tests conducted at 40°C

4.2.2. Effect of seeding

It can be deduced from Figure 4.12 that iron phosphate precipitation, in both seeded and unseeded precipitation experiments, was completed and attained equilibrium after about 20 minutes.

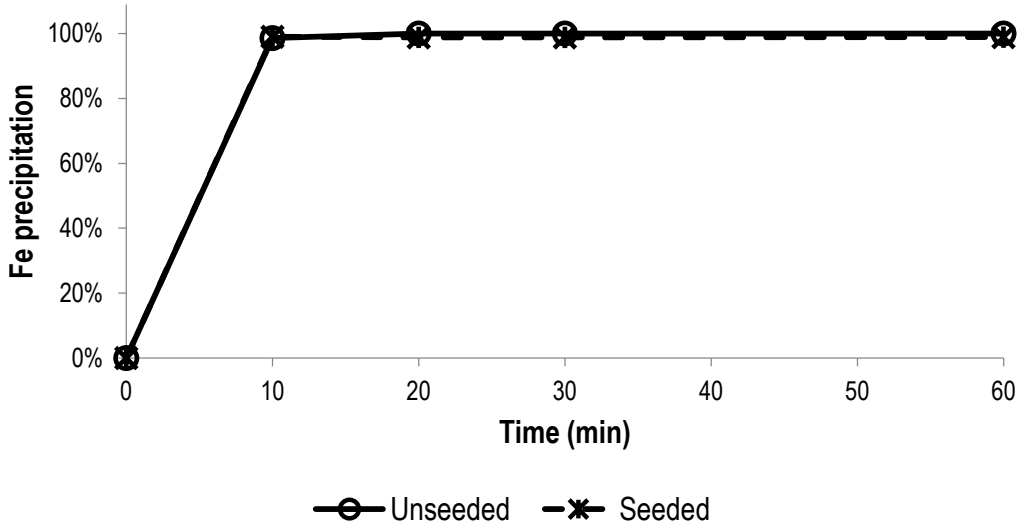

Figure 4.12. Seeded and unseeded iron phosphate precipitation at 40°C and pH 1 with respect to time.

It can be seen in Figure 4.13 and Figure 4.14 that nickel and copper losses for seeded and unseeded iron precipitation had different profiles. Repeat experimental results for seeded and unseeded runs are recorded in APPENDIX E: EXPERIMENTAL DATA, Table E 31 and Table E 32 respectively. Seeded precipitation provides more nucleation sites than unseeded precipitation because of the introduction of particles of the same kind as those desired to precipitate. The dissolution of smaller and impure precipitates is enhanced in seeded precipitation compared to unseeded precipitation. Hove et al. (2009) reported that seeding favors formation of larger, more pure and more stable particles at the expense of the smaller, impure and kinetically unfavorable particles (Hove et al., 2009).

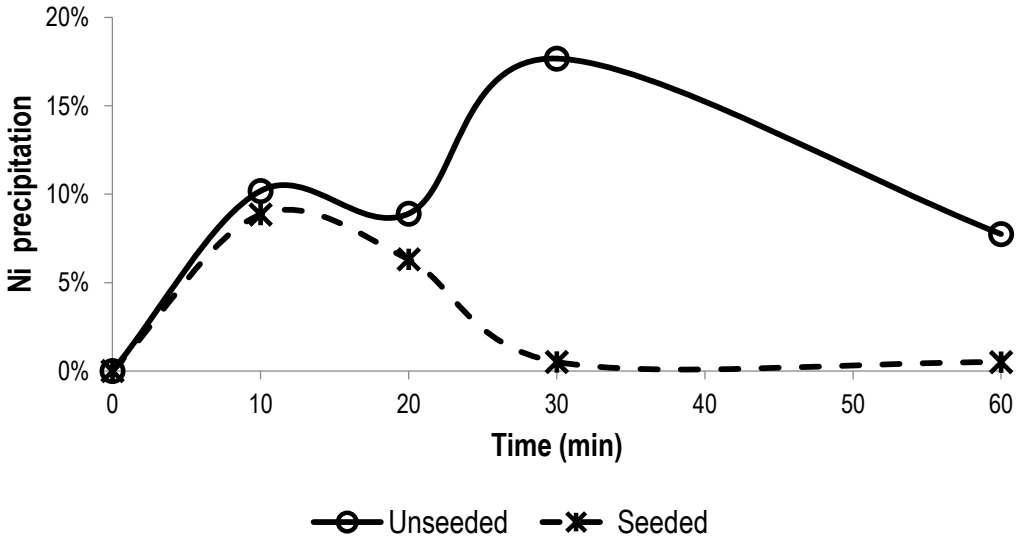

Figure 4.13. Co-precipitation of nickel during seeded and unseeded iron phosphate precipitation at 40°C and pH 1 with respect to time

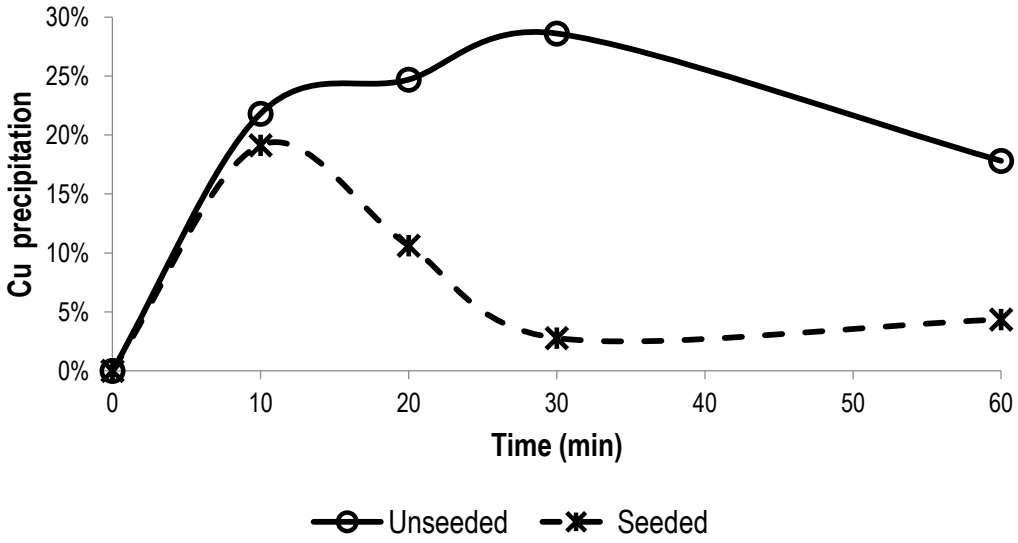

Figure 4.14. Co-precipitation of copper during seeded and unseeded iron phosphate precipitation at 40°C and pH 1 with respect to time

4.2.3. Simultaneous oxidation and iron phosphate precipitation

Dilution is one way of controlling supersaturation and thereby a means of producing high quality precipitates. It was expected that simultaneous oxidation and precipitation would not only improve the oxidation rate but it would also

produce purer precipitates because of lower supersaturation (i.e. lower concentration of iron(III) at a given point).

It can be seen in Figure 4.15 that even though almost 99% iron was precipitated out of solution after 120 minutes, it was at the expense of over 28% nickel co-precipitation. Unexpectedly, the copper losses were observed to be consistently lower than nickel losses. After 120 minutes, the copper losses were above 20%. It is not clear at this point why lower copper losses were observed compared to nickel losses in simultaneous oxidation and precipitation experiments. For extended reaction times, complete iron removal was achieved with lower nickel and copper co-precipitation. After 480 minutes, complete iron removal was observed with the co-precipitation of nickel and copper of about 12% and 3% respectively.

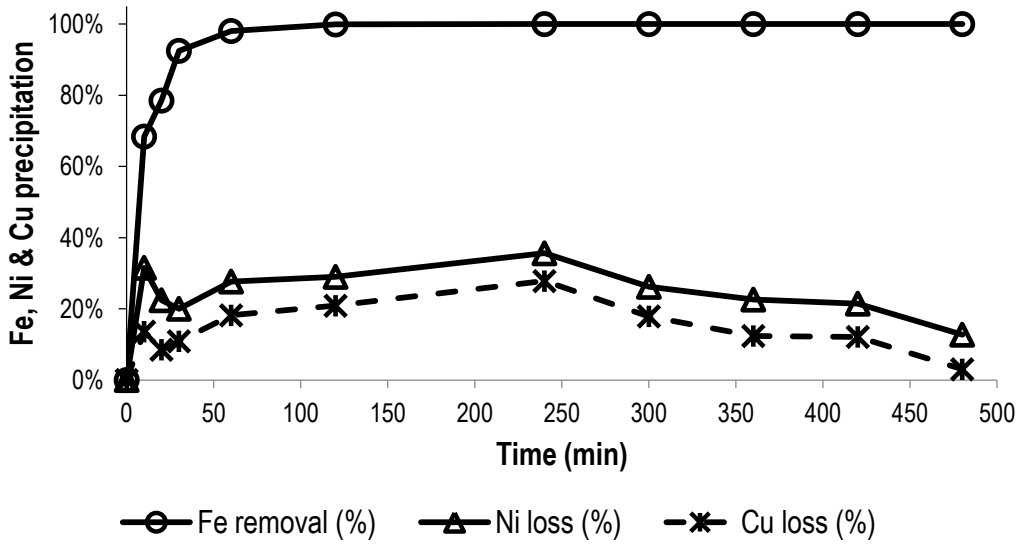

Figure 4.15. Simultaneous oxidation and seeded precipitation of iron phosphate at 80^{o}C and 1 M [HCl]

It is suggested that the process of precipitation was compromised due to the need for balancing oxidation optimal conditions with the seemingly optimized precipitation parameters. A temperature of 80^{o}C was maintained as opposed to 40^{o}C, because it was observed in oxidation experiments that the oxidation rate reduced with reduction in temperature. It is however possible to compromise the

oxidation retention time for precipitation temperature. The effect of dissolved oxygen on speciation during precipitation is also not clear at this point.

4.2.4. Iron phosphate characterization

4.2.4.1. SEM analysis

Figure 4.16 [A] to [E] shows an image of iron phosphate precipitate and maps of elements presents in the precipitate produced at 40^{o}C and pH 1. On the individual element maps, the increase in elemental presence is denoted by an increase in colour brightness.

Figure 4.16 [A] shows an image of iron phosphate precipitate with flakes of sodium chloride. It can be seen that the iron phosphate morphology is dense and spherical particles (and agglomerates of spherites) with high surface area. It is because of this kind of morphology that iron phosphate traps fewer impurities by surface adsorption.

Figure 4.16 [B] and [C] shows the distribution of nickel and copper losses in the iron phosphate matrix. Because the distribution of the nickel and copper appears so evenly distributed in the iron phosphate matrix, it is proposed that the mode of co-precipitation was occlusion (occlusion is discussed in Section 2.3.1.6).

Chen and Dutrizac (1990) reported that SEM can be singularly used to suggest the compounds present in a material by utilizing images and maps. From Figure 4.16 [D] and [E] it can be seen that the intensity of iron follows that of phosphorous. It therefore can be suggested that the iron compound in precipitate produced in the presence of a phosphorous source was iron phosphate. XRF analysis also indicated iron to phosphorous ratio of approximately 1.8 which is typically the stoichiometric ratio of iron to phosphorous in iron phosphate.

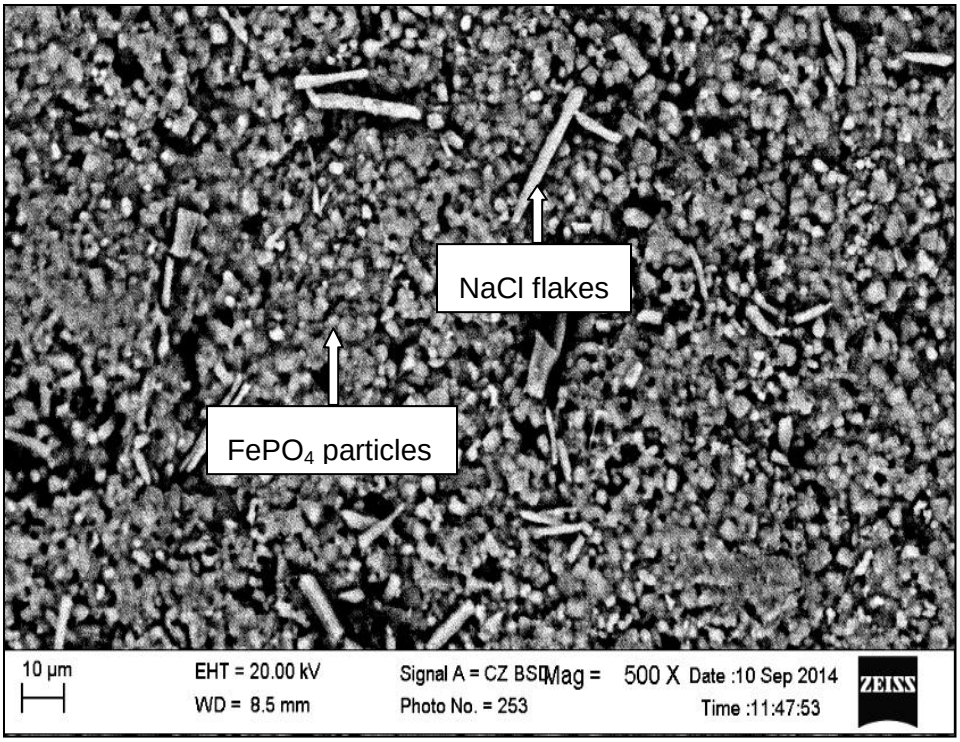

[A]

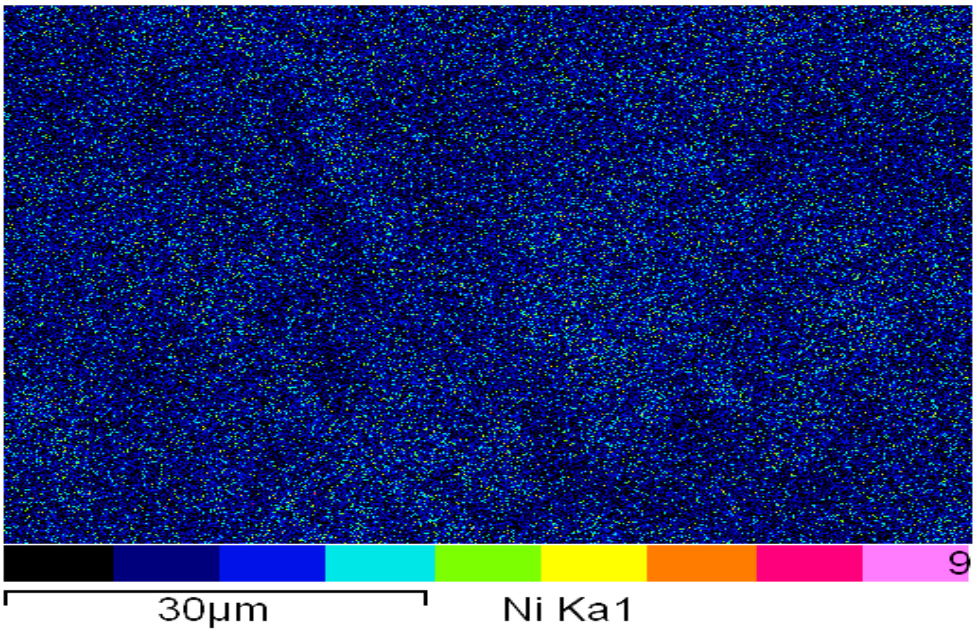

[B]

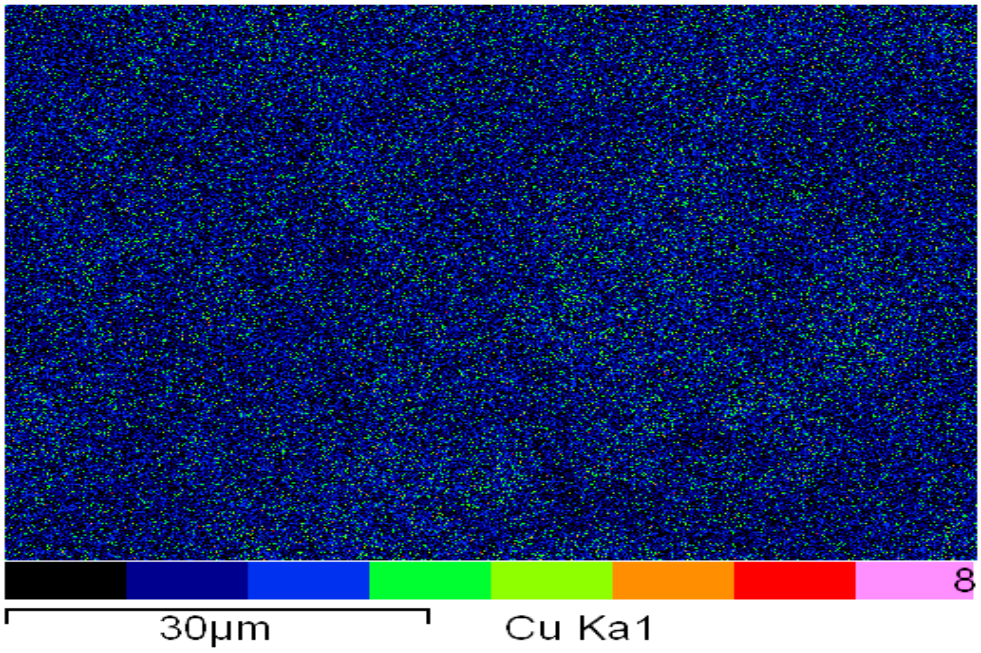

[C]

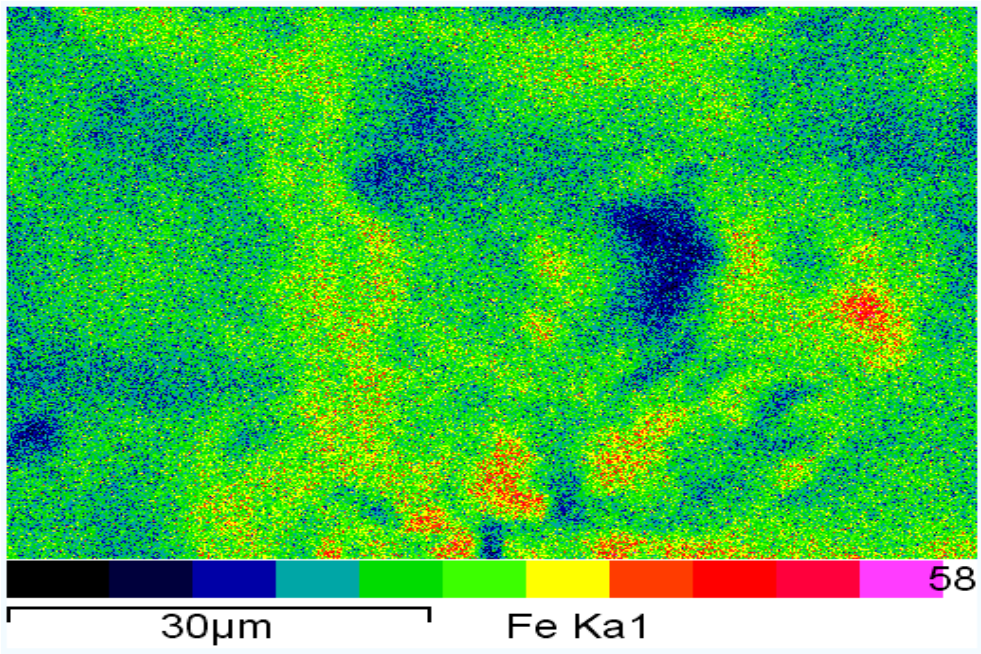

[D]

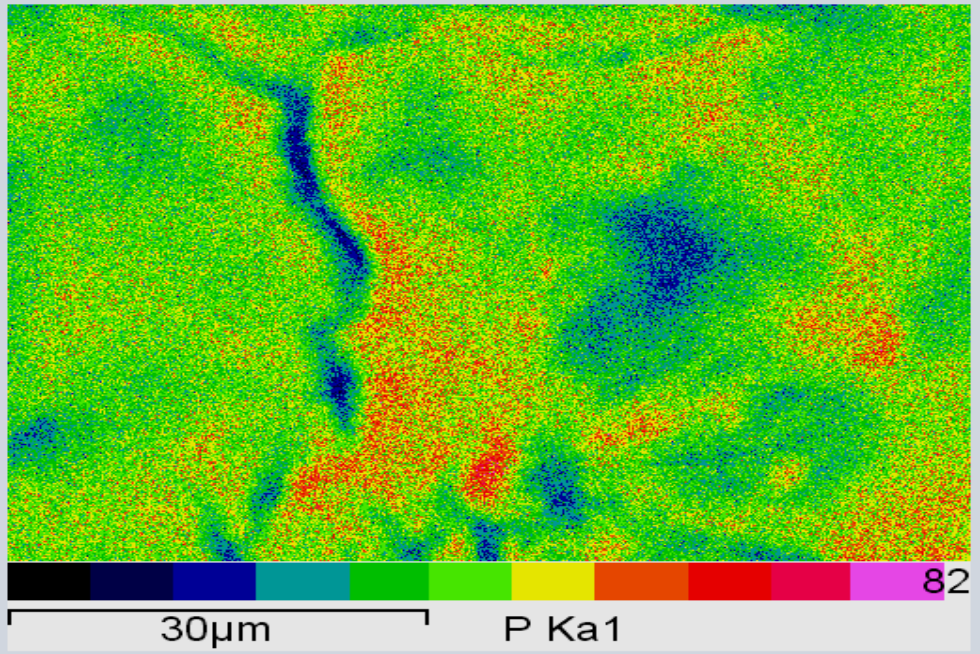

[E]

Figure 4.16. Scanning electron microscopy (SEM) image and maps of seeded iron precipitate produced at 40°C and pH 1. [A]-iron phosphate image, [B]-Ni distribution map, [C]-Cu distribution map, [D]-Fe distribution map and [E]-P distribution map

4.2.4.2. XRD analysis

Figure 4.17 shows results of XRD analysis for seeded iron phosphate precipitates produced at 40°C and pH 1. The iron phosphate precipitates produced at all conditions tested were reported to be largely amorphous with traces of sodium chloride. Beck et al. (2011) reported the precipitation of amorphous iron phosphate from the reaction of ferric iron and sodium phosphate unless deliberate additional processes were involved. In Section 2.3.2.4, additional steps that can be taken to prepare crystalline iron phosphate are discussed.

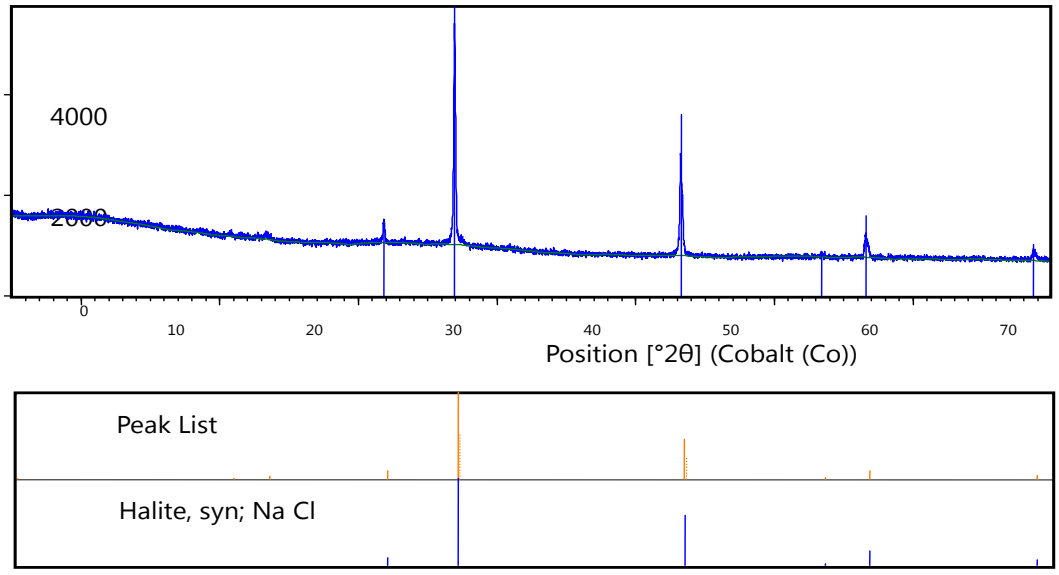

Figure 4.17. XRD analysis of seeded iron phosphate precipitate produced at 40°C and pH 1

4.3. Hematite precipitation

4.3.1. Effect of pH and temperature on hematite purity

The effects of pH variations on the precipitation of hematite and the resulting nickel and copper lose were similar to those observed during the precipitation of iron phosphate. The base solution contained about 45 g/L iron(III), 3 g/L nickel and 3 g/L copper. From Figure 4.18 [A] to [D], it can be shown that iron precipitation was almost complete (above 99% removal) after 20 minutes at pH points 1, 2 and 3. The nickel and copper losses were observed to increase with increase in pH.

From Figure 4.18 [A], it can be seen that the co-precipitation of nickel and copper initially increased with time, to about 10% and 11% respectively, then after 20 minutes the losses gradually reduced with time, until after 60 minutes. After 60 minutes, the nickel and copper losses were below 5%. Repeat experimental results are recorded in APPENDIX E: EXPERIMENTAL DATA, Table E 15. It was assumed that the losses of nickel and copper, even after iron precipitation was almost complete, were due to the initial precipitation of some amount of akaganeite even in seeded experiments. The losses of nickel and copper were

attributed to occlusion of liquid nickel and copper within the akaganeite structure. The minor changes in the concentration of nickel and copper suggested the possibility of solid nickel and copper occlusion. It was thought that as the akaganeite transformed to hematite with time, the trapped liquid was released back into solution. When the pH was increased to 2 (Figure 4.18 [C]), the nickel and copper losses were respectively above 11% and 12% after 60 minutes.

From Figure 4.18 [A] and [B], it can be seen that precipitation at pH 1 while varying temperature at 80^{o}C and 60^{o}C had similar iron removal profiles. The nickel and copper losses were however different. As discussed in Section 2.3.2.3, hematite is traditionally precipitated at temperatures above 100^{o}C. Reducing the temperature favors the precipitation of akaganeite (goethite for sulphate systems). The concentration of akaganeite in the precipitate generally increases with temperature reduction. Akaganeite is more susceptible to trap nickel and copper in its crystal lattice compared to hematite.

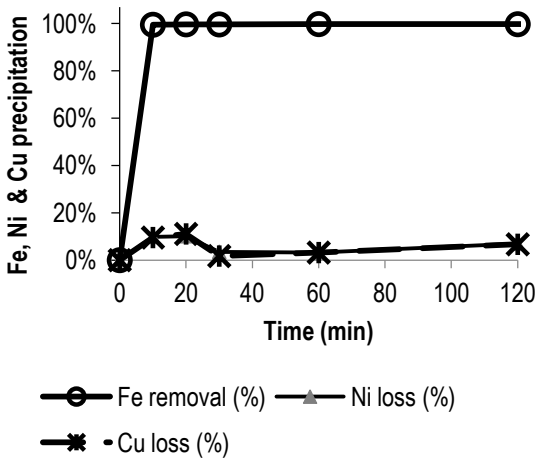

[A]

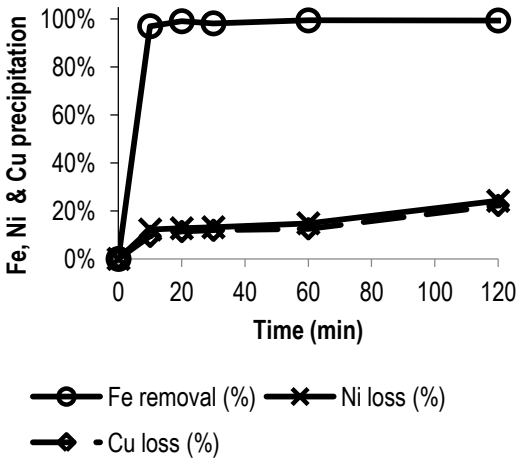

[B]

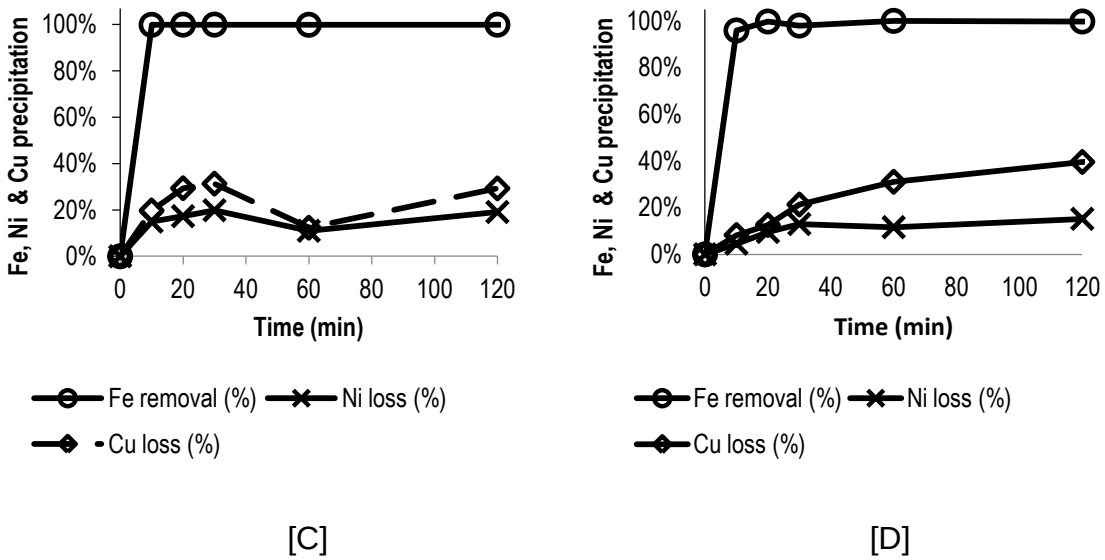

Figure 4.18. Seeded hematite precipitation and loss of nickel and copper at varying pH and temperature: [A] pH 1 at 80°C, [B] pH 1 at 60°C, [C] pH 2 at 80°C, [D] pH 3 at 80°C

4.3.2. Effect of seeding

Figure 4.19 to Figure 4.21 compares iron removal, nickel and copper co-precipitation for seeded and unseeded precipitation at 80°C and pH of 1. Repeat experimental results for seeded and unseeded runs are recorded in APPENDIX E: EXPERIMENTAL DATA, Table E 14 and Table E 15 respectively. It was noted that although iron removal was rapid in both seeded and unseeded precipitation, nickel and copper losses were higher in unseeded precipitation.

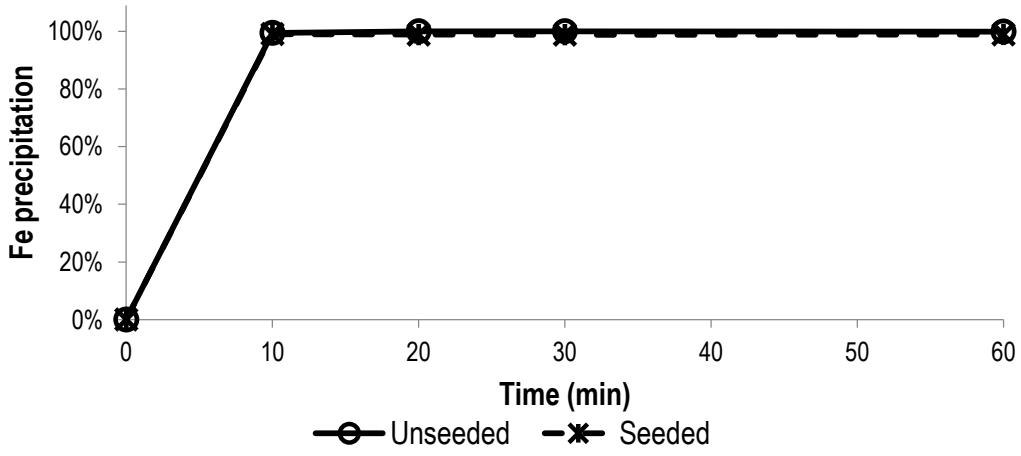

Figure 4.19. Seeded and unseeded hematite precipitation at 80°C and pH 1 with respect to time

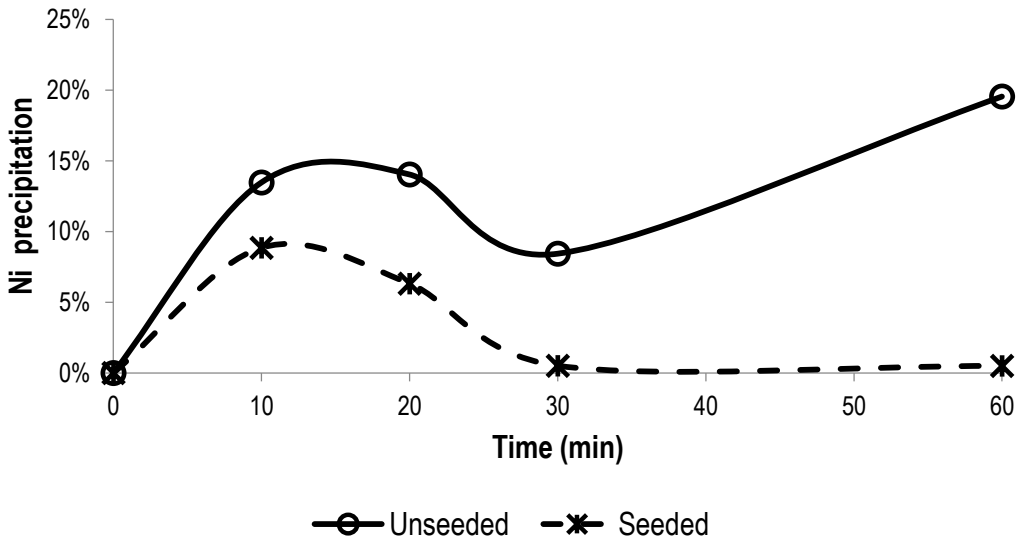

Figure 4.20. Co-precipitation of nickel during seeded and unseeded hematite precipitation at 80°C and pH 1 with respect to time

Dutrizac and Riveros (1999) demonstrated that hematite can be precipitated at temperatures as low as 60°C when precipitation is seeded. It was however reported that even in seeded experiments, akaganeite precipitation was not entirely avoided but seeding accelerated its transformation to hematite.

As discussed in Section 2.3.2.3, compared to other iron hydroxides precipitates, hematite has a more compact structure and therefore less likely to trap foreign materials. It is proposed that the lower nickel and copper losses in seeded precipitation compared to unseeded precipitation are attributed to the formation of hematite in seeded precipitation as opposed to the formation of akaganeite in unseeded experiments. The precipitation of hematite in seeded precipitation is qualified in Section 4.3.4.2.

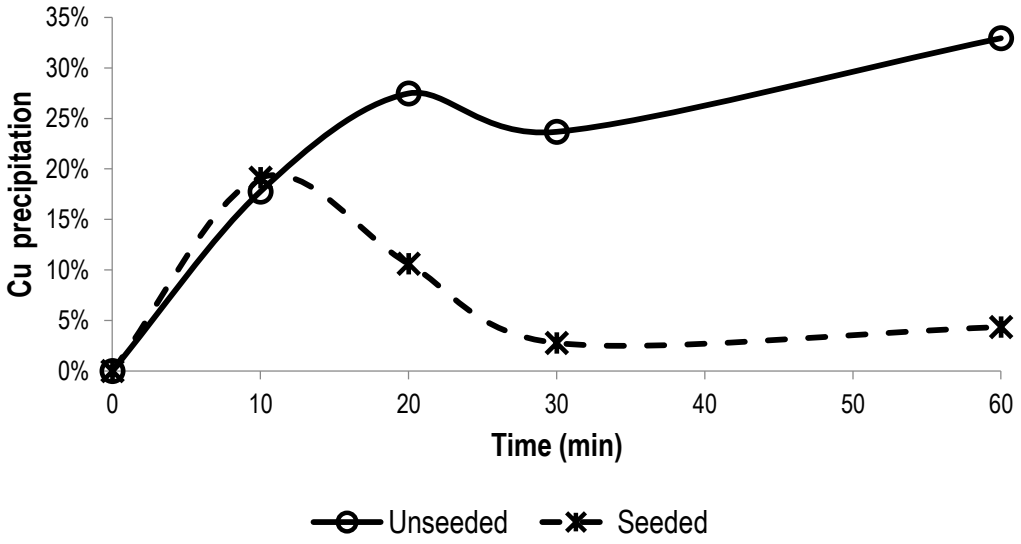

Figure 4.21. Co-precipitation of copper during seeded and unseeded hematite precipitation at 80°C and pH 1 with respect to time

4.3.3. Simultaneous oxidation and hematite precipitation

Figure 4.22 shows average results obtained from the simultaneous oxidation and seeded hematite precipitation conducted at 80°C and 1 M HCl. Similar to results obtained in the iron phosphate precipitation at the same conditions, iron removal was almost complete after 120 minutes while nickel and copper losses were higher compared to those obtained from dedicated oxidation and precipitation experiments.

It was expected that since the availability of iron(III) was controlled by the rate of oxidation of iron(II), supersaturation would have been controlled by limiting the amount of iron(III) present for precipitation and thereby controlling the precipitate quality. Results obtained however did not support this. It is not clear why almost 20% nickel and above 15% copper was lost compared to below 4% nickel and below 5% copper co-precipitation during dedicated oxidation and precipitation experiments.

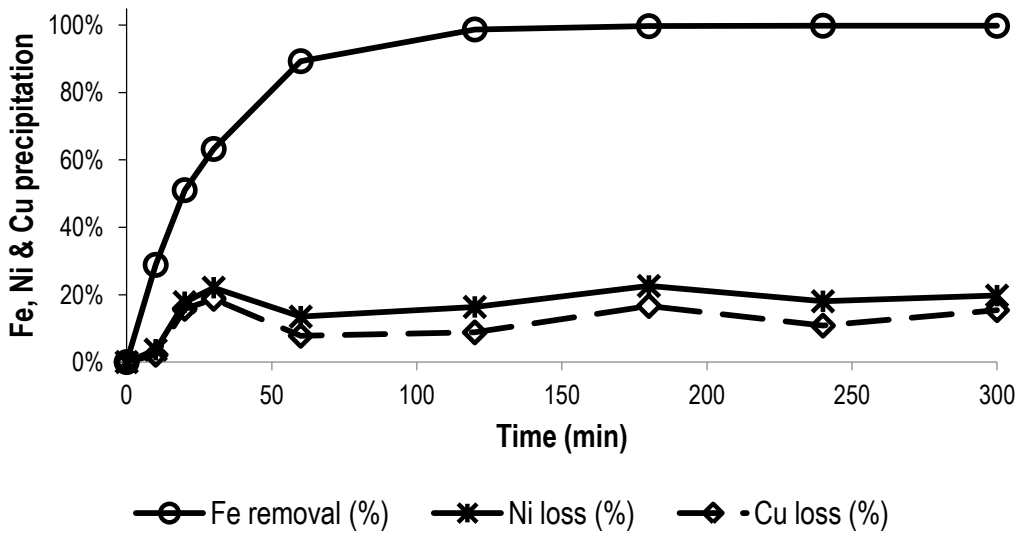

Figure 4.22. Simultaneous oxidation and precipitation of hematite at 80°C and 1 M [HCl]

4.3.4. Hematite characterization

4.3.4.1. SEM analysis

Figure 4.23 [A] shows an image of hematite precipitate produced at 80°C and pH 1 in a seeded process. It can be noticed that the morphology of the particles appears to be compact with a number of agglomerates and aggregates.

On the individual element maps, the increase in elemental presence is denoted by an increase in colour brightness. The intensity of iron shown in Figure 4.23 [B] may suggest a high iron content compound. Hematite has the highest iron content among iron oxides and hydroxides. It contains approximately 70% iron. XRD results, reported in Section 4.3.4.2, confirmed that hematite was the major phase precipitated (above 95%) at 80°C and pH 1.

Similar to the observation made in the iron phosphate precipitates, it can be seen in Figure 4.23 [C] and [D] that nickel and copper losses were evenly distributed in the hematite precipitate as well. It is suggested that the major co-precipitation mechanism of nickel and copper, during the precipitation of hematite, was occlusion.

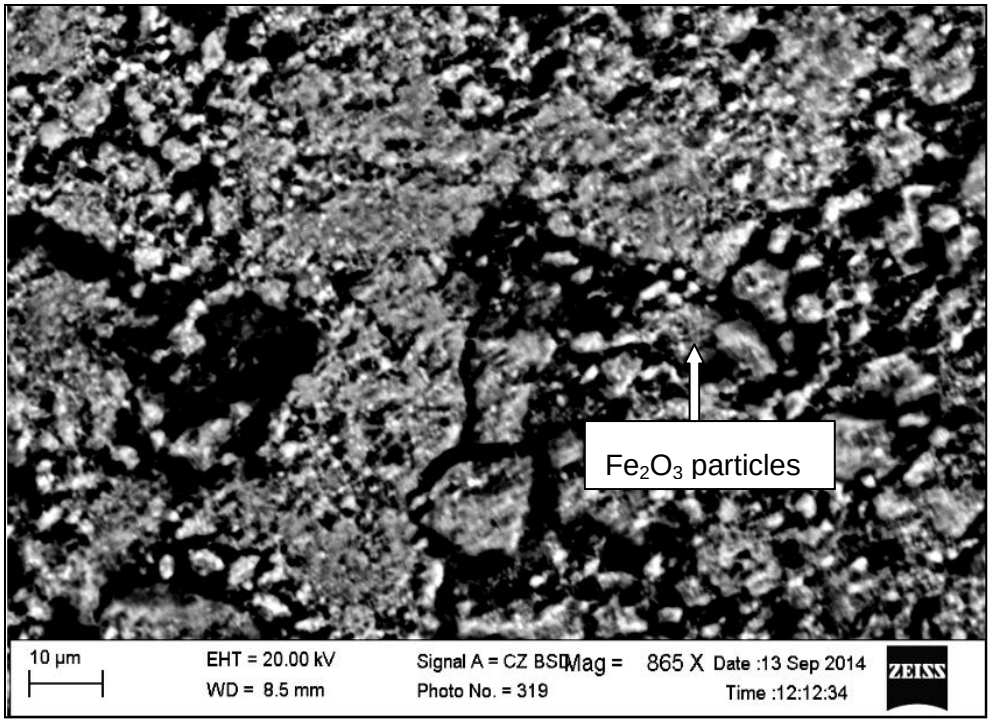

[A]

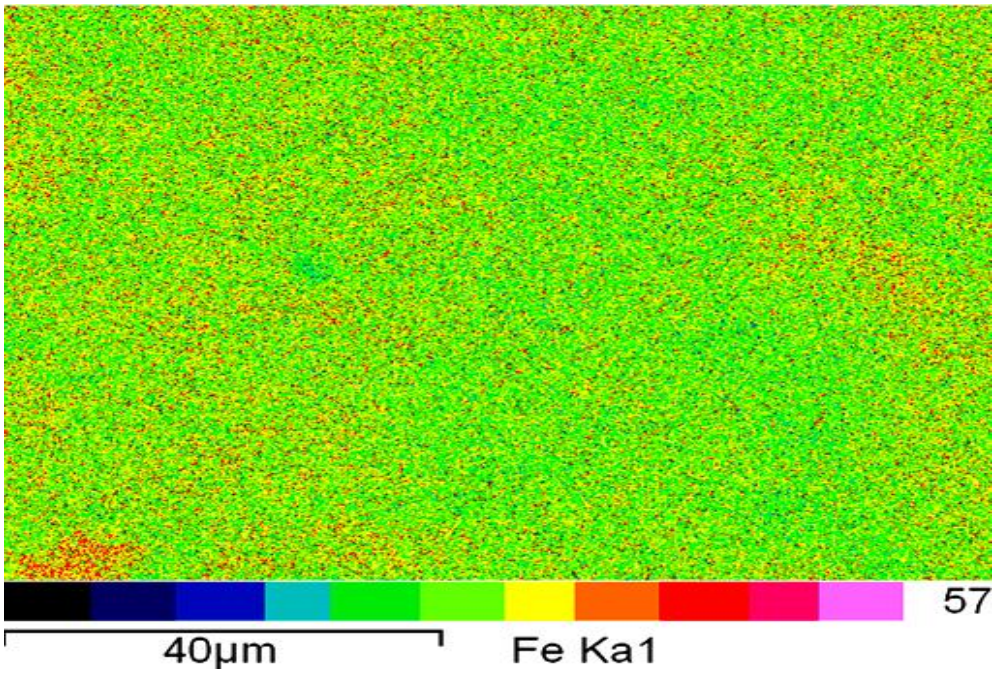

[B]

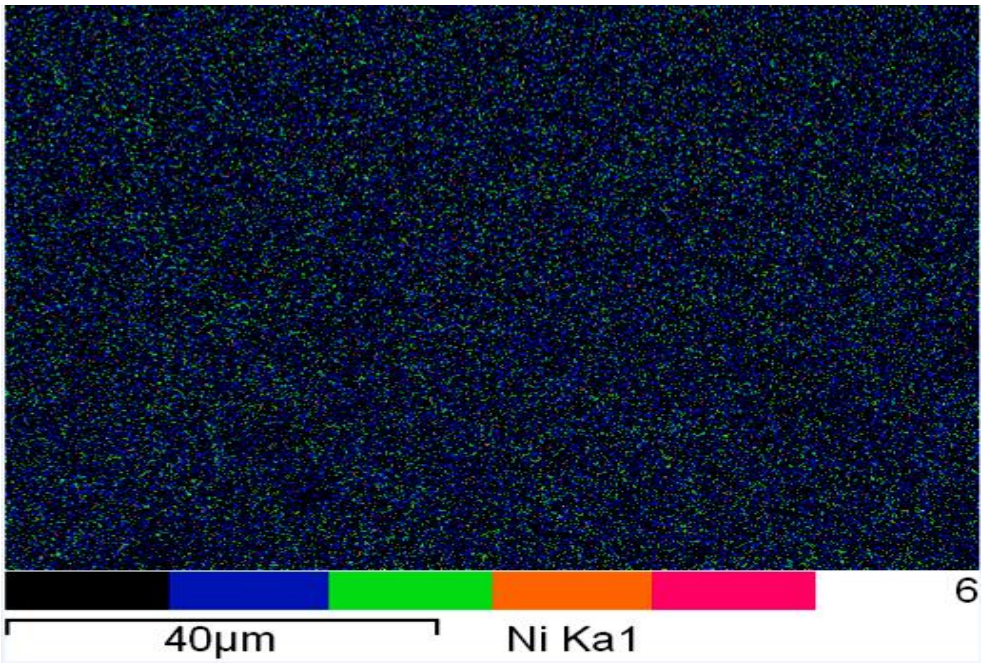

[C]

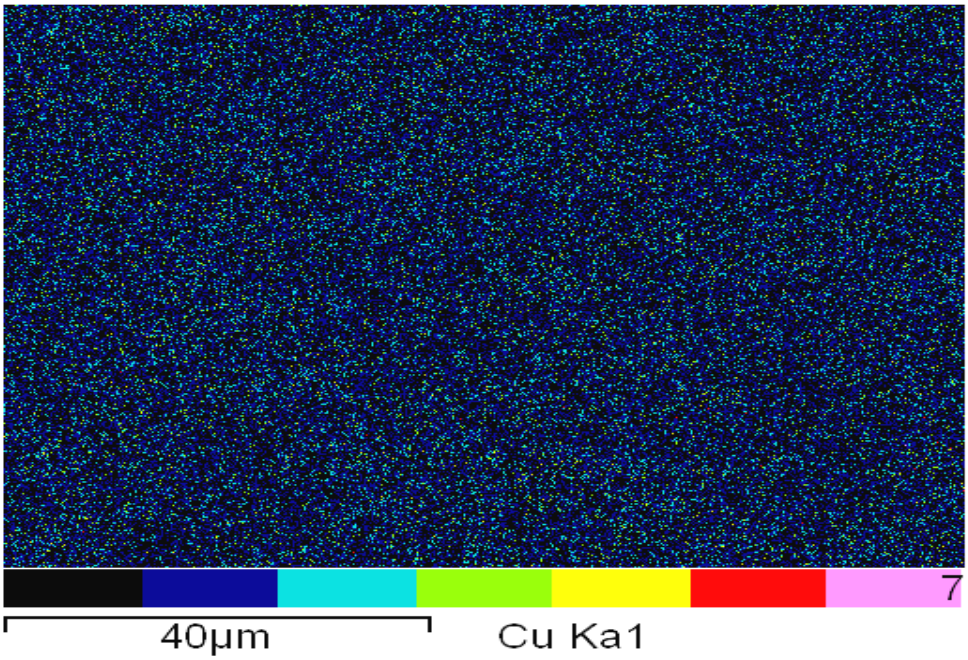

[D]

Figure 4.23. Scanning electron microscopy (SEM) image and maps of seeded hematite produced at 80^{o}C and pH 1. [A]-hematite image, [B]-Fe distribution map, [C]-Ni distribution map and [D]-Cu distribution map

4.3.4.2. XRD analysis

Figure 4.24 [A] to [E] shows XRD analysis of seeded precipitation from iron(III) chloride at various temperatures and pH.

It can be seen from Figure 4.24 [A] and [D] that hematite was the dominate phase for seeded precipitates produced at all tested conditions. The percentage of hematite increased with increase in temperature and appeared to increase with reduction in pH.

Cohen et al. (2005) reported the precipitation of hematite at 80^{o}C and pH 0.9 to minimize the co-precipitation of impurities. Dutrizac and Riveros (1999) proposed that akaganeite transforms itself to hematite with time. This transformation was reported to be rapid at elevated temperature and controlled supersaturation.

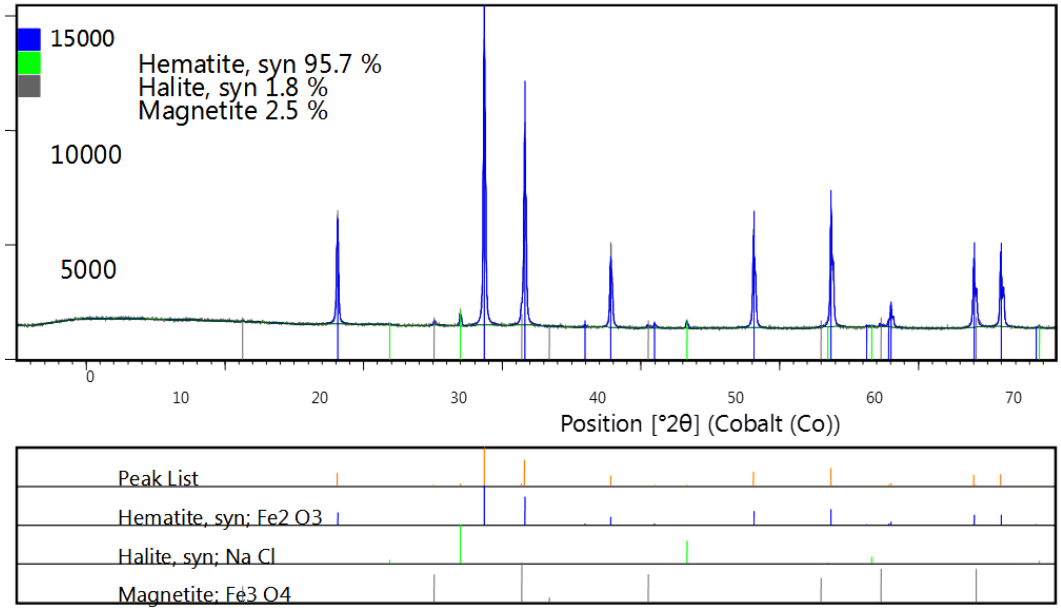

[A]: pH 1, Temperature 80^{o}C

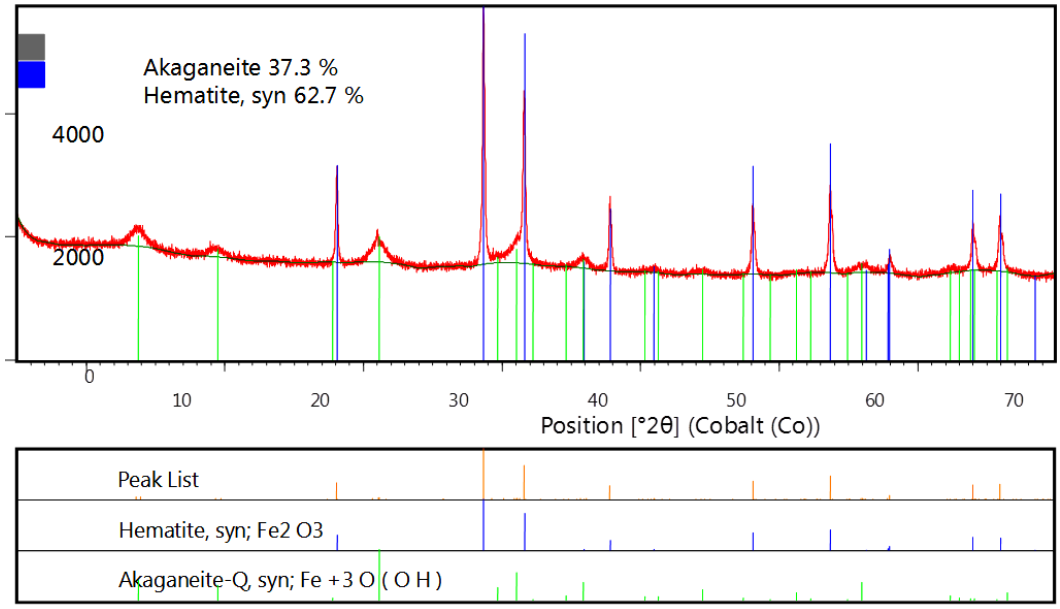

[B]: pH 1, Temperature 60^{o}C

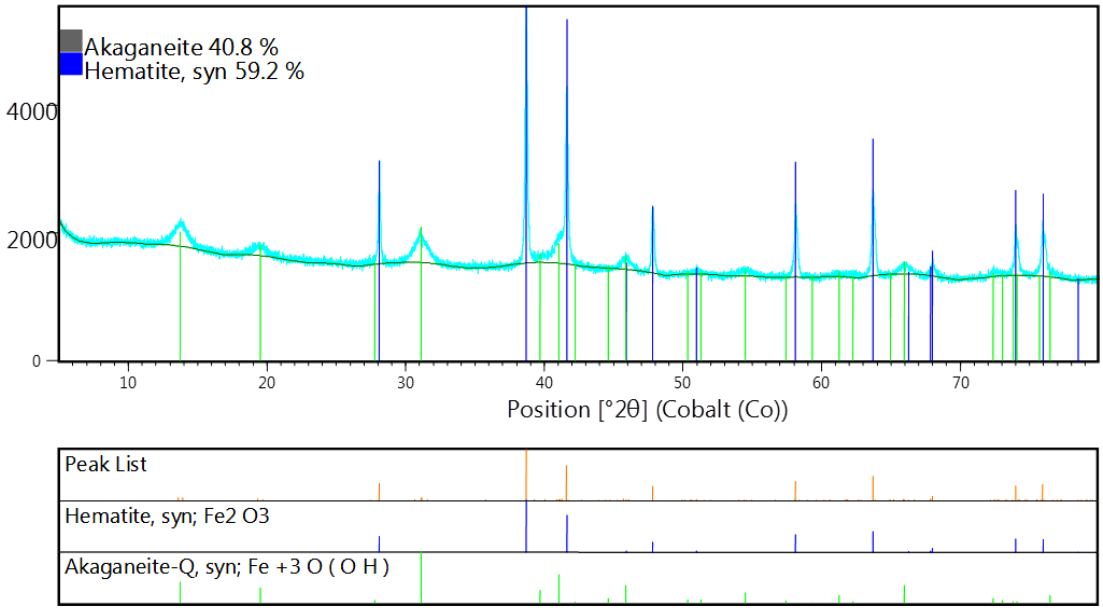

[C]: pH 2, Temperature 80^{o}C

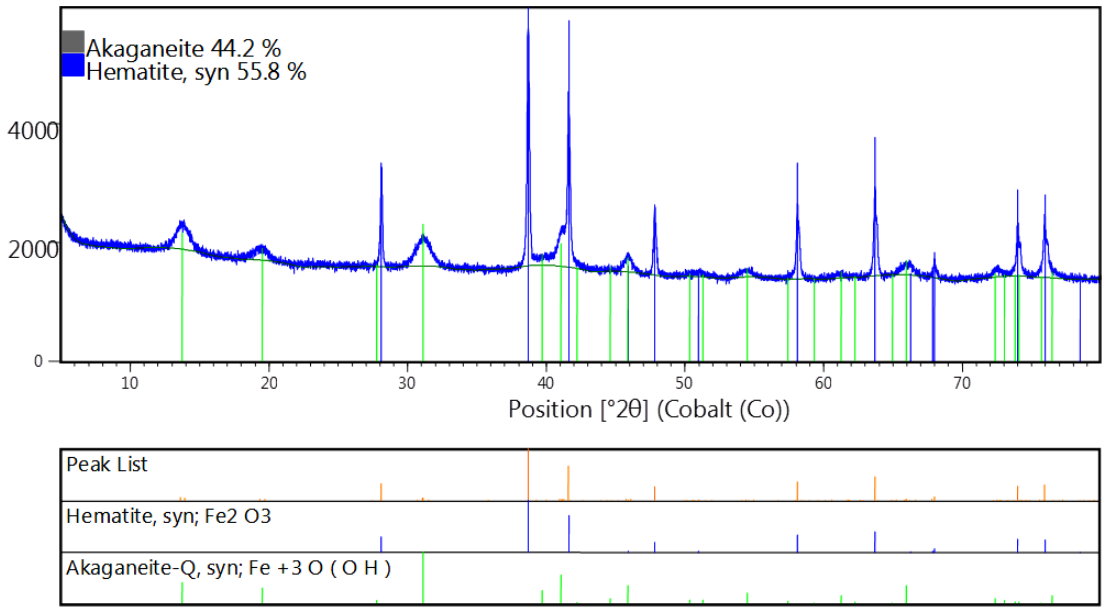

[D]: pH 3, Temperature 80^{o}C

Figure 4.24. XRD analysis of seeded hematite precipitate produced at varying temperature and pH

4.4. Solid–liquid separation

4.4.1. Filtration

4.4.1.1. Iron phosphate filtration

From Figure 4.25, it can be seen that iron phosphate precipitates produced at all conditions tested were easily filterable. The filtration rates ranged from 50 mL/min to over 100 mL/min. The filtration rates increased with increase in temperature and appeared to be influenced by the pH. The increase in filtration rate with temperature may be attributed to the increase in filter cake porosity.

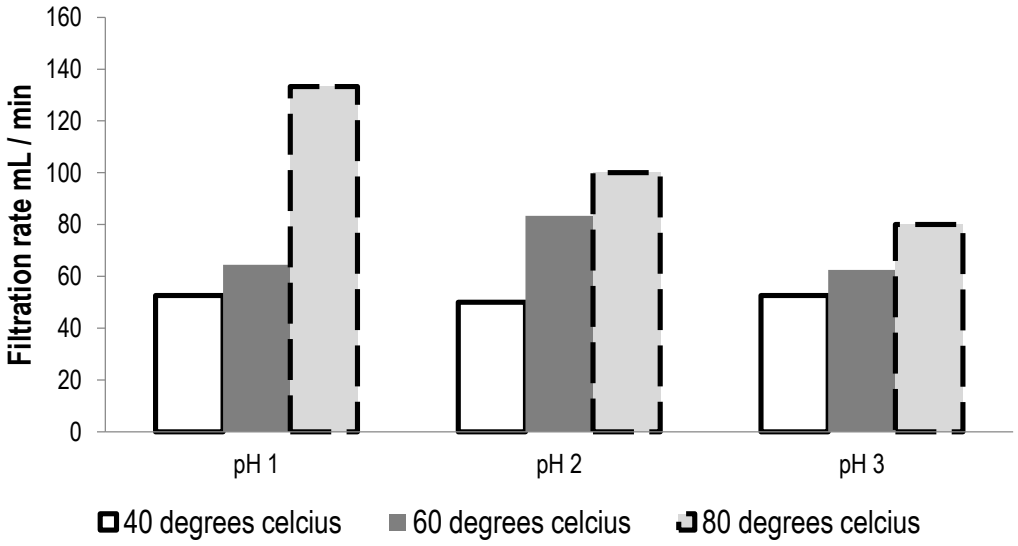

Figure 4.25. Iron phosphate filtration rates as a function of pH at various temperatures

It can be seen from Figure 4.26 that the particle sizes of the precipitated iron phosphate were significantly large. At 40°C the D50 particle sizes were in close range, regardless of the precipitation pH. At 40°C, the D50 particle sizes were 27 µm, 29 µm and 28 µm at pH 1, 2 and 3 respectively. As the temperature was increased to 60°C and 80°C, the D50 particle sizes varied more widely with pH change.

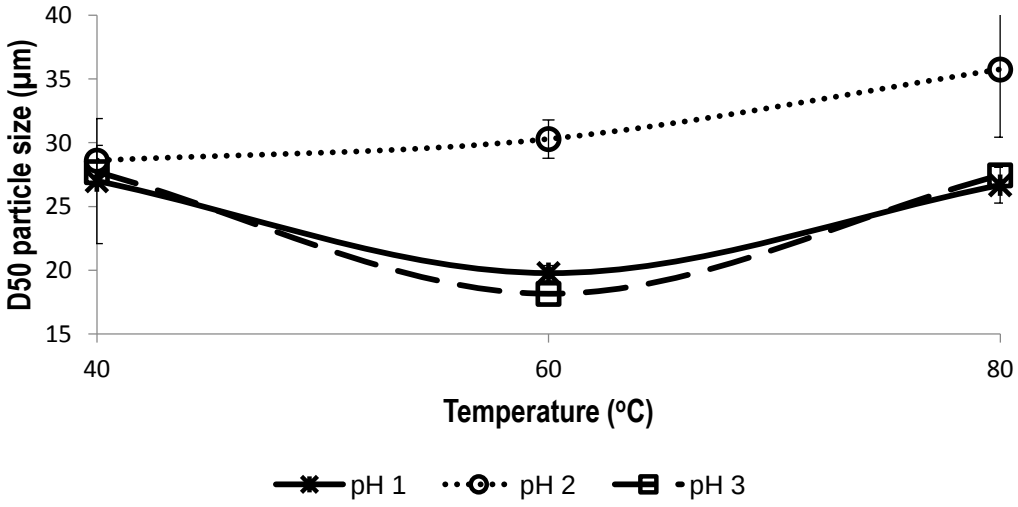

Figure 4.26. Iron phosphate D50 particle size as a function of temperature at various pH points including error bars depicting the standard deviations obtained from 3 runs for each point

As discussed in Section 2.4.1, resistance to filtration is inversely proportional to the particle size because larger particles are expected to have higher void fractions. Assuming uniform cake thickness and similar Van der Waals attractions between primary particles, the rate of filtration is expected to increase with increase in particle size. As can be seen in Figure 4.25 and Figure 4.26, the expected trend was not entirely satisfied. The filtration rate at 80^{o}C did not follow the particle size distribution. At this point, it is not clear why this was the case.

4.4.1.2. Hematite filtration

It was practically impossible to filter precipitates produced without hematite seed. It took 120 minutes to filter about 200 mL. All seeded experiments were easily filtered. The filtration rate was between 35 mL/min to over 100 mL/min, depending on the operating pH and temperature.

Cohen et al. (2005) reported similar results. Seeding improved the filtration rate of precipitates produced at pH 0.9 and 70^{o}C, 100^{o}C and 110^{o}C temperature points. This was attributed to the formation of hematite in seeded precipitation as opposed to unseeded precipitation which yielded akaganeite. It was reported that it took 430 minutes to filter a litre of unseeded precipitates produced at pH 0.9, 100^{o}C and retention time of 24 h. However, seeded experiments took 10 to 40 minutes to filter 500 mL.

From Figure 4.27, it can be seen that filtration rate increased with increase in pH. This increase in filtration rate with pH can be attributed to the formation of aggregates and agglomerates. Comparing Figure 4.26 and Figure 4.28, it can be observed that the phosphate D50 particle sizes were larger than the hematite D50 particle sizes. Smaller particles have a higher tendency to form aggregates and agglomerates than larger particles. The formation of aggregates and agglomerates is enhanced by decreasing the potential difference between the surfaces of the precipitate and the parent solution (zeta potential). The zeta potential decreases with increase in solution pH.

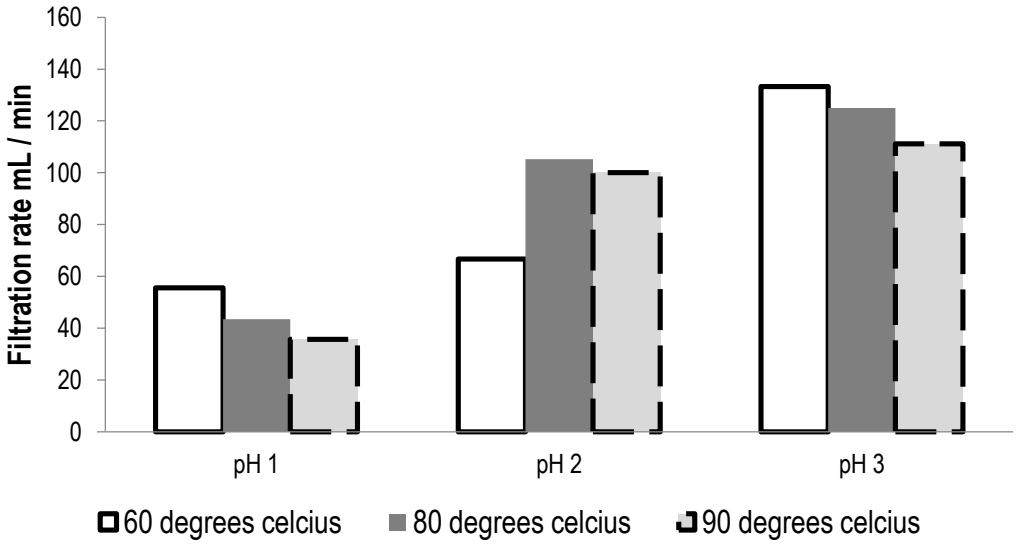

Figure 4.27. Hematite filtration rates as a function of pH at various temperatures

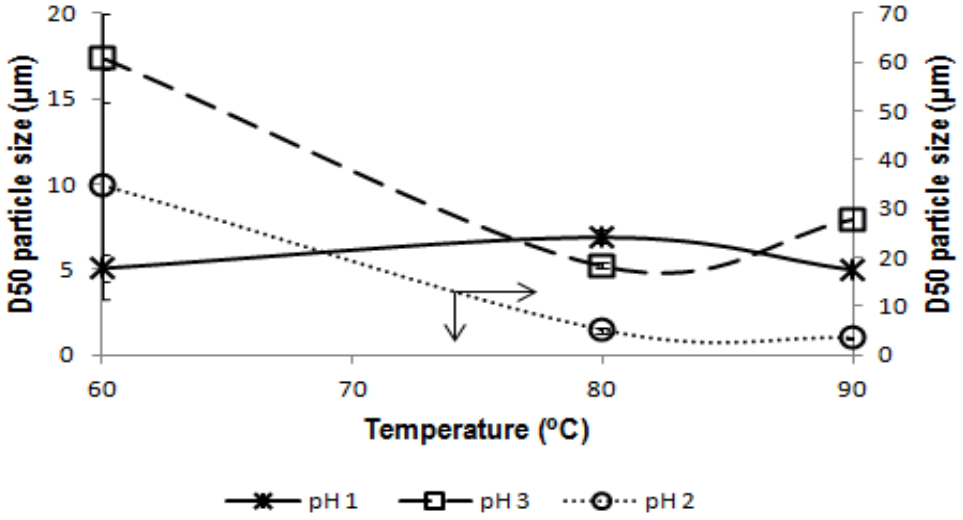

Figure 4.28. Hematite D50 particle size as a function of temperature at various pH points including error bars depicting the standard deviations obtained from 3 runs for each point

4.4.2. Settling rates

4.4.2.1. Iron phosphate settling

Figure 4.29 shows the settling profile of seeded iron phosphate, precipitated at pH 1 and 40°C, as obtained from MATLAB interface tool. The different color profiles indicate the distinction of solids from liquids. The color threshold of 0.1 and below signifies clear liquid while the color profile of 0.8 and above signifies

the solid phase. It can be seen that after 1572 seconds, iron phosphate completely settled with a definite solid-liquid interface.

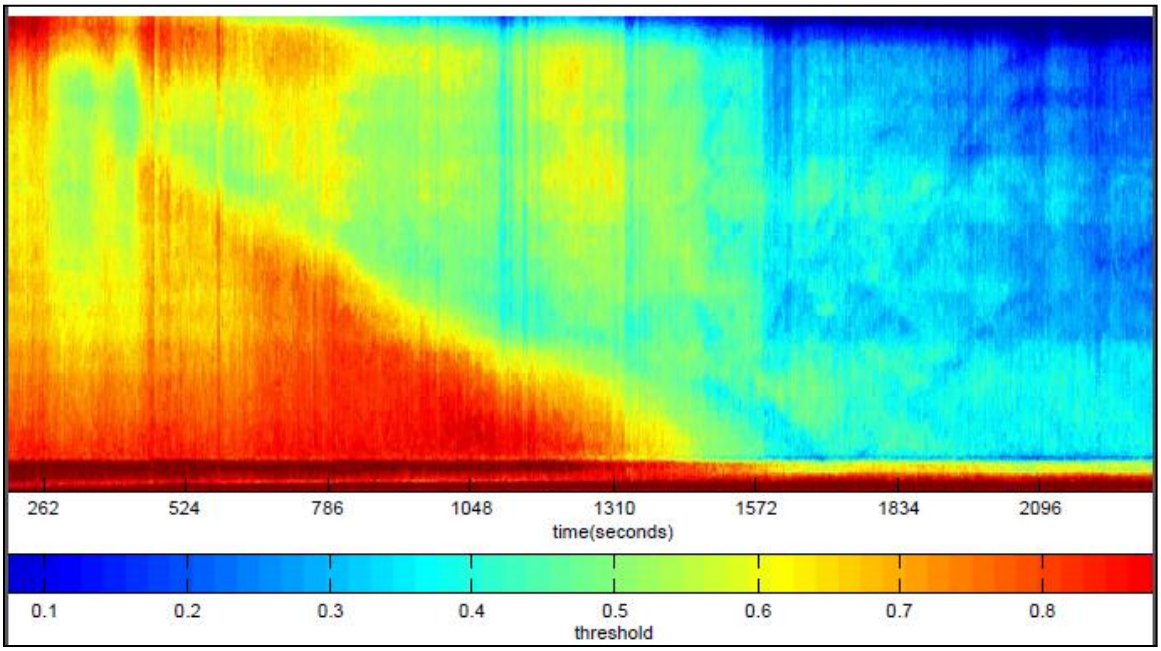

Figure 4.29. Settling profile of seeded, unfloculated iron phosphate precipitated at pH 1 and 40^{o}C

It can be noted from Figure 4.30 that as the pH was increased, the clarity of the solid-liquid interface slightly reduced, although the D50 particle sizes (at pH 1 and pH 2) are comparable at 40^{o}C. It is not clear at the moment why this was the case.

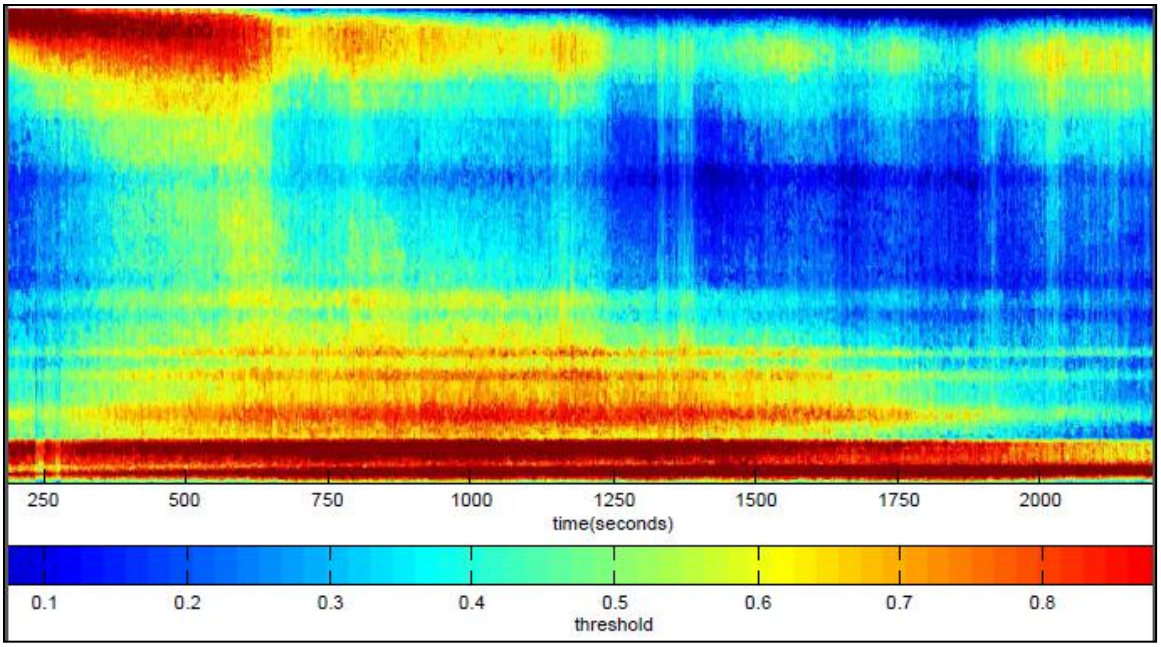

Figure 4.30. Settling profile of seeded, unfloculated iron phosphate precipitated at pH 2 and 40^{o}C

4.4.2.2. Hematite settling

Figure 4.31 and Figure 4.32 shows the settling profiles of hematite precipitates produced at pH 1 and 2 respectively. Similar to images obtained during iron phosphate settling tests, the different color profiles indicate the distinction of solids from liquids. It can be seen that it was practically impossible to settle hematite by gravity. This may be attributed to the particle morphology, particle size, particle density and particle surface characteristics of hematite.

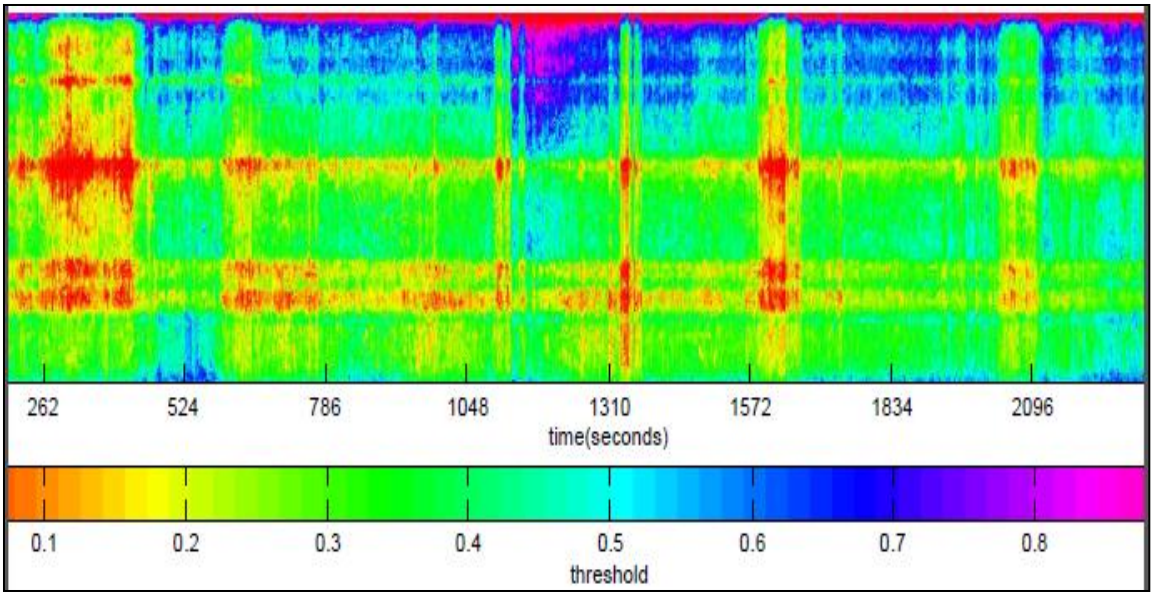

Figure 4.31. Settling profile of seeded and unfloculated hematite precipitated at pH 1 and 80°C

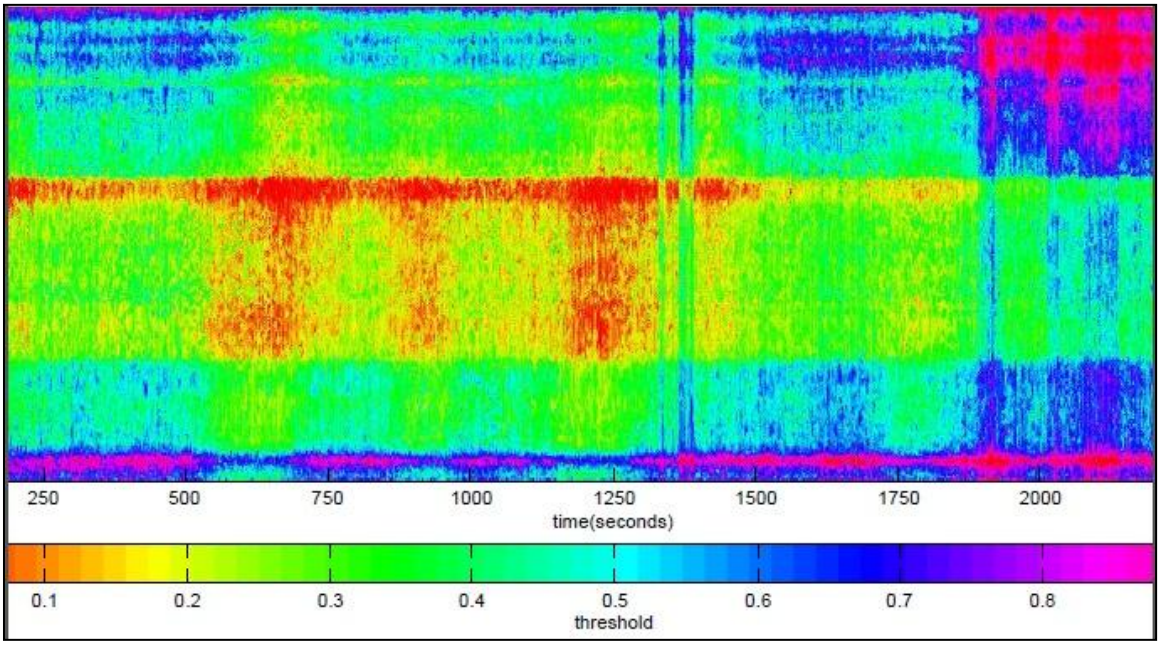

Figure 4.32. Settling profile of seeded and unfloculated hematite precipitated at pH 2 and 80°C

4.5. Comparison of the Phosphate and the Hematite process

Based on the experimental results obtained, a comparison of key parameters in iron phosphate precipitation and hematite precipitation is summarized in Table 4.4.

Table 4.4. Summarized comparison of key parameters in iron phosphate and hematite precipitation

Parameter	**Iron phosphate**	**Hematite**
Iron removal	98.8% iron is removed from solution	99.78% removal
Nickel loss	1% minimum - 9% maximum	3% minimum - 10% maximum
Copper loss	3% minimum - 19% maximum	2% minimum - 11% maximum
Retention time	30 min	60 min
pH	pH 1	pH 1
Temperature	40^{o}C	80^{o}C
Seeding	Unseeded precipitation resulted in increased nickel and copper loss	Unseeded precipitation not only resulted in higher nickel and copper loss but also poor filtration
Filtration	50 mL/min to over 100mL/min	35 mL/min to over 100 mL/min
Sedimentation	Settling was almost complete after 26 min	No settling observed
Reagents	Neutralizing reagent (NaOH) and PO_4^{3-} are required. The $PO4^{3-}$ has been reported to be regenerated	Only a neutralizing reagent is required (NaOH)
Precipitate color	Bright yellow, easy to clean precipitates	Deep red, difficulty to clean precipitates

5. PLANT SOLUTION EXPERIMENTS AND MASS BALANCE

Results obtained using synthetic solutions suggested a significant basis for exploring the potential for iron removal by molecular oxygen oxidation followed by either iron phosphate precipitation or hematite precipitation, at atmospheric conditions. It was expected that real plant solutions would contain varying concentrations of iron, nickel, copper and additional ions. To check the direct applicability of the results obtained using synthetic solutions, plant solutions were obtained and further experiments conducted.

5.1. Plant solution characterization

The plant solution chemical composition, as analysed by the Stellenbosch University Central Analytical Facility (CAF) laboratory and Stellenbosch University Department of Process Engineering laboratory are shown in Table 5.1.

Table 5.1. Plant solution chemical composition

Plant solution composition (g/L)							
	Fe	Ni	Cu	Co	P	Na	Cl^-
Sample 1	125.6	12.6	0.1	0.1	8.8	0.7	368.0
Sample 2	116.0	11.6	0.1	0.1	8.9	0.0	340.0
Sample 3	114.2	11.5	0.1	0.1	8.8	0.0	310.0

The acidity of the plant solutions was calculated. The analysed total chloride ion was used to calculate the HCl concentration in the plant solution. It was assumed that the chloride ions were paired with cations present in solution (Fe^{3+}, Fe^{2+}, Ni^{2+}, Cu^{2+}, Co^{2+} and Na^{+}) so that the compounds did not have net charges. The remaining chloride ions were assumed to be paired with the hydrogen ions (Dorfling, 2012). The calculated concentration of HCl in the plant solution was

about 5 M. The calculations are documented in APPENDIX H: [HCl] CALCULATIONS.

5.2. Oxidation runs

Figure 5.1 shows results obtained from plant solution oxidation experiments conducted using the experimental setup and procedure described in Section 3.1.2.2 and 3.1.2.3 respectively.

In order to ensure 1:1 complexation of iron with associated [HCl] (as discussed in Section 4.1.3); about 1.4 moles of HCl were added to a liter of plant solution. Dedicated oxidation experiments were conducted at about 6.4 M [HCl] and 80^{o}C. In the case of simultaneous oxidation and precipitation runs, plant solutions were neutralized from 6.4 M [HCl] to pH 0 using 15 M NaOH standard solutions. Simultaneous oxidation and precipitation experiments were conducted at pH 0 and 80^{o}C.

It can be seen from Figure 5.1 that over 97% oxidation of iron(III) was achieved within 180 minutes for dedicated oxidation experiments. This compares well with oxidation achieved (96%) using synthetic solutions containing 0.3 g/L copper concentration, 4.6 M [HCl] and about 50 g/L iron for the same temperature and reaction time. It was also noted that simultaneous oxidation and precipitation resulted in higher iron(III) yields, for the same reaction times. This is in line with the observations made using synthetic solutions.

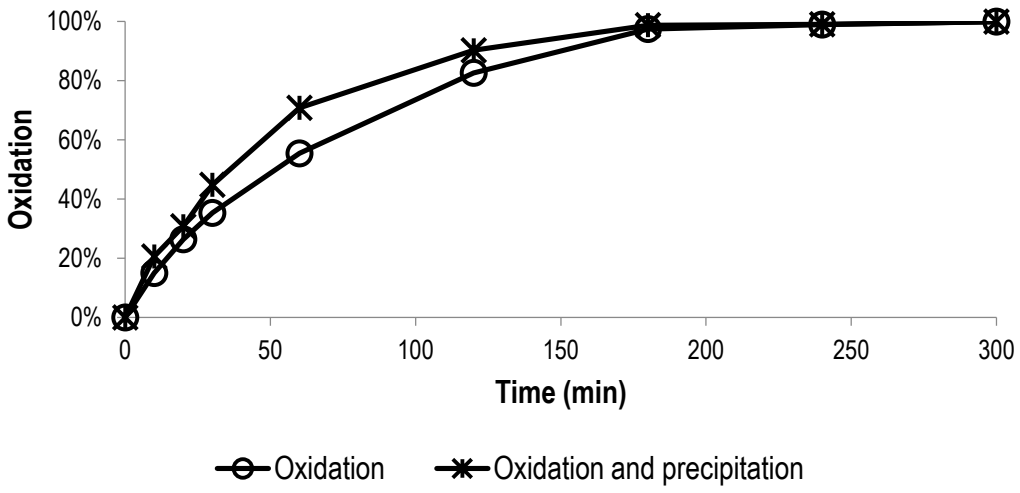

Figure 5.1. Plant solution average oxidation at 80°C for dedicated oxidation runs and simultaneous oxidation and precipitation runs

5.3. Precipitation runs

After conducting a number of trial runs, it was observed that it was not feasible to precipitate over 110 g/L iron while attempting to minimize nickel losses. It was evidenced that precipitating 110 g/L iron resulted in poor mixing. It was thought that poor mixing could lead to high nickel losses due to uneven supersaturated spots within the reactor. It was therefore decided to dilute the oxidized solutions about 2.5 times for the precipitation feed to contain about 45 – 40 g/L of iron and about 4.5 - 4 g/L of nickel.

5.3.1 Phosphate precipitation

It can be observed from Figure 5.2 that iron removal was complete within 20 minutes during iron phosphate precipitation at 40°C and pH 1. After 60 minutes, the nickel loss was 9.8%. After 120 minutes, the nickel loss reduced to 7.8%. A similar trend was noted during iron phosphate precipitation using synthetic solutions. The nickel losses increased with time during the initial stages of precipitation and thereafter the losses reduced, to some extent, with time. This could be caused by the dissolution and recrystallization of the precipitate with time.

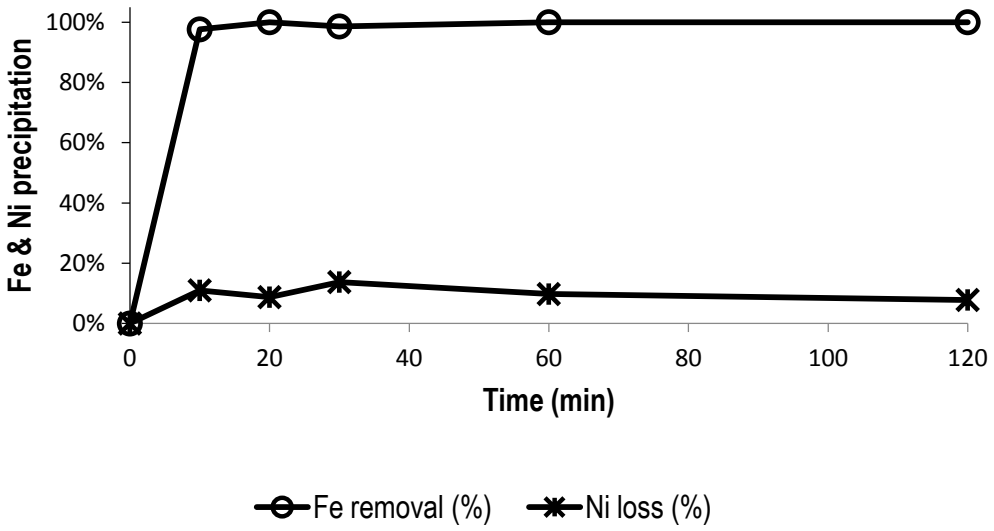

Figure 5.2. Iron removal and co-precipitation of nickel during seeded iron phosphate precipitation at 40°C and pH 1 as a function of time

Figure 5.3 shows the precipitation of iron and the loss of nickel during iron phosphate precipitation at 40°C and pH 0. It can be noticed that only 92% of iron was precipitated after 120 minutes. The corresponding nickel loss was lower than that observed at pH 1. The nickel loss was below 5%. It was expected that the nickel loss would reduce with reduction in pH but at the expense of iron removal.

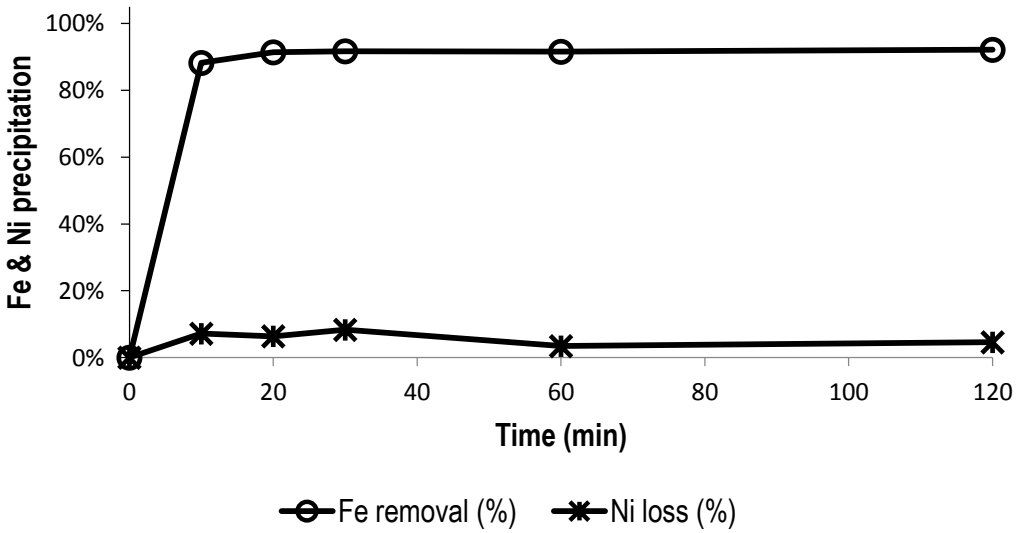

Figure 5.3. Iron removal and co-precipitation of nickel during seeded iron phosphate precipitation at 40°C and pH 0 as a function of time

Figure 5.4 shows iron removal and the co-precipitation of nickel during simultaneous oxidation and precipitation of ferric phosphate at 80°C and pH 0. It was observed that after 180 minutes, only about 97% of the initial iron was removed from solution. The nickel loss was however about 8%. Similar experiments conducted using synthetic solutions resulted in over 99% iron removal at the expense of over 20% nickel co-precipitation. Apart from the presence of additional ions that could influence speciation during precipitation of iron in plant solutions compared to synthetic solutions, the difference in results obtained under these conditions is unclear at this point.

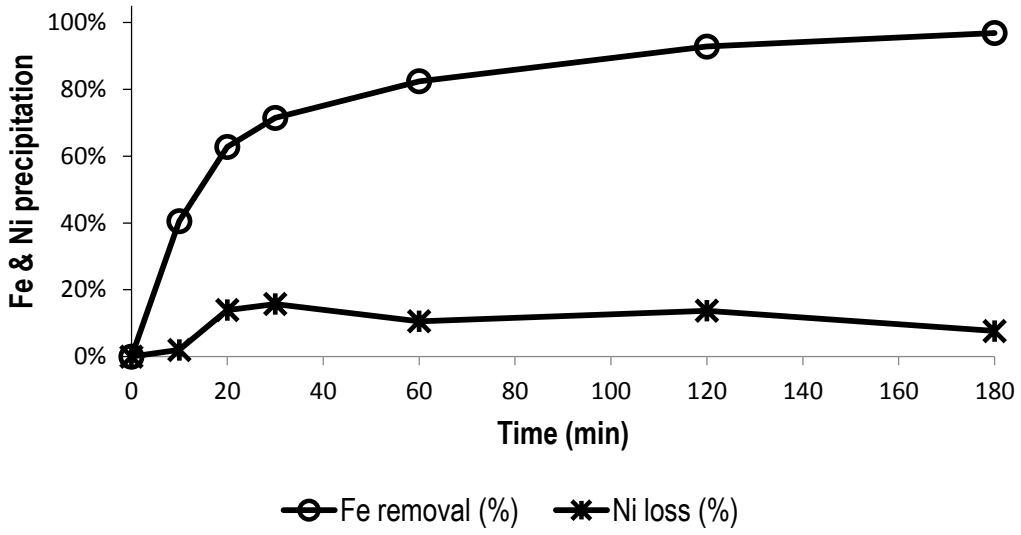

Figure 5.4. Iron removal and the co-precipitation of nickel during simultaneous oxidation and seeded precipitation at 80°C and pH 0 as a function of temperature

5.3.2 Hematite precipitation

Figure 5.5 shows the removal of iron and the resulting nickel loss with time, during seeded hematite precipitation at 80°C and pH 1. It was observed that iron removal was complete after 60 minutes. The corresponding nickel loss at 60 minutes was about 18% and reduced to 12% after 120 minutes of reaction. Even in seeded precipitation setups, metastable phases are known to precipitate and then transform into stable and relatively more pure phases with time. It is proposed that the concentration of akaganeite (a metastable phase) after 60

minutes of precipitation is higher than after 120 minutes, hence the reduction in nickel co-precipitation with time.

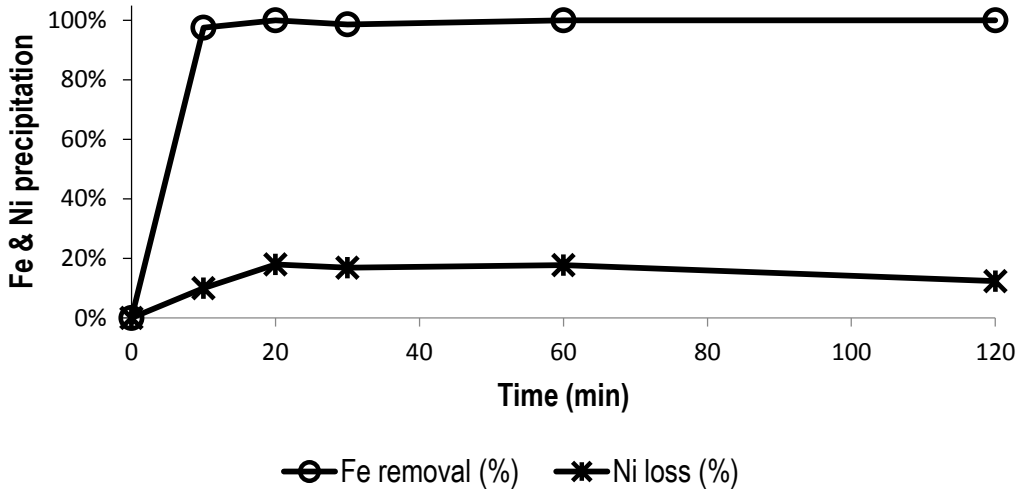

Figure 5.5. Iron removal and co-precipitation of nickel during seeded hematite precipitation at 80°C and pH 1 as a function of time

Similar to observations made during iron phosphate precipitation at 40°C and pH 0, Figure 5.6 shows that 92% of the initial iron was removed after 120 minutes. As expected, the nickel co-precipitation (8%) was lower at pH 0 compared to pH 1.

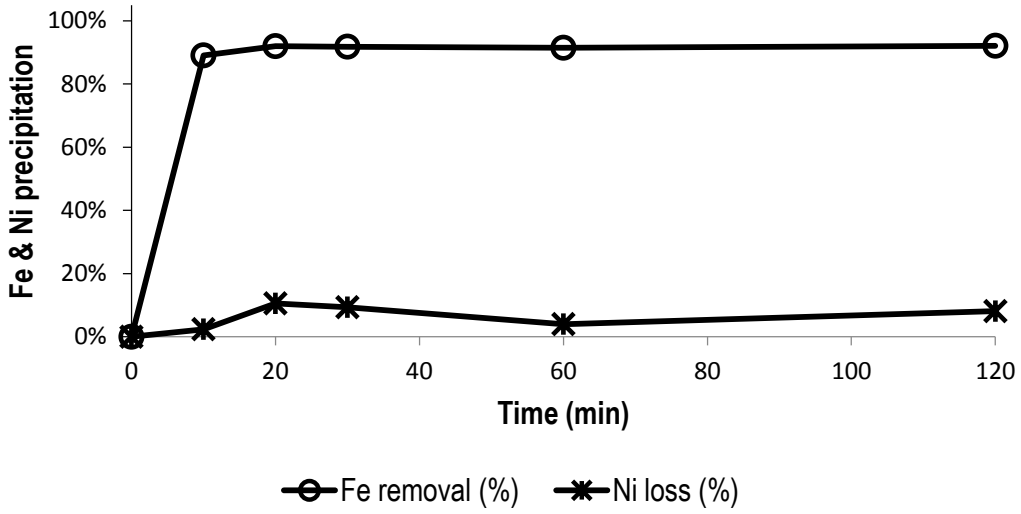

Figure 5.6. Iron removal and co-precipitation of nickel during seeded hematite precipitation at 80°C and pH 0 as a function of time

5.4. Suggested flowsheets and mass balances

Simultaneous oxidation and precipitation was observed to have a shorter overall residence time than separate oxidation and precipitation. Furthermore, separate oxidation and precipitation steps would have a greater equipment requirement compared to simultaneous oxidation and precipitation. Simultaneous oxidation and precipitation therefore appears feasible however, the extent of iron removal (only 97% removal) suggests further improvement was required.

Figure 5.7 and Figure 5.8 shows the proposed iron phosphate and hematite precipitation flowsheets respectively. The stream balances are shown in Table 5.2 and Table 5.3 respectively. The individual stream balances are calculated on the basis of 1 liter plant solution, ICP analysis of plant solutions and the iron depleted solutions, and the stoichiometric calculated reagent addition. The stream calculations are documented in APPENDIX F: MASS BALANCE STREAMS.

In both phosphate and hematite processes, it is suggested that HCl be added at oxidation stage to satisfy the complete complexation of iron by associated HCl for rapid oxidation of iron(II). For decent mixing and handling of the precipitation process, the plant solution containing over 110 g/L iron can be diluted 2.5 times after the oxidation process and prior to the precipitation process. Solid-liquid separation can be achieved by filtration, in both the iron phosphate process and the hematite process.

In both iron phosphate and hematite process, complete iron removal was achieved at pH 1. The operating temperature in the iron phosphate process was 40^{o}C, compared to 80^{o}C in the case of hematite process. At pH 1 and 40^{o}C, after 120 minutes, the nickel loss in the iron phosphate process was reduced to 7.8%. In the hematite process, at pH 1 and 80^{o}C, the nickel loss was reduced to 12%. In the case of the iron phosphate process, as demonstrated in Section 4.4.2, sedimentation is a viable option. The iron phosphate process had more sodium and phosphorous reporting in the iron depleted solution compared with the

hematite process. Treatment of 1 L plant solution resulted in about 140.6 g sodium and 10.3 g phosphorous reporting in the iron depleted solution, in the case of iron phosphate process. In the hematite process, 85 g of sodium reported in the iron depleted solution. All the phosphorous initially present in the plant solution (about 8.8 g) reported in the hematite precipitate. Provided that the consequences of sodium and phosphorous in iron depleted solution are fully evaluated with regards to the downstream processing of nickel, iron phosphate flowsheet appears more suitable to implement, mainly due to the lower nickel loss and lower operating temperature compared with the hematite flowsheet.

The solution depleted of iron can proceed to nickel recovery. Options for downstream nickel and copper recovery have been suggested in APPENDIX G: GENERAL PROCESS OPTIONS.

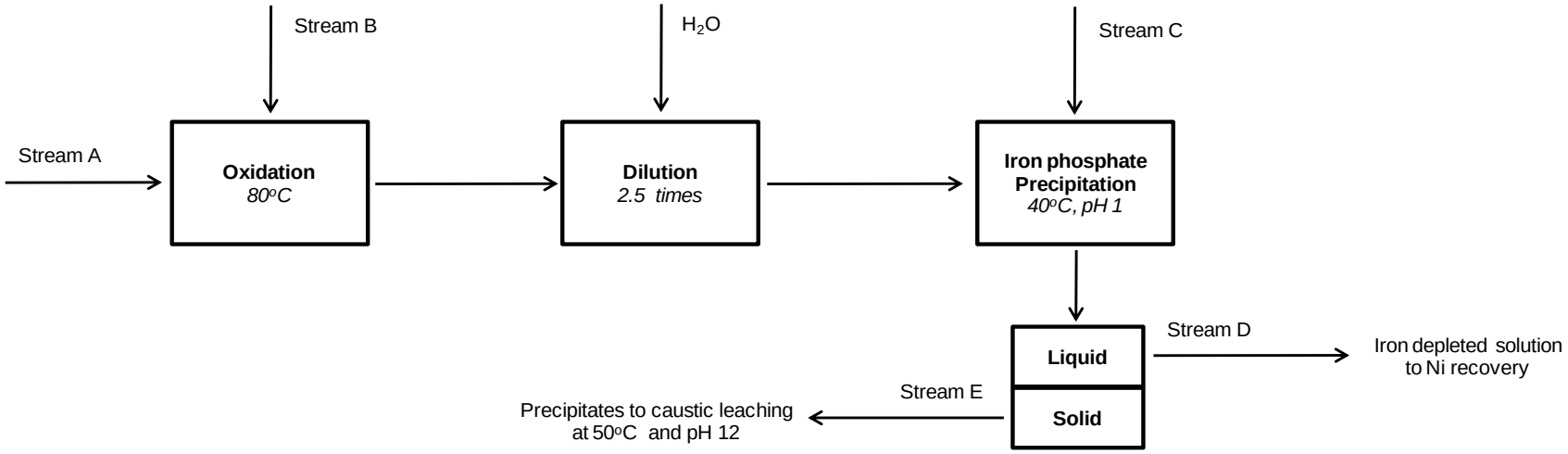

Figure 5.7. Iron phosphate - oxidation and precipitation process flowsheet

Table 5.2. Iron phosphate flowsheet mass balance

Stream	Stream name	System species per Litre of plant solution (g)						
		Fe	**Ni**	**Cu**	**Co**	**Na**	**P**	**Cl**
A	Plant solution	125.6	12.6	0.1	0.1	0.7	8.8	368.0
B	HCl addition							49.7
C	Reagent - $FePO_4$ seed, Na_3PO_4, NaOH	8.9				278.0	74.4	
	Total input	*134.5*	*12.6*	*0.1*	*0.1*	*278.7*	*83.2*	*417.7*
D	Fe depleted solution	0.0	11.6	0.1	0.1	140.6	10.3	204.5
E	$FePO_4$ precipitate	134.5	1.0	0.0	0.0	138.1	72.9	213.2
	Total output	*134.5*	*12.6*	*0.1*	*0.1*	*278.7*	*83.2*	*417.7*

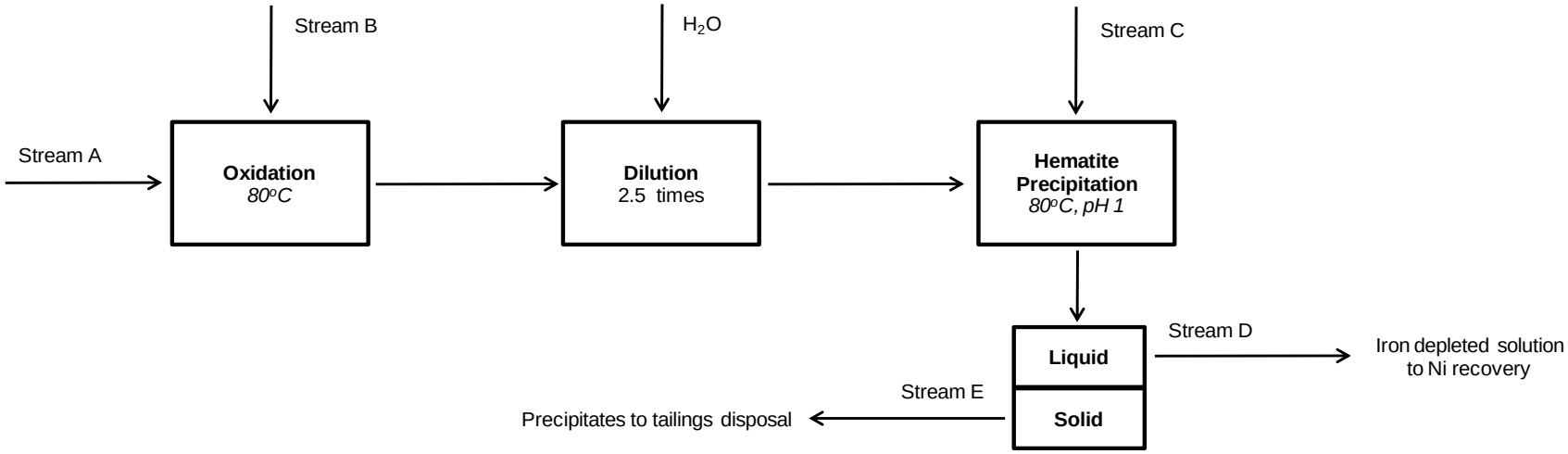

Figure 5.8. Hematite – oxidation and precipitation flowsheet

Table 5.3. Hematite flowsheet mass balance

Stream	Stream name	System species per Litre of plant solution (g)						
		Fe	**Ni**	**Cu**	**Co**	**Na**	**P**	**Cl**
A	Plant solution	125.6	12.6	0.1	0.1	0.7	8.8	368.0
B	HCl addition							49.7
C	Reagent - Fe_2O_3 seed, NaOH	20.9				124.0		
	Total input	*146.5*	*12.6*	*0.1*	*0.1*	*124.7*	*8.8*	*417.7*
D	Fe depleted solution	0.0	11.0	0.1	0.1	85.3	0.0	355.0
E	Fe_2O_3 precipitate	146.5	1.6	0.0	0.0	39.4	8.8	62.7
	Total output	*146.5*	*12.6*	*0.1*	*0.1*	*124.7*	*8.8*	*417.7*

6. CONCLUSIONS AND RECOMMENDATIONS

The oxidation mechanism of iron(II) in chloride medium has been illustrated. It has been shown that nickel and copper losses are significantly affected by the quality of iron precipitate. The quality of iron precipitate is affected by the supersaturation level during precipitation. Hematite and iron phosphate precipitation has been evaluated and compared using experimental data.

The objectives of the study were achieved and the conclusions are summarized in this chapter.

6.1. Effect of [HCl] and Cu concentration on oxidation

Data from a series of experiments was analysed to determine the effect of hydrochloric acid on iron(II) oxidation by molecular oxygen. At [HCl] above 4 M, oxidation of about 0.9 M iron(II) was rapid, compared to below 4 M.

Equilibrium calculations were performed using specific HCl equilibrium dissociation constants to determine the equilibrium concentrations of associated and dissociated HCl for various acid concentrations. Experimental data and equilibrium calculations proved that rapid oxidation of iron(II) was triggered when the associated [HCl] to iron ratio was equal to 1 and above. This ratio satisfies the stoichiometric requirement of associated HCl for complete complexation with iron.

Although the mechanism by which copper catalyses iron(II) oxidation was not clear, it is suggested that copper(II) gains an electron from iron(II) to produce copper(I) and iron(III) in a redox reaction. Experimental data proved the catalytic effect of copper during the oxidation of iron(II). This catalytic effect was more emphasized at low acid concentrations.

6.2. Effect of operating conditions on precipitate quality

It has been shown that supersaturation influences the level of nickel and copper co-precipitation during the precipitation of both hematite and iron phosphate. It has been demonstrated that the lower the supersaturation, the lower the co-precipitation of nickel and copper. This is because lower supersaturation promotes growth controlled precipitation rather than nucleation controlled precipitation. Growth controlled precipitation is less likely to trap the solution containing nickel and copper. The pH and temperature proved to be effective ways of controlling supersaturation levels.

Iron phosphate precipitation at pH 3 and temperature 80^{o}C for 30 minutes retention time resulted in over 99% iron removal however, with high nickel and copper co-precipitation (50% and 53%, respectively). Reducing the pH and temperature to 1 and 40^{o}C resulted in minimal nickel and copper co-precipitation (less than 1% and 4%, respectively) for the same reaction time.

Hematite precipitation at pH 1 and temperature 80^{o}C, for a reaction time of 60 minutes, resulted in 3% nickel and copper co-precipitation with almost complete iron removal. Increase in the pH, from 1 to 3, also ensured almost complete iron removal (above 99%) but at the expense of nickel and copper co-precipitation of 28% and 58% respectively.

Iron phosphate precipitation was almost complete and attained equilibrium, with minimal co-precipitation, after 30 minutes. In the hematite process, complete iron removal with minimal nickel and copper loss was established after 60 minutes.

It was shown that seeding was essential to precipitate hematite. Precipitates produced at pH 1 and 80^{o}C (after 60 minutes reaction time) in the absence of the hematite seed could not be practically filtered and the nickel and copper co-precipitation were as high as 19% and 33% respectively. It was observed that in the absence of seed, iron phosphate also co-precipitated higher nickel and copper, 17% and 28% respectively, at pH 1 and 40^{o}C (after 30 minutes reaction

time). The losses however reduced to 8% and 18% after 60 minutes retention time.

In order to minimize co-precipitation of nickel and copper in the iron phosphate precipitation process, by means of supersaturation control, low pH and low temperatures should be maintained. Seeding greatly reduces the amount of co-precipitation.

Seeding is critical for the precipitation of hematite at temperatures below 100^{o}C. A lower pH should be adopted as a means of controlling supersaturation during the precipitation of hematite.

6.3. Comparison of hematite and iron phosphate precipitation

The quality of seeded hematite precipitates produced at pH 1 and 80^{o}C and the quality of seeded iron phosphate precipitates produced at pH 1 and 40^{o}C were compared in terms iron removal, copper and nickel co-precipitation, retention time, sodium chloride contamination and solid-liquid separation.

Iron phosphate precipitation attained equilibrium, with less than 1% and 4% nickel and copper loss respectively; within 30 – 60 minutes while it took 60 – 120 minutes for hematite precipitation to attain equilibrium with 3% nickel and copper loss. Both seeded iron phosphate and seeded hematite were easily filterable. The average filtration rates for iron phosphate and hematite were 53 mL/minute and 43 mL/minute respectively. A clear solid–liquid interface was obtained in the case of iron phosphate after 26 minutes of gravity sedimentation, however in the case of hematite; no settling was seen after 8 h.

In this study, it has been made clear that the traditionally superior iron removal method, the Hematite process, can be replaced by the low temperature iron phosphate precipitation process. The degree of iron removal in iron phosphate precipitation process and hematite precipitation process are comparable while lower losses of nickel and copper are generally observed in iron phosphate precipitation compared to hematite precipitation.

6.4. Recommendations

The following are the study recommendations:

- Experimental verification of the recovery of nickel and copper from a solution depleted of iron, as outlined in this study, should be considered for future work.
- In order to accurately predict the rate of oxidation and precipitation, it is recommended that rate expressions should be derived, building from the experimental data and knowledge of key parameters obtained from this study.

7. REFERENCES

Allen, R.W, Haigh, C.J., Hamdorf, C.J., 1970. An improved method of removing dissolved ferric iron from iron bearing solutions. *Australian Patent*, Patent number 424095

Asokan, P., Saxena, M., Asolekar, S.R., 2006. Hazardous jarosite use in developing non-hazardous product for engineering application. *Journal of Hazardous Materials* 137, 1589 – 1599

Astanina, A.N., Rudenko, A.P., 1971. Effect of acids on homogenous oxidation of iron(II) by molecular oxygen in aqueous solution. *Russian Journal of Physical Chemistry* 47, 194

Awakura, Y., Majima, H., Iwai, M., 1986. Oxidation of iron(II) in HCl and H_2SO_4 solutions with dissolved molecular oxygen in the presence and absence of a cupric catalyst, In: J.E. Dutrizac and A.J. Monhemius (eds.), *Iron Control in Hydrometallurgy*. Ellis Horwood Ltd., Chichester pp. 202 – 222

Babcan, J., 1971. Die synthese von jarosit $KFe_3(SO_4)_2(OH)_6$. Geologicky Zbornik - *Geologica Carpathica* 22, 299 – 304

Beck, L.W., Soltani, M., Wang, L., 2011. Ferric phosphate and methods of preparation thereof. *United States Patent*, Patent number US 2011/0068295 A1

Betancourt, F., Burger, R., Diehl, S., Faras, S., 2013. A model of clarifier - thickener control with time dependent feed properties. *Presented at Physical Separation 2013, Falmouth, United Kingdom*

Birch, D., Ahmed, N., 1995. Gas sparging in vessels agitated by mixed flow impellers. *Powder Technology* 88, 33 – 38

Burger, R., Wendland, W.L., 2001. Sedimentation and suspension flows: Historical perspective and some recent developments. *Journal of Engineering Mathematics* 41, 101 – 116

Chang, Y., Zhai, X., Li, B., Fu, Y., 2010. Removal of iron from acidic leach liquor

of lateritic nickel ore by goethite precipitate. *Hydrometallurgy* 101, 84 – 87

Chen, T.T., Dutrizac, J.E., 1990. Practical mineralogical techniques for the characterization of hydrometallurgical products. *The Minerals, Metals and Material Society*, Warrendale Pennsylvania, 289 – 309

Claassen, J.O., Meyer, E.H.O., Rennie, J., Sandenbergh, R.F., 2002. Iron precipitation from zinc-rich solutions: defining the Zincor Process. *Hydrometallurgy* 67, 87 – 108

Claassen, J.O., Sandenbergh, R.F., 2006. Particle growth parameters in the precipitation of metastable iron phases from zinc - rich solutions. *Hydrometallurgy* 84, 165 – 174

Claassen, J.O., Sandenbergh, R.F., 2007a. Influence of temperature and pH on the quality of metastable iron phases produced in zinc - rich solutions. *Hydrometallurgy* 86, 178 – 190

Claassen, J.O., Sandenbergh, R.F., 2007b. Influence of mixing on the quality of iron precipitates in zinc - rich solutions. *Hydrometallurgy* 87, 112 – 123

Claassen, J.O., 2006. Product quality parameters in the reaction crystallization of metastable iron phases from zinc - rich solutions. *Ph.D. thesis*, Department of Material Science and Metallurgical Engineering, University of Pretoria, Pretoria South Africa

Cohen, B., Shipley, D.S., Tong, A.R., Casaroli, S.J.G., Petrie, J.G., 2005. Precipitation of iron from concentrated chloride solutions: Literature observations, challenges and preliminary experimental results. *Minerals Engineering* 18, 1344 – 1347

Colborn, R.P., Nicol, M.J., 1973. An investigation into the kinetics and mechanism of the oxidation of iron (II) by oxygen in aqueous chloride solutions. *The Journal of The South African Institute of Mining and Metallurgy* 73(9), 281 – 289

Coll, M.T., Fortuny, A., Kedari, C.S., Sastre, A.M., 2012. Studies on the extraction of Cobalt(II) and Nickel(II) from aqueous chloride solutions using Primene JMT-Cyanex 272 ionic liquid extractant. *Hydrometallurgy* 125 - 126, 24 – 28

Crundwell, F.K., Moats, M.S., Ramachandran, V., Robinson, T.G., Davenport, W.G., 2011a. Separation of Nickel and Cobalt by Solvent Extraction. In: *Extractive Metallurgy of Nickel, Cobalt and Platinum Group Metals*. Elsevier, pp. 315 – 326

Crundwell, F.K., Moats, M.S., Ramachandran, V., Robinson, T.G., Davenport, W.G., 2011b. Hydrometallurgical Production of High - Purity Nickel and Cobalt. In: *Extractive Metallurgy of Nickel, Cobalt and Platinum Group Metals*. Elsevier, pp. 281 – 299

Cruz, A., Lastra, M., Menacho, J., 1980. Removal of iron from copper leach solutions by using phosphate compounds. *Mining and Metallurgical Research Centre*, Santiago, Chile, pp. 105 – 112

Danckwerts, P.V., 1970. *Gas - Liquid Reactions*. McGraw - Hill, New York

Davey, P.T., Scott, T.R., 1975. Removal of iron from leach liquors by the “Goethite” process. *Hydrometallurgy* 2, 25 – 33

Demopoulos, G.P., 2009. Aqueous precipitation and crystallization for the production of particulate solids with desired properties. *Hydrometallurgy* 96, 199 – 214

Demopoulos, G.P., Gefvert, D.L., 1984. Iron(III) removal from base metal electrolyte solutions by solvent extraction. *Hydrometallurgy* 12, 299 – 315

Dirksen, J.A., Ring, T.A., 1991. Fundamentals of crystallization: kinetic effects on particle size distributions and morphology. *Chemical Engineering Science* 46, 2389 – 2427

Dorfling, C., 2012. Characterisation and dynamic modelling of the behaviour of platinum group metals in high pressure sulphuric acid/oxygen leaching systems. *Ph.D. Dissertation*, Department of Process Engineering, Stellenbosch University, South Africa

Dreisinger, D.B., Peters, E., 1989. The oxidation of ferrous sulphate by molecular oxygen under zinc pressure-leach conditions. *Hydrometallurgy* 22, 101 – 119

Dutrizac, J.E., 1991. The precipitation of lead jarosite from chloride media. *Hydrometallurgy* 26, 327 – 346

Dutrizac, J.E., Riveros, P.A., 1999. The precipitation of hematite from ferric chloride media at atmospheric pressure. *Metallurgical and Materials Transactions* B 30, 993 – 1001

Dutrizac, J.E., Monhemius, A.J., 1986. *Iron control in hydrometallurgy*. Ellis Horwood Ltd

Filippou, D., Cheng, T.C., Demopoulos, G.P., 2000. Gas – liquid oxygen mass transfer; from fundamentals to applications in hydrometallurgical Systems. *Mineral Processing and Extractive Metallurgy Review* 20, 447 – 502

Free, M.L., 2013. *Hydrometallurgy: Fundamentals and Applications*. Hoboken, New Jersey: Wiley

Garole, D.J., Garole, V.J., Dalal, D.S., 2012. Recovery of metal value from electroplating sludge. *Research Journal of Chemical Sciences* 2, 61 – 63

George, P., 1954. Oxidation of Ferrous Perchlorate by Molecular Oxygen, *Journal of the Chemical Society*, 4349 – 4359

Georges, B., Gaunand, A., Renon, H., 1987. Oxidation of iron(II) by Oxygen in Concentrated NaCl solutions: Prediction of stirred gas - liquid reactor performance from homogeneous kinetic data. *Hydrometallurgy* 19, 25 – 35

Gupta, C.K., 2003. *Chemical Metallurgy Principals and Practice*, 1st ed. Wiley - VCH, India

Habashi, F., 1999. *A Text Book of Hydrometallurgy*, 2nd ed. Metallurgie Extractive Quebec

Haber, F., Weiss, J., 1934. The decomposition of hydrogen peroxide by iron salts, *Proceedings of the Royal Society of London, Series A*, 147,332

Harris, G.B., White, C., 2008. Recent developments in the high-strength chloride leaching of base metal sulphide ores. *Presented at ALTA Nickel/Cobalt 2008* Perth, Australia

Hove, M., Van Hille, R.P., Lewis, A.E., 2009. The effect of different types of seeds on the oxidation and precipitation of iron. *Hydrometallurgy* 97, 180 – 184

Hsing, H.J., Wang, F.K., Chiang, P.C., Yang, W.F., 2004. Hazardous wastes transboundary movement management: a case study in Taiwan. *Resources, Conservation and Recycling* 40, 329 – 342

Huang, H.H., 2001. Stabcal equilibrium calculational program. *Montana Tech. of the University of Montana*, Department of Metallurgical and Materials Engineering, Montana, U.S.A

Hudson, M.J., 1982. An introduction to some aspects of solvent extraction chemistry in hydrometallurgy. *Hydrometallurgy* 9, 149 – 168

Ismael, M.R.C., Carvalho, J.M.R., 2003. Iron recovery from sulphate leach liquors in zinc hydrometallurgy. *Minerals Engineering* 16, 31– 39

Iwai, M., Majima, H., Izaki, T., 1979. A kinetic study on the oxidation of ferrous ion with dissolved molecular oxygen. *Denki Kagaku* 47, 409 – 414

Jenkins, D., Ferguson, J.F., Menar, A.B., 1971. Chemical processes for phosphate removal. *Water Research* 5, 369 – 389

Koo, S., 2009. Estimation of hindered settling velocity of suspensions. *Journal of Industrial and Engineering Chemistry* 15, 45 – 49

Kynch, G.J., 1952. A theory of sedimentation. *Transactions of the Faraday Society* 48, 166 – 176

Lamb, A.B., Elder, L.W., 1931. The electromotive activation of oxygen. *Journal of the American Chemical Society* 53, 137 – 163

Leclerc, N., Meux, E., Lecuire, J.M., 2003. Hydrometallurgical extraction of zinc from zinc ferrites. *Hydrometallurgy* 70, 175 – 183

Loan, M., Newman, O.M.G., Cooper, R.M.G., Farrow, J.B., Parkinson, G.M., 2006. Defining the Paragoethite process for iron removal in zinc hydrometallurgy. *Hydrometallurgy* 81, 104 – 129

Lowson, R.T., 1982. Aqueous Oxidation of Pyrite by Molecular Oxygen. *Chemical*

Review 82, 477 – 485

McBain, J.W., 1901. Oxidation of Ferrous Solutions by Free Oxygen. *The Journal of Physical Chemistry* 5, 623 – 638

Montgomery, D.C., 2008. *Design and analysis of experiments*. John Wiley and Sons

Mudd, G.M., 2009. Nickel sulfide versus laterite: the hard sustainability challenge remains. In: *Proceeding of the 48th Annual Conference of Metallurgists*, Canadian Metallurgical Society, Sudbury, Ontario, Canada, 23 – 26

Narita, E., Lawson, F., Han, K.N., 1983. Solubility of oxygen in aqueous electrolyte solutions. *Hydrometallurgy* 10, 21 - 37

Ostwald, F.W., 1896. Lehrbuch der Allgemeinen Chemie. *Leipzig Germany* 2, part 1

Posner, A.M., 1953. The kinetics of autoxidation of ferrous ions in concentrated HCl solutions. *Transactions of the Faraday Society* 49, 382 – 388

Posnjak, E., Merwin, H.E., 1922. The system, Fe_2O_3 - SO_3 - H_2O. *Journal of the American Chemical Society* 44, 1965 – 1994

Raos, S.R., Finch, J.A., Kuyucak, N., 1995. Technical note ferrous - ferric oxidation in acidic mineral process effluents: comparison of methods. *Minerals Engineering* 8, 905 – 911

Richardson, J.F., Harker, J.H., Backhurst, J.H., 2002. *Coulson and Richardson's Chemical engineering*, 5th ed. Butterworth - Heinemann

Ritcey, G.M., 1980. Crud in solvent extraction processing - A review of causes and treatment. *Hydrometallurgy* 5, 97 – 107

Riveros, P.A., Dutrizac, J.E., 1997. The precipitation of hematite from ferric chloride media. *Hydrometallurgy* 46, 85 – 104

Robins, L.G. Twidwell, D.R. Dahnke, S.F. McGrath, G.H. Khoe, 1991. The solubility of metal phosphates. EPD Congress 1991, Edited by Caskell, D.R., *Minerals Metals and Material Society*

Salas, A., Vermet, F., Finch, J.A., 1993. Apparatus and technique to measure settling velocity and holdup of solids in water slurries. *Chemical Engineering Science* 48, 815 – 819

Scaccia, S., Carewska, M., Prosini, P.P., 2003. Thermoanalytical study of iron(III) phosphate obtained by homogeneous precipitation from different media. *Thermochimica acta* 413, 81 – 86

Schwertmann, U., Cornell, R.M., 2000. *Iron oxides in the laboratory: preparation and characterization*. Wiley-VCH, Weinheim; New York

Shen, Y., Xue, W.Y., Niu, W.Y., 2008. Recovery of Co (II) and Ni (II) from hydrochloric acid solution of alloy scrap. *Transactions of Nonferrous Metals Society of China* 18, 1262 – 1268

Sohnel, O., Garside, J., 1992. *Precipitation: Basic Principals and Industrial Applications*, 1st ed. Butterworth-Heinemann

Stumm, W., Lee, G.F., 1961. Oxygenation of ferrous iron. *Industrial and Engineering Chemistry* 53, 143 – 146

Tagirov, B.R., Zotov, A.V., Akinfiev, N.N., 1997. Experimental study of dissociation of HCI from 350 to 500°C and from 500 to 2500 bars: Thermodynamic properties of $HCl_{(aq)}$. *Geochimica et Cosmochimica acta* 61, 4267 – 4280

Threlfall, T., 2003. Structural and thermodynamic explanations of Ostwald's Rule. *Organic Process Research and Development* 7, 1017 – 1027

Tromans, D., 1998. Temperature and pressure dependent solubility of oxygen in water: a thermodynamic analysis. *Hydrometallurgy* 48, 327 – 342

Twidwell, L.G., Dahnke, D.R., Arthur, B.W., Nordwick, S.M., 1986. Recovery of metal values from metal finishing hydroxides sludges by phosphate precipitation. Presented at the Land disposal, remedial action, incineration and treatment of hazardous waste. *Proceedings of the 12th annual research symposium*, Cincinnati, Ohio, United States, 338 – 351

Twidwell, L.G., Dahnke, D.R., 2001. Treatment of metal finishing sludge for

detoxification and metal value. *European Journal of Mineral Processing and Environmental Protection* 1, 76 – 88

Twidwell, L.G., Robins, R.G., Dahnke, D.R., 1987. Method for recovering metal values from mixed metal aqueous solutions by selective phosphate precipitation. *European Patent*, Patent number 0221760 A2

Wang, K., Li, J., McDonald, R.G., Browner, R.E., 2011. The effect of iron precipitation upon nickel losses from synthetic atmospheric nickel laterite leach solutions: Statistical analysis and modelling. *Hydrometallurgy* 109, 140 – 152

Weiss, J., 1935. Electron transition process in the mechanism of oxidation- and reduction reactions in solutions. *Naturwissenschaften* 23, 64 – 69

Zhu, Z., Zhang, W., Cheng, C.Y., 2012. A synergistic solvent extraction system for separating copper from iron in high chloride concentration solutions. *Hydrometallurgy* 113 - 114, 155 – 159

APPENDIX A: OLI SIMULATIONS

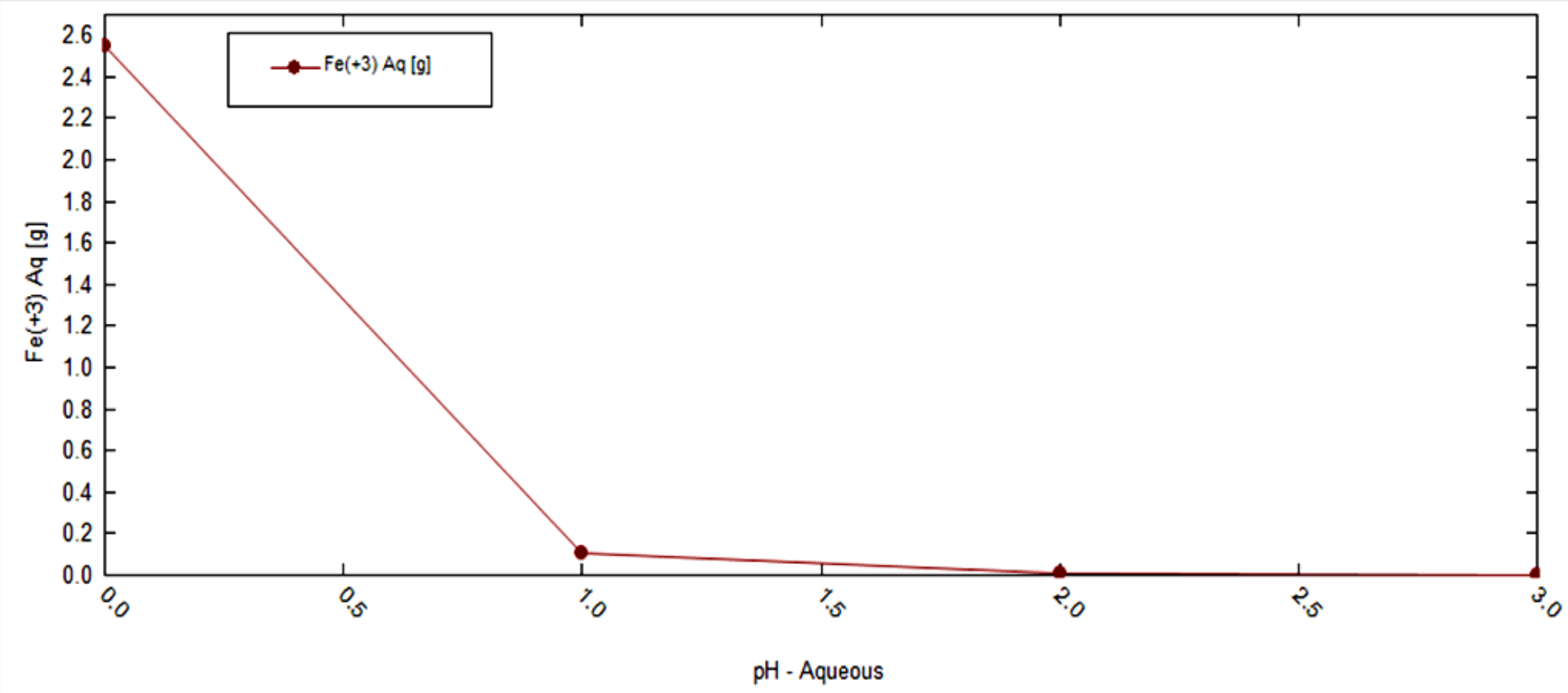

Figure A 1. OLI software simulation of iron removal by iron phosphate precipitation, at 40^{o}C as a function of solution pH, showing the quantity of iron left in a 1 L solution initially containing 45 g iron

APPENDIX B: LEACH SOLUTION PREPARATION

The procedure followed during the preparation of synthetic leach solutions was as follows:

- 500 mL of deionised water was added into a 1 L beaker and then a desired molarity of acid was added according to Equation B - 1.
- A calculated amount of iron(II) chloride salt was added into the beaker containing deionised water with a specific acid molarity.
- Calculated amounts of nickel chloride and copper chloride salts were then added into the beaker.
- Deionised water was toped up to a volume of 800 mL.
- The mixture was heated to 40^{o}C and agitated at 400rpm for about 1h, at which point all the salts had dissolved completely.

Fresh synthetic solution was prepared in the manner outlined for each experimental run to avoid iron transformations or oxidation with time.

$$\mathrm{Vol}_{acid} = 36.5 \frac{\mathrm{M}}{\sigma_{acid}} \left(\%\mathrm{Purity}_{acid}\right).\left(\mathrm{Vol}_{mixture}\right) \qquad B - 1$$

Where; Vol_{acid} is the volume of acid to be added, M is the molarity of the mixture desired and $\mathrm{Vol}_{mixture}$ is the total volume of the synthetic solution.

APPENDIX C: ANALYSIS OF IRON (II)

Wet chemistry was used to determine the amount of iron(II) in solution during oxidation investigations. ICIP analysis was used to determine the total iron. The following was the wet chemistry procedure;

- At least 10 mL of deionised water was added into a 250 mL Erlenmeyer flask.
- 1 mL of sample was added into the 250 mL Erlenmeyer flask using a 5 mL adjustable pipetman.
- 5 mL of 98% phosphoric acid and 5 mL sulphuric acid was added into the 250 mL Erlenmeyer flask to mask the iron(III)
- 3 to 5 drops of sodium diphenylamine indicator was then added into the flask
- The burette was set with 0.0084 M potassium dichromate ($K_2Cr_2O_7$)
- The potassium dichromate was then titrated against the contents of the Erlenmeyer flask to a purple end point.
- The concentration of iron(II) was then calculated as per the balanced Equation C - 1 using the formula indicated in Equation C - 2.

$$Cr_2O_7^{2-} + 6Fe^{2+} + 14H^+ \rightarrow 2Cr^{3+} + 6Fe^{3+} + 7H_2O \qquad C - 1$$

$$C_{Fe(II)} = 6 \times 55.85 \times M_{K_2Cr_2O_7} \times \frac{Vol_{Titrant}}{Vol_{Sample}} \qquad C - 2$$

APPENDIX D: ASSOCIATED AND DISSOCIATED [HCl]

Given the dissociation of HCl shown in Equation D – 1, the equilibrium concentration of dissociated and associated acid can be calculated using a specific dissociation constant *K*, at a given temperature and pressure for a particular concentration of HCl.

$$HCl \leftrightarrow H^{+} + Cl^{-} \qquad D - 1$$

ICE (Initial, Change, Equilibrium) tables can be used to facilitate the calculation. Let $[HCl]_{int}$ and *x* be the initial associated acid concentration and acid molarity change upon dissociation. The ICE table for the respective species can be seen in Table D 1. *K* can be expressed as shown in Equation D – 2 and *x* can be calculated using the quadratic formula. The equilibrium concentrations of the specific species can be read off the ICE table by replacing the calculated value of *x* in the table.

Table D 1. Initial, Change, Equilibrium (ICE) table for calculating equilibrium associated and dissociated [HCl]

	[HCl] (M)	**$[H^+]$ (M)**	**$[Cl^-]$ (M)**
Initial	$[HCl]_{int}$	0	0
Change	(-) *x*	(+) *x*	(+) *x*
Equilibrium	$[HCl]_{int}$ - *x*	*x*	*x*

$$K = \left(\frac{x^2}{[HCl] - x} \right) \qquad D - 2$$

For a solution containing 125.6 g/L iron, 2.24 moles of associated HCl is needed for complete complexation.

K at 80^{o}C and atmospheric pressure is obtained to be approximately 7.9.

Total HCl – dissociated HCl = 2.24

Using Equation D – 2,

$7.9 \times 2.24 = \{\text{dissociated HCl}\}^2$

Total HCl required = 6.4 M

APPENDIX E: EXPERIMENTAL DATA

Oxidation experiments

Oxidation screening and optimization runs

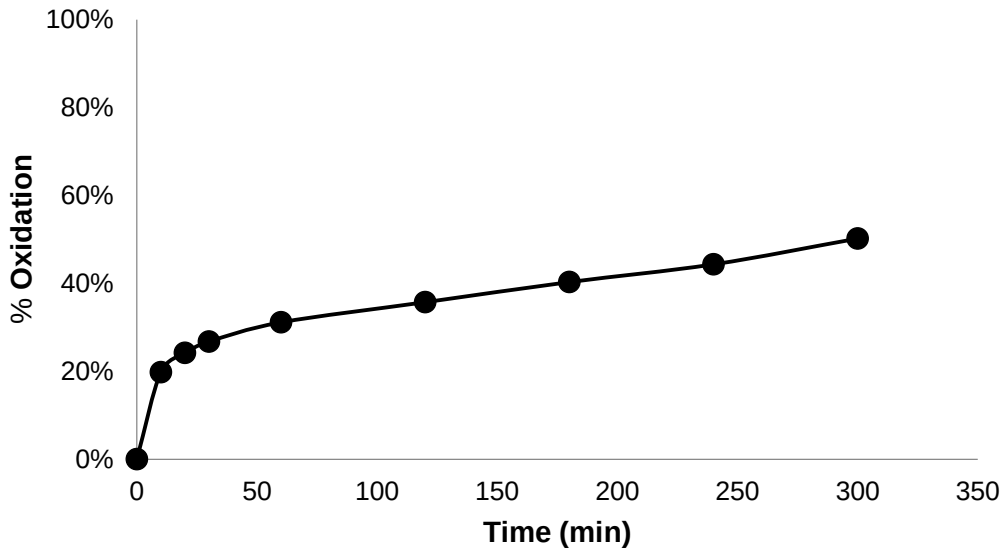

.Figure E 1 Oxidation test 1: Cu concentration 3 g/L, [HCl] 2 M, Temperature 80^{o}C

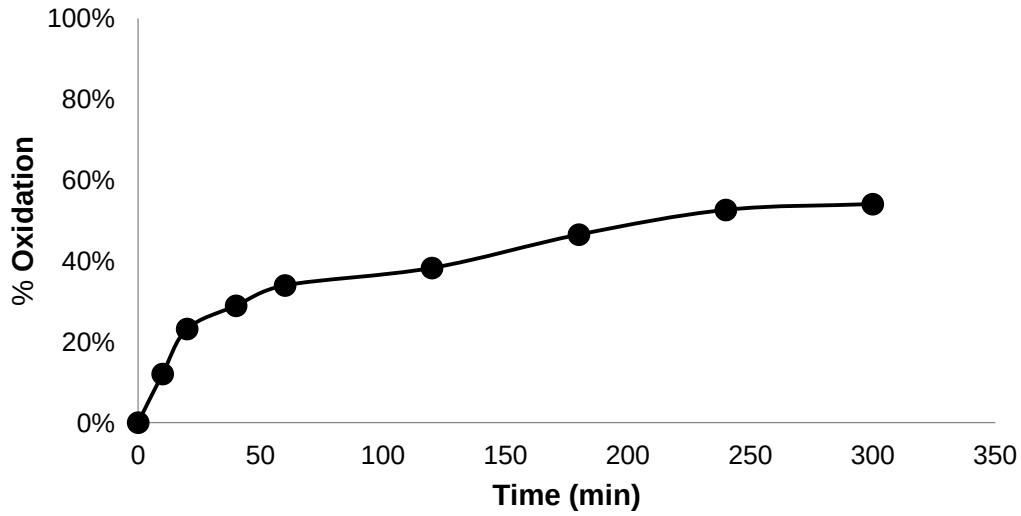

Figure E 2. Oxidation test 2: Cu concentration 0.3 g/L, [HCl] 4 M, Temperature 80^{o}C

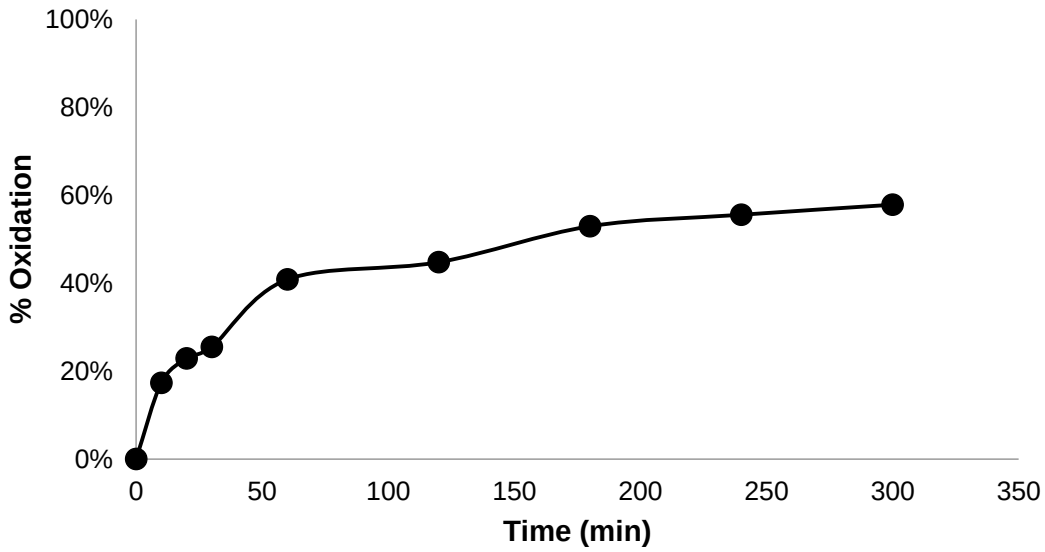

Figure E 3. Oxidation test 3: Cu concentration 3 g/L, [HCl] 4 M, Temperature 50^{o}C

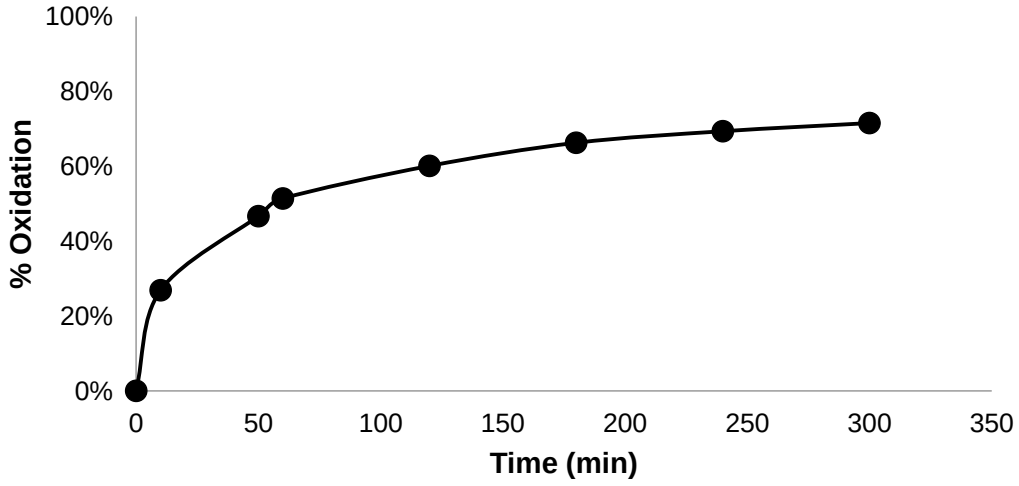

Figure E 4. Oxidation test 4: Cu concentration 3 g/L, [HCl] 4 M, Temperature 80^{o}C

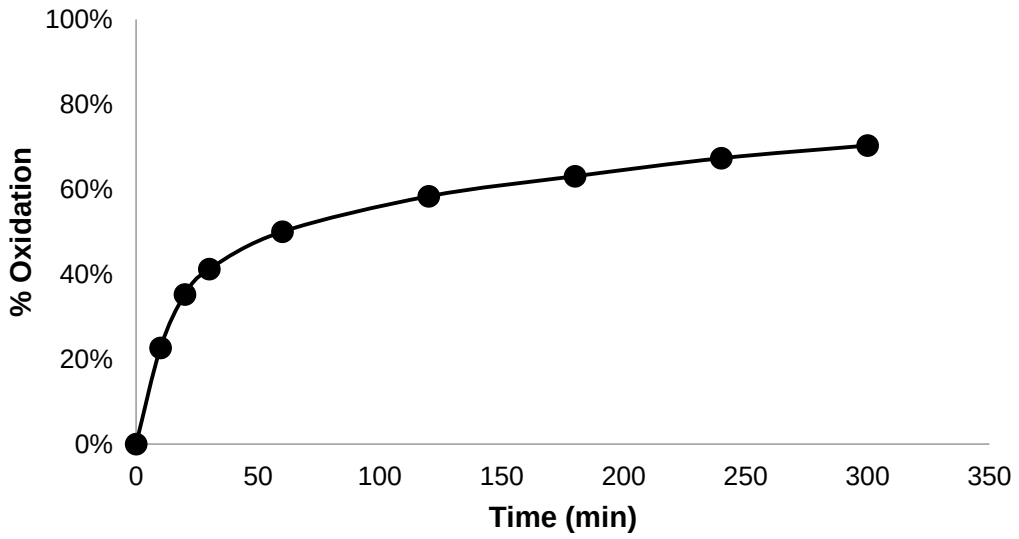

Figure E 5. Oxidation test 5 (repeat of Test 4 with a new batch of titrant reagent): Cu concentration 3 g/L, [HCl] 4 M, Temperature 80°C

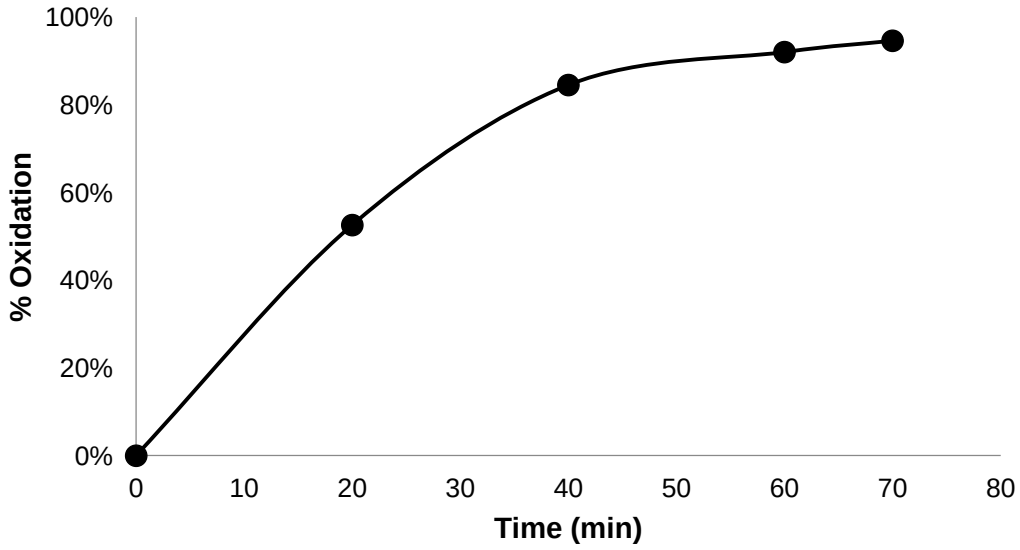

Figure E 6. Oxidation test 6: Cu concentration 3 g/L, [HCl] 4.6 M, Temperature 80°C (70 min)

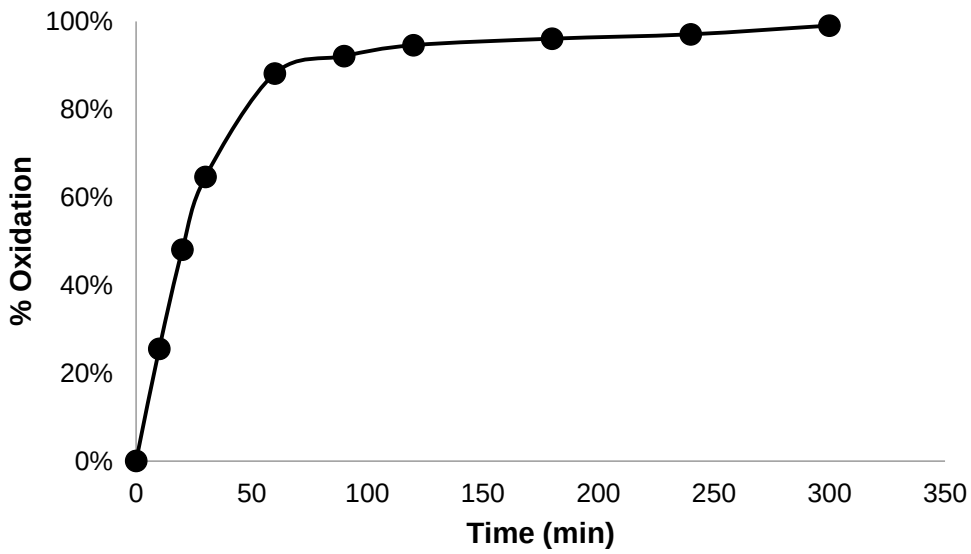

Figure E 7. Oxidation test 7: Cu concentration 0.3 g/L, [HCl] 4.6 M, Temperature 80°C

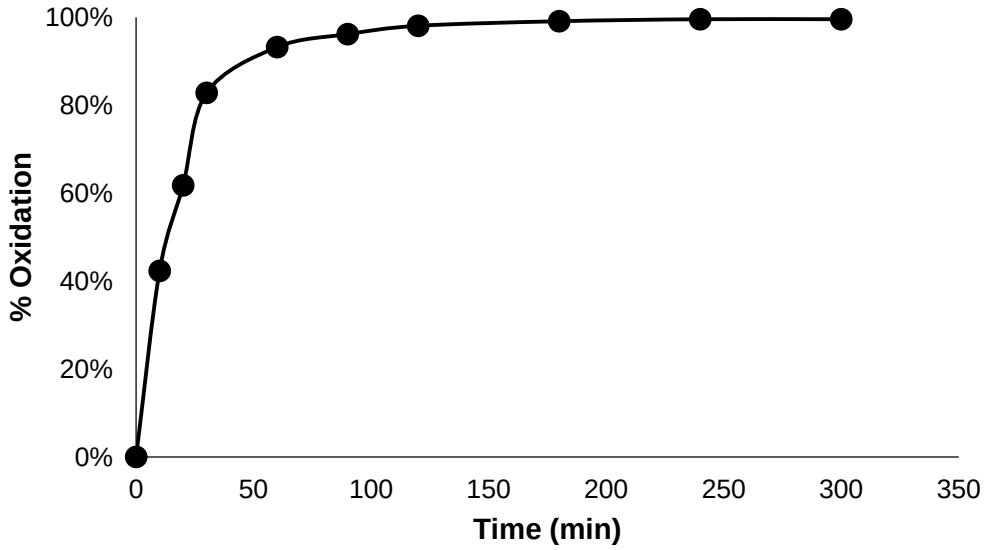

Figure E 8. Oxidation test 8: Cu concentration 3 g/L, [HCl] 4.6 M, Temperature 80°C

Oxidation confirmatory and discovery runs

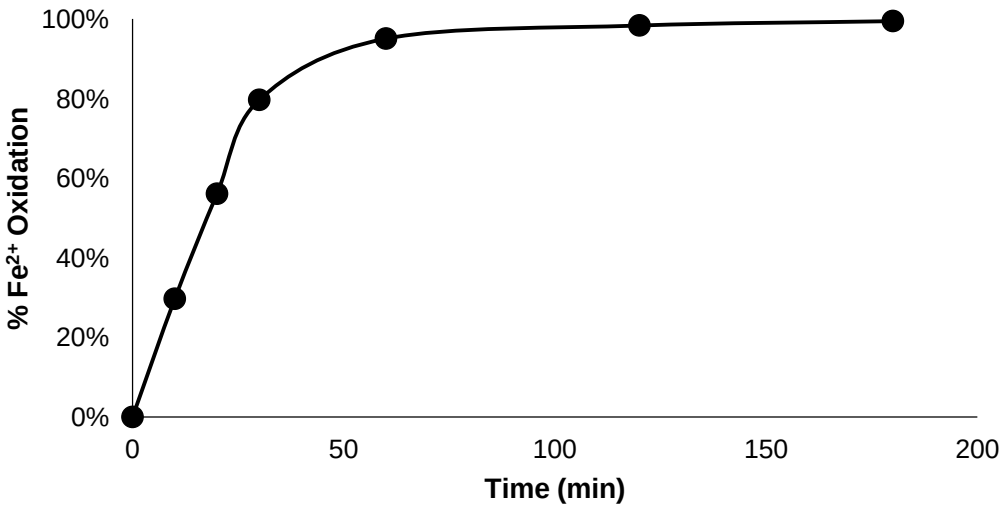

Figure E 9.Oxidation test 13: 3 M [HCl] and 1.6 M NaCl (Cu 3 g/L, 80°C)

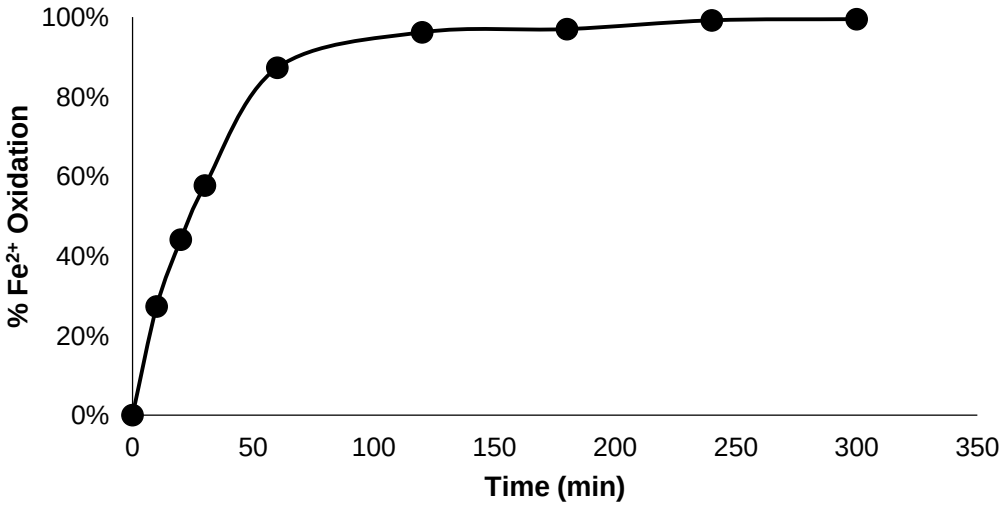

Figure E 10. Oxidation test 14: 2 M [HCl] and 2.6 M NaCl (Cu 3 g/L, 80°C)

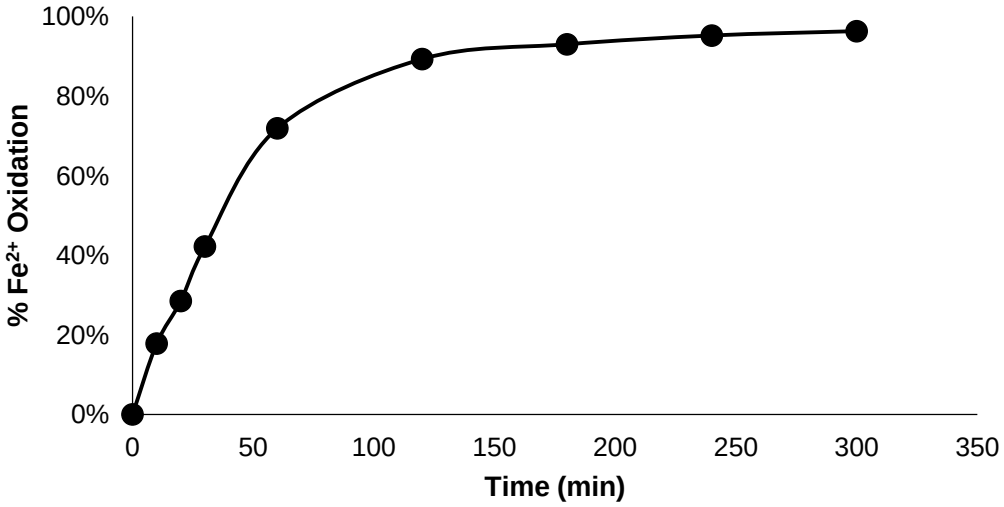

Figure E 11. Oxidation test 15: 1 M [HCl] and 3.6 M NaCl (Cu 3 g/L, 80°C)

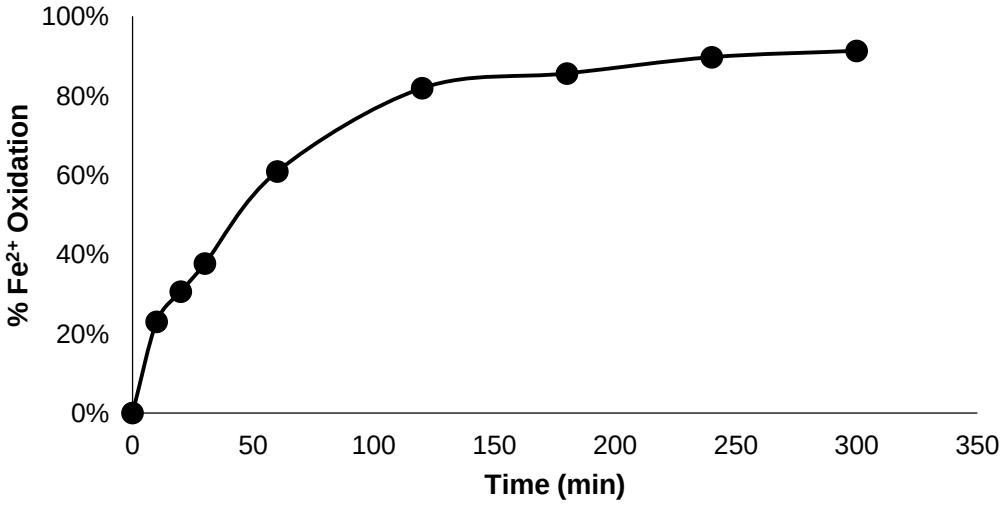

Figure E 12. Oxidation test 16: 0.65 M [HCl] and 3.95 M NaCl (Cu 3 g/L, 80°C)

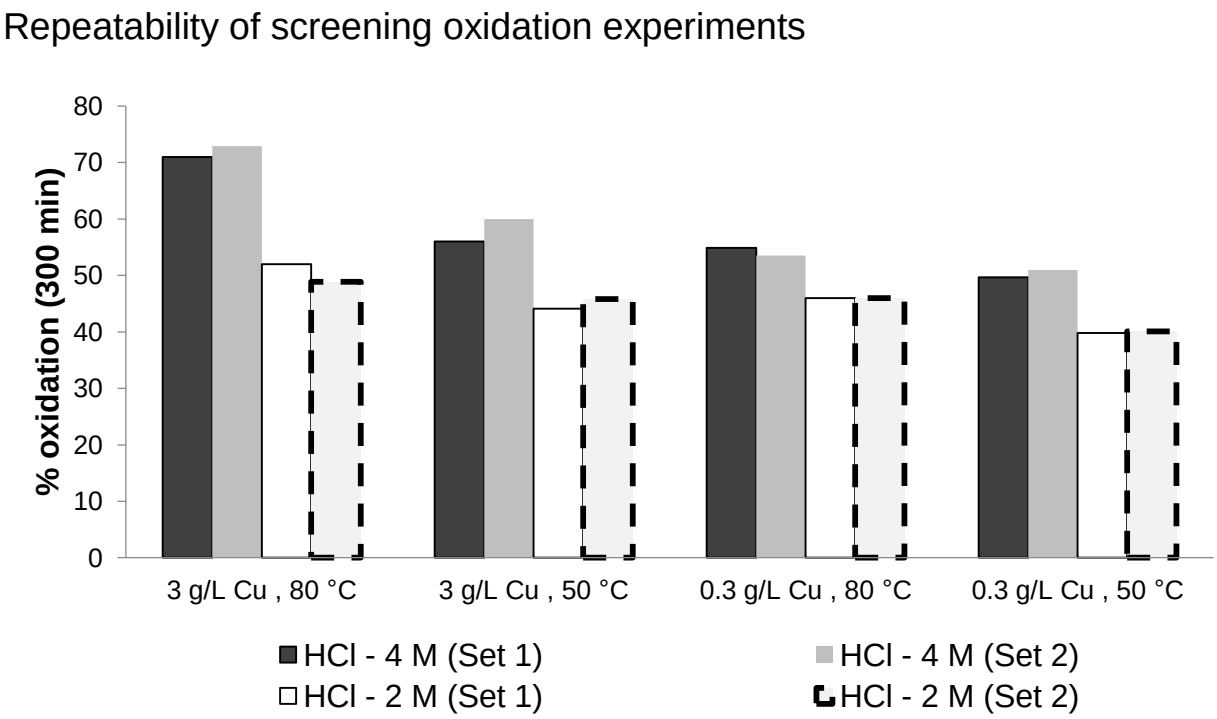

Figure E 13: Oxidation of iron(II) after 300 minutes at 4M and 2 M [HCl] with varying Cu concentration and temperature reported for Set 1 and Set 2 experiments

Analysis of variance for set 1 and set 2 experiments, ANOVA Table 4.1, indicated that the R-Squared was 0.8984, Adjusted R-Squared was 0.8731 and the Standard deviation was 3.41. The R-squared of 0.8984 is within reasonable agreement with the adjusted R-squared value of 0.8731.

Repeatability of optimization oxidation experiments

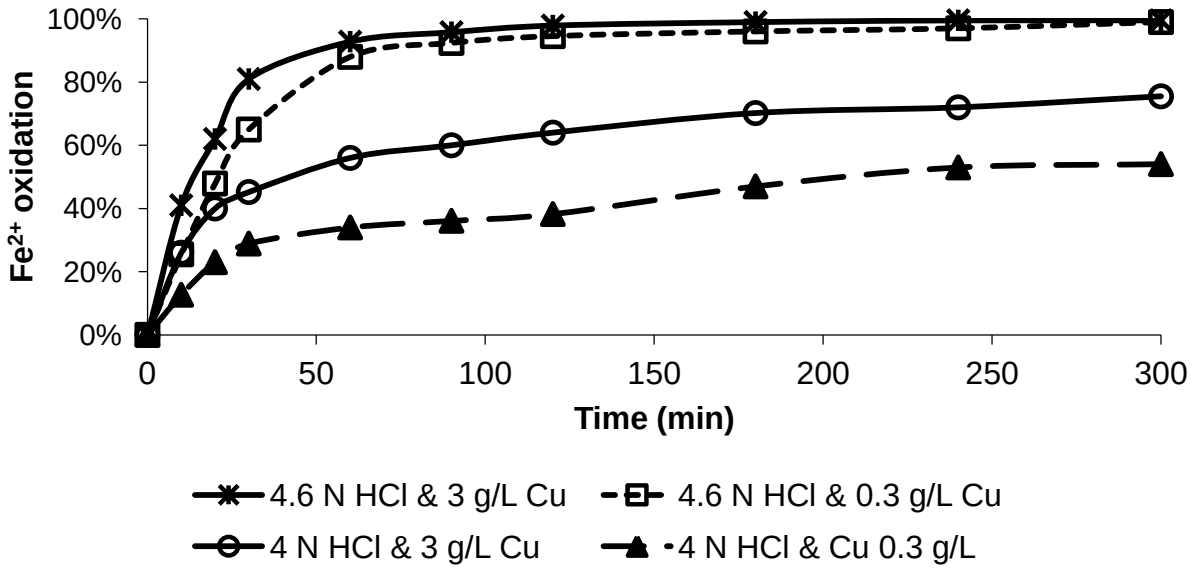

Figure E 14. Repeat oxidation tests (12, 13 and 14): 80°C as a function of [HCl] and copper concentration

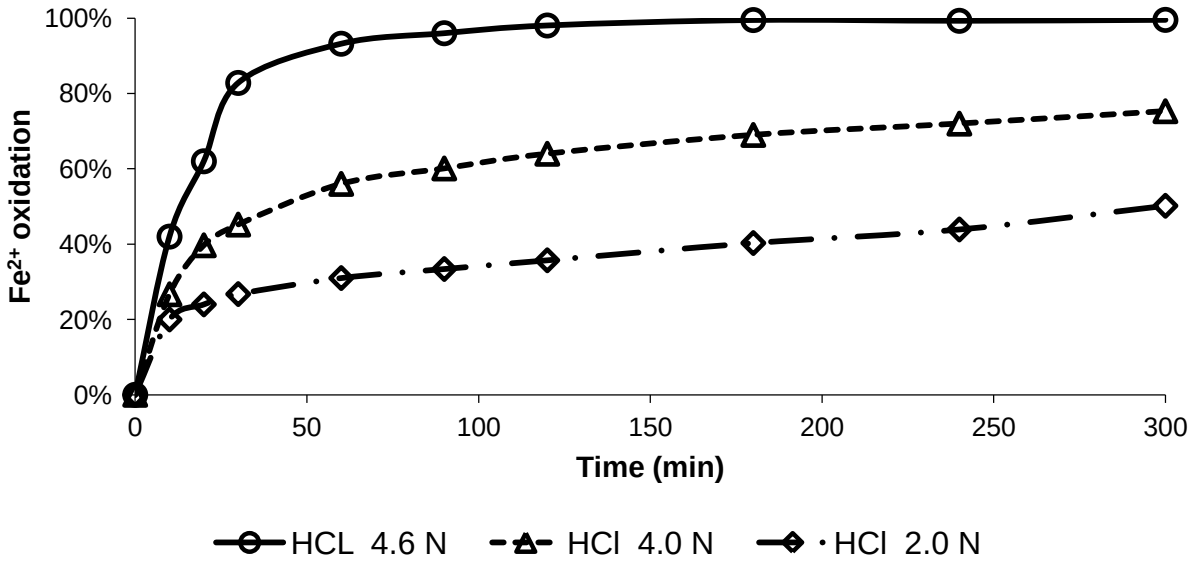

Figure E 15. Repeat oxidation tests (9, 10 and 11): 3 g/L Cu concentration, 80°C and varying [HCl]

Hematite precipitation

Screening experiments

Table E 1. Hematite screening, test 1 ICP results

Conditions	Time (min)	Fe removal (%)	Ni loss (%)	Cu loss (%)
Test 1 - seeded pH 1, 60°C	0	0	0	0
	10	96.99%	12.25%	9.41%
	20	99.06%	12.77%	11.44%
	30	98.18%	13.18%	11.94%
	60	99.42%	14.84%	12.57%
	120	99.37%	24.21%	22.30%

Table E 2. Hematite screening, test 2 ICP results

Conditions	Time (min)	Fe removal (%)	Ni loss (%)	Cu loss (%)
Test 2 - seeded pH 1, 80°C	0	0	0	0
	10	99.51%	9.87%	9.56%
	20	99.68%	10.14%	11.09%
	30	99.64%	3.53%	1.74%
	60	99.78%	3.26%	3.22%
	120	99.74%	6.94%	6.71%

Table E 3. Hematite screening, test 3 ICP results

Conditions	Time (min)	Fe removal (%)	Ni loss (%)	Cu loss (%)
Test 3 - seeded pH 1, 90°C	0	0	0	0
	10	99.77%	16.94%	15.70%
	20	99.69%	13.22%	13.83%
	30	99.84%	13.00%	14.05%
	60	99.87%	21.02%	22.30%
	120	99.85%	12.37%	12.77%

Table E 4. Hematite screening, test 4 ICP results

Conditions	Time (min)	Fe removal (%)	Ni loss (%)	Cu loss (%)
Test 4 - seeded pH 2, 60°C	0	0	0	0
	10	98.35%	18.03%	24.65%
	20	99.97%	15.41%	29.16%
	30	99.99%	19.74%	32.75%
	60	99.99%	15.26%	29.58%
	120	99.99%	18.65%	32.92%

Table E 5. Hematite screening, test 5 ICP results

Conditions	Time (min)	Fe removal (%)	Ni loss (%)	Cu loss (%)
Test 5 - seeded pH 2, 80°C	0	0	0	0
	10	99.88%	14.95%	19.78%
	20	99.97%	17.30%	29.37%
	30	99.98%	19.86%	31.33%
	60	99.90%	11.00%	12.33%
	120	99.95%	19.10%	29.30%

Table E 6. Hematite screening, test 6 ICP results

Conditions	Time (min)	Fe removal (%)	Ni loss (%)	Cu loss (%)
Test 6- seeded pH 2, 90°C	0	0	0	0
	10	99.92%	12.06%	20.13%
	20	99.99%	10.30%	23.33%
	30	99.99%	10.68%	23.68%
	60	100.00%	14.03%	26.02%
	120	100.00%	17.52%	30.28%

Table E 7. Hematite screening, test 7 ICP results

Conditions	Time (min)	Fe removal (%)	Ni loss (%)	Cu loss (%)
Test 7 - seeded pH 3, 60°C	0	0	0	0
	10	97.78%	25.70%	52.5%
	20	99.84%	26.57%	53.7%
	30	99.59%	33.78%	58.0%
	60	99.92%	33.67%	58.9%
	120	99.97%	39.30%	64.2%

Table E 8. Hematite screening, test 8 ICP results

Conditions	Time (min)	Fe removal (%)	Ni loss (%)	Cu loss (%)
Test 8 - seeded pH 3, 80°C	0	0	0	0
	10	95.88%	4.57%	8.3%
	20	99.69%	9.61%	12.5%
	30	97.97%	12.97%	21.3%
	60	99.97%	11.64%	31.1%
	120	99.72%	15.21%	39.5%

Table E 9. Hematite screening, test 9 ICP results

Conditions	Time (min)	Fe removal (%)	Ni loss (%)	Cu loss (%)
Test 9 - seeded pH 1, 90°C	0	0	0	0
	10	97.59%	18.37%	48.34%
	20	99.99%	25.14%	56.43%
	30	99.99%	20.68%	51.64%
	60	99.99%	27.79%	58.32%
	120	99.91%	31.93%	60.70%

Optimization experiments

Table E 10. Hematite optimization, test 10 ICP results

Conditions	Time (min)	Fe removal (%)	Ni loss (%)	Cu loss (%)
Test 10 - unseeded pH 1, 80°C	0	0	0	0
	10	99.43%	13.47%	17.75%
	20	99.99%	14.03%	27.46%
	30	100.00%	8.43%	23.67%
	60	99.88%	19.54%	32.93%
	120	100.00%	17.21%	28.34%

Table E 11. Hematite optimization, test 11 ICP results

Conditions	Time (min)	pH	Fe removal (%)	Ni loss (%)	Cu loss (%)
Test 11 - seeded stepwise pH control to pH 0.5, 80°C	0	0	0	0	0
	10	0	96.65%	14.35%	11.97%
	20	0.2	96.29%	4.71%	0.28%
	30	0.2	96.98%	10.80%	5.44%
	40	0.5	98.26%	6.81%	2.02%
	50	0.5	98.50%	20.06%	16.34%
	60	0.5	98.49%	16.67%	11.66%

Table E 12. Hematite optimization, test 12 ICP results

Conditions	Time (min)	Fe removal (%)	Ni loss (%)	Cu loss (%)
Test 12 - seeded pH 1, 80°C	0	0	0	0
	10	96.80%	3.88%	1.90%
	20	99.07%	6.52%	6.32%
	30	99.42%	12.03%	13.29%

Table E 13. Hematite optimization, test 13 ICP results

Conditions	Time (min)	Fe removal (%)	Ni loss (%)	Cu loss (%)
Test 13 - seeded pH 1, 80°C	0	0	0	0
	10	99.66%	2.82%	1.12%
	20	99.87%	0.00%	0.00%
	30	99.91%	13.48%	16.18%
	60	99.73%	15.31%	19.11%

Confirmatory experiments

Table E 14. Hematite confirmatory run, test 1 Repeat ICP results

Conditions	Time (min)	Fe removal (%)	Ni loss (%)	Cu loss (%)
Repeat (Test 1) - seeded pH 1, 80°C	0	0	0	0
	10	99.31%	8.29%	10.56%
	20	99.48%	8.01%	9.09%
	30	99.64%	4.03%	5.74%
	60	99.56%	2.87%	3.42%
	120	99.84%	5.89%	5.91%

Table E 15. Hematite confirmatory run, test 10 Repeat ICP results

Conditions	Time (min)	Fe removal (%)	Ni loss (%)	Cu loss (%)
Repeat (Test 10) - unseeded pH 1, 80°C	0	0	0	0
	10	98.43%	15.47%	18.75%
	20	98.99%	14.03%	25.46%
	30	99.00%	10.43%	20.67%
	60	98.88%	20.54%	34.03%
	120	99.10%	15.21%	24.34%

Table E 16. Hematite confirmatory run, test 14 ICP results

Conditions	Time (min)	Fe removal (%)	Ni loss (%)	Cu loss (%)
Test 14 - seeded pH 0, 80°C	0	**0**	0	0
	10	**99.5%**	21.82%	27.65%
	20	**99.5%**	24.02%	27.96%
	30	**99.3%**	7.04%	10.91%
	60	**99.2%**	7.04%	5.88%

Robustness experiment

Table E 17. Hematite robustness run, test 15 ICP results

Conditions	Time (min)	Fe removal (%)	Ni loss (%)	Cu loss (%)
Test 15- seeded pH 0, 80°C oxidation - precipitation	0	0	0	0
	10	28.85%	3.66%	2.17%
	20	51.02%	17.78%	15.79%
	30	63.26%	22.07%	18.76%
	60	89.31%	13.48%	7.80%
	120	98.72%	16.37%	8.81%
	180	99.70%	22.59%	16.63%
	240	99.84%	18.05%	10.83%
	300	99.82%	19.72%	15.39%

Iron phosphate precipitation

Screening experiments

Table E 18. Iron phosphate screening, test 16 ICP results

Conditions	Time (min)	Fe removal (%)	Ni loss (%)	Cu loss (%)
Test 16 - seeded pH 1, 40°C	0	0	0	0
	10	99.00%	8.85%	19.13%
	20	98.81%	6.32%	10.62%
	30	98.80%	0.51%	2.78%
	60	98.88%	0.50%	4.35%
	120	98.92%	3.40%	5.99%

Table E 19. Iron phosphate screening, test 17 ICP results

Conditions	Time (min)	Fe removal (%)	Ni loss (%)	Cu loss (%)
Test 17 - seeded pH 1, 60°C	0	0	0	0
	10	99.82%	12.60%	25.89%
	20	99.85%	13.58%	31.37%
	30	99.89%	9.23%	33.10%
	60	99.83%	8.58%	25.57%
	120	99.83%	9.40%	28.17%

Table E 20. Iron phosphate screening, test 18 ICP results

Conditions	Time (min)	Fe removal (%)	Ni loss (%)	Cu loss (%)
Test 18 - seeded pH 1, 80°C	0	0	0	0
	10	99.84%	11.78%	27.62%
	20	99.78%	6.37%	18.20%
	30	99.81%	8.67%	20.82%
	60	99.81%	9.20%	22.45%
	120	99.80%	7.23%	19.34%

Table E 21. Iron phosphate screening, test 19 ICP results

Conditions	Time (min)	Fe removal (%)	Ni loss (%)	Cu loss (%)
Test 19 - seeded pH 2, 40°C	0	0	0	0
	10	99.91%	12.58%	76.23%
	20	99.99%	11.71%	77.13%
	30	99.94%	14.02%	76.91%
	60	99.98%	14.87%	71.40%
	120	99.89%	11.51%	70.13%

Table E 22. Iron phosphate screening, test 20 ICP results

Conditions	Time (min)	Fe removal (%)	Ni loss (%)	Cu loss (%)
Test 20 - seeded pH 2, 60°C	0	0	0	0
	10	99.95%	1.92%	50.31%
	20	99.98%	-4.64%	53.85%
	30	99.99%	5.73%	54.93%
	60	99.99%	5.93%	57.37%
	120	99.94%	2.49%	50.58%

Table E 23. Iron phosphate screening, test 21 ICP results

Conditions	Time (min)	Fe removal (%)	Ni loss (%)	Cu loss (%)
Test 21- seeded pH 2, 80°C	0	0	0	0
	10	99.91%	5.67%	45.09%
	20	99.79%	2.99%	44.10%
	30	99.92%	3.72%	41.78%
	60	99.99%	8.84%	69.39%
	120	99.99%	11.61%	73.33%

Table E 24. Iron phosphate screening, test 22 ICP results

Conditions	Time (min)	Fe removal (%)	Ni loss (%)	Cu loss (%)
Test 22 - seeded pH 3, 40°C	0	0	0	0
	10	99.95%	34.70%	29.4%
	20	99.98%	33.46%	30.1%
	30	99.98%	34.84%	14.9%
	60	99.98%	31.87%	17.1%
	120	99.76%	34.61%	33.5%

Table E 25. Iron phosphate screening, test 23 ICP results

Conditions	Time (min)	Fe removal (%)	Ni loss (%)	Cu loss (%)
Test 23 - seeded pH 3, 60°C	0	0	0	0
	10	99.69%	33.97%	66.2%
	20	99.71%	31.77%	72.7%
	30	100.00%	35.50%	80.1%
	60	100.00%	36.54%	81.4%
	120	99.92%	41.21%	79.9%

Table E 26. Iron phosphate screening, test 24 ICP results

Conditions	Time (min)	Fe removal (%)	Ni loss (%)	Cu loss (%)
Test 24 - seeded pH 3, 80°C	0	0	0	0
	10	99.96%	39.46%	46.48%
	20	99.99%	46.80%	62.73%
	30	100.00%	49.73%	53.36%
	60	99.99%	59.08%	51.62%
	120	100.00%	61.71%	61.90%

Optimization experiments

Table E 27. Iron phosphate optimization, test 25 ICP results

Conditions	Time (min)	Fe removal (%)	Ni loss (%)	Cu loss (%)
Test 25 - unseeded pH 1, 40°C	0	0	0	0
	10	99.55%	10.18%	21.80%
	20	99.97%	8.89%	24.69%
	30	99.99%	17.66%	28.61%
	60	99.99%	7.74%	17.81%
	120	99.77%	9.98%	18.39%

Table E 28. Iron phosphate optimization, test 26 ICP results

Conditions	Time (min)	pH	Fe removal (%)	Ni loss (%)	Cu loss (%)
Test 26 - seeded stepwise pH control to pH 0.5, 40°C	0	0	0	0	0
	10	0	97.30%	0.00%	0.00%
	20	0.2	97.76%	10.05%	12.67%
	30	0.2	97.60%	9.61%	8.64%
	40	0.5	97.99%	21.72%	22.13%
	50	0.5	97.61%	19.48%	17.47%
	60	0.5	97.12%	5.10%	1.26%

Table E 29. Iron phosphate optimization, test 27 ICP results

Conditions	Time (min)	Fe removal (%)	Ni loss (%)	Cu loss (%)
Test 27 - seeded pH 1, 40°C	0	0	0	0
	10	96.07%	0.00%	2.5%
	20	96.86%	6.12%	9.7%
	30	97.13%	5.72%	6.9%

Table E 30. Iron phosphate optimization, test 28 ICP results

Conditions	Time (min)	Fe removal (%)	Ni loss (%)	Cu loss (%)
Test 28 - seeded pH 1, 40°C	0	0	0	0
	10	99.95%	9.88%	14.1%
	20	99.99%	3.84%	8.0%
	30	99.99%	8.81%	10.9%
	60	99.99%	7.39%	13.3%

Confirmatory experiments

Table E 31. Iron phosphate confirmatory run, test 16 repeat ICP results

Conditions	Time (min)	Fe removal (%)	Ni loss (%)	Cu loss (%)
Repeat (Test 16) - seeded pH 1, 40°C	0	0	0	0
	10	97.90%	10.85%	18.13%
	20	98.41%	8.32%	12.62%
	30	99.00%	2.41%	3.78%
	60	98.88%	3.50%	4.55%
	120	99.22%	2.99%	6.09%

Table E 32. Iron phosphate confirmatory run, test 25 repeat ICP results

Conditions	Time (min)	Fe removal (%)	Ni loss (%)	Cu loss (%)
Repeat (Test 25) - unseeded pH 1, 40°C	0	0	0	0
	10	98.10%	8.68%	18.80%
	20	99.45%	9.42%	22.94%
	30	98.80%	12.02%	25.61%
	60	99.99%	8.42%	15.81%
	120	99.90%	10.47%	16.92%

Table E 33. Iron phosphate confirmatory run, test 29 ICP results

Conditions	Time (min)	Fe removal (%)	Ni loss (%)	Cu loss (%)
Test 29 - seeded pH 0, 40°C	0	0	0	0
	10	98.60%	1.90%	6.07%
	20	100.00%	0.68%	4.81%
	30	100.00%	5.51%	8.80%
	60	100.00%	7.32%	8.77%

Robustness experiment

Table E 34. Iron phosphate robustness run, test 30 ICP results

Conditions	Time (min)	Fe removal (%)	Ni loss (%)	Cu loss (%)
Test 30- seeded pH 0, 80°C oxidation - precipitation	0	0	0	0
	10	68.4%	31.54%	13.59%
	20	78.5%	22.43%	8.51%
	30	92.5%	20.02%	10.88%
	60	98.1%	27.68%	18.17%
	120	99.9%	28.98%	20.87%
	240	100.0%	35.61%	27.79%
	300	100.0%	26.20%	17.89%
	360	100.0%	22.61%	12.37%
	420	100.0%	21.46%	12.11%
	480	100.0%	12.74%	3.01%

Energy dispersive X-ray spectroscopy

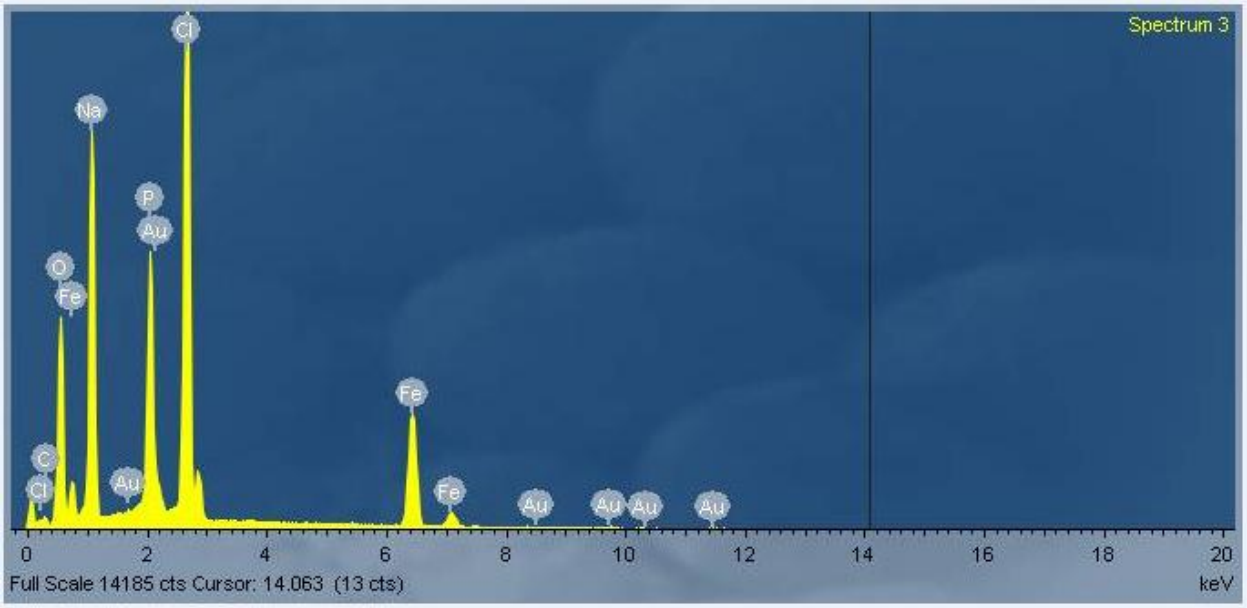

Figure E 16. Solid analysis of seeded iron phosphate precipitates produced at pH 1 and 40°C

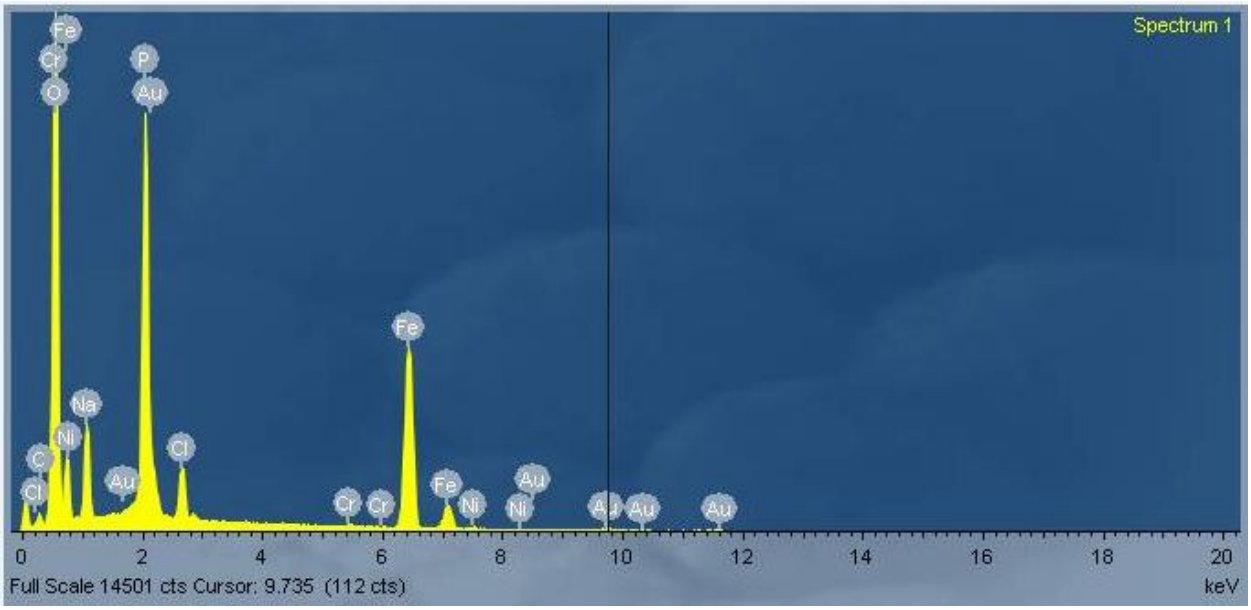

Figure E 17. Solid analysis of seeded iron phosphate precipitates produced at pH 3 and 40°C

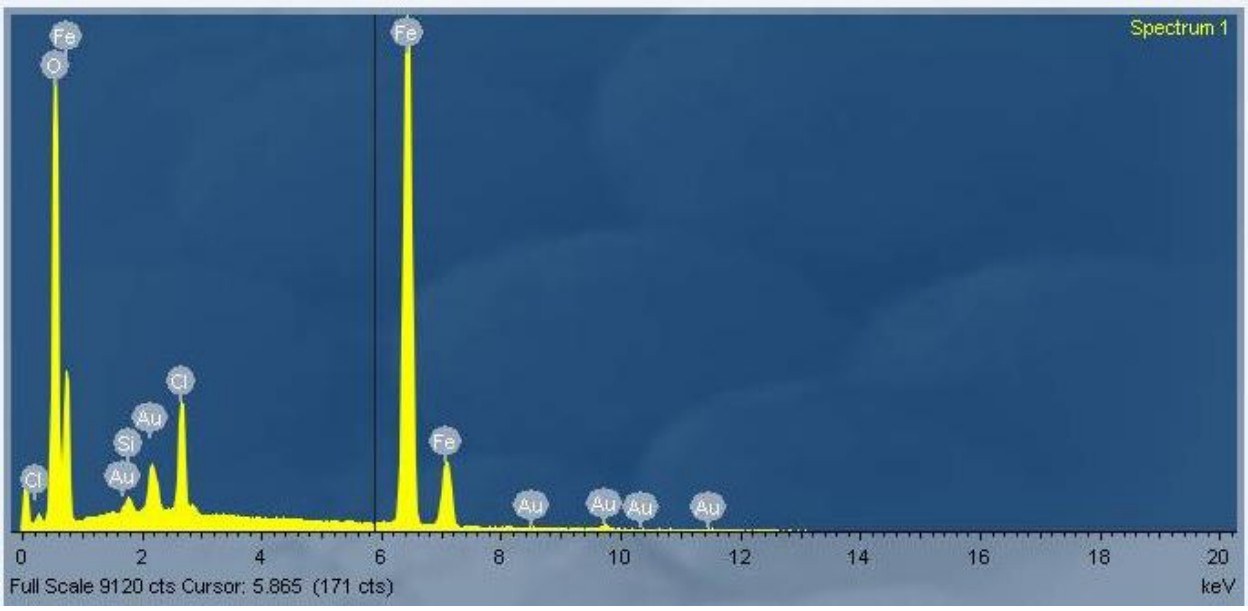

Figure E 18. Solid analysis of seeded hematite precipitates produced at pH 1 and 80^{o}C

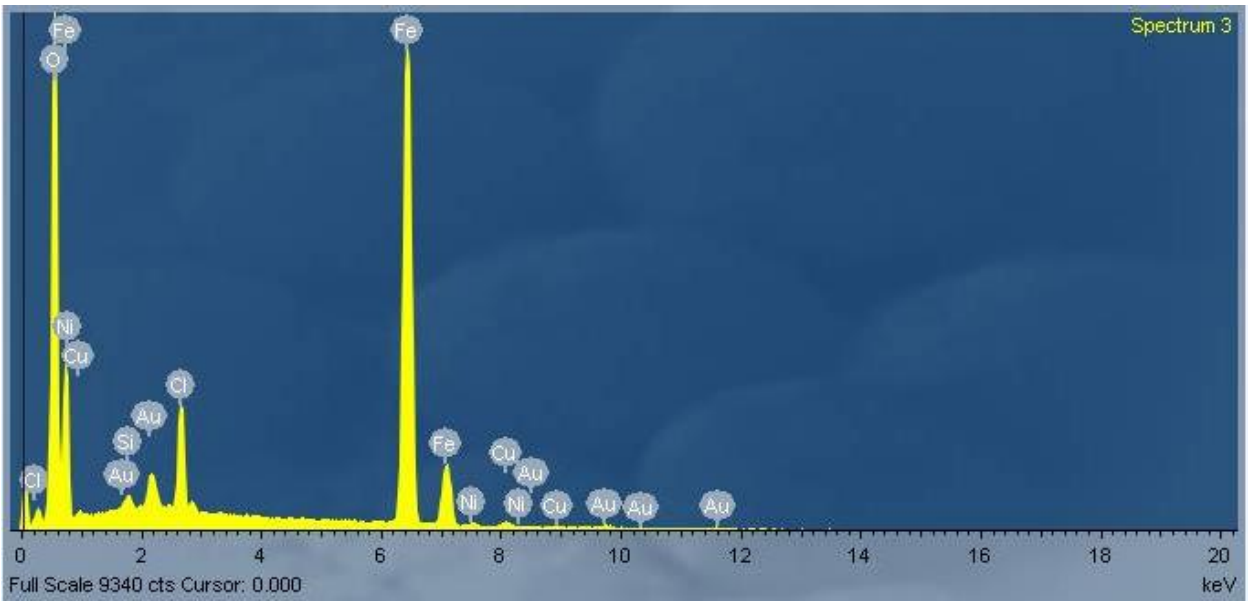

Figure E 19. Solid analysis of seeded hematite precipitates produced at pH 3 and 80^{o}C

X-ray fluorescence

Table E 35. XRF analysis of iron phosphate and hematite precipitates

Process	pH	Temperature (°C)	Ni composition in solids	Cu composition in solids
Iron phosphate	pH 1	80	0.26%	0.11%
		60	0.22%	0.23%
		40	0.20%	0.17%
	pH 2	80	0.29%	0.77%
		60	0.29%	0.98%
		40	0.20%	0.68%
	pH 3	80	1.10%	0.52%
		60	0.66%	1.05%
		40	0.66%	1.05%
Hematite	pH 1	60	0.32%	0.14%
		80	0.15%	0.11%
		90	0.14%	0.12%
	pH 2	60	0.17%	0.28%
		80	0.38%	0.60%
		90	0.21%	0.32%
	pH 3	60	0.51%	1.29%
		80	0.48%	0.61%
		90	0.56%	1.23%

APPENDIX F: MASS BALANCE STREAMS

Iron phosphate streams

Stream A – plant solution

ICP analysis

Stream B – HCl addition

Based on the need to completely complex 125.6 g/L of iron contained in the plant solution, the calculated total HCl required, as shown in APPENDIX D: ASSOCIATED AND DISSOCIATED [HCl], is 6.4 M. The plant solutions contain about 5 M HCl. Therefore the additional HCl is 1.4 M.

Added chloride ions = 1.4 x 35.5 = 49.7 g

Stream C - reagent addition

$FePO_4$. $2H_2O$ seed:

The seed addition was at a rate of 30 g/L.

Iron contained in 30 g of seed = 30 x 55.85 / 186.9 = 8.9 g

Phosphorous contained in 30 g of seed = 30 x 31 / 186.9 = 5 g

NaOH acid neutralizing agent:

In order to neutralize 6.4 M of HCl to pH 0 (1 M HCl) the amount of NaOH needed is equal to 5.4 M.

Na in 5.4 M NaOH = 5.4 x 23 = 124 g

Na_3PO_4 as the phosphate source:

Stoichiometric amounts of Na_3PO_4 were added as the source for phosphorous to the plant solution during phosphate precipitation (the initial 8.8 g of phosphate in the plant solutions was to be considered as excess).

Na the added Na_3PO_4 = 125 / 55.85 x 3 x 23 = 154.4 g

P contained in the Na_3PO_4 = 125 / 55.85 x 31 = 69.4 g

Stream D

Stream D is based on ICP analysis and the obtaining percentage precipitation and co-precipitation during phosphate precipitation at pH 1 and 40^{o}C.

Stream E

It is assumed that the balance components of the unaccounted for inputs reports to the solids.

Hematite streams

Stream A – plant solution

ICP analysis

Stream B – HCl addition

Based on the need to completely complex 125.6 g/L of iron contained in the plant solution, the calculated total HCl required, as shown in APPENDIX D: ASSOCIATED AND DISSOCIATED [HCl], is 6.4 M. The plant solutions contain about 5 M HCl. Therefore the additional HCl is 1.4 M.

Added chloride ions = 1.4 x 35.5 = 49.7 g

Stream C - reagent addition

Fe_2O_3 seed:

The seed addition was at a rate of 30 g/L.

Iron contained in 30 g of seed = 30 x 111.7 / 159.7 = 20.9 g

NaOH acid neutralizing agent:

In order to neutralize 6.4 M of HCl to pH 0 (1 M HCl) the amount of NaOH needed is equal to 5.4 M.

Na in 5.4 M NaOH = 5.4 x 23 = 124 g

Stream D

Stream D is based on ICP analysis and the obtaining percentage precipitation and co-precipitation during hematite precipitation at pH 1 and 40^{o}C.

Stream E

It is assumed that the balance components of the unaccounted for inputs reports to the solids.

APPENDIX G: GENERAL PROCESS OPTIONS

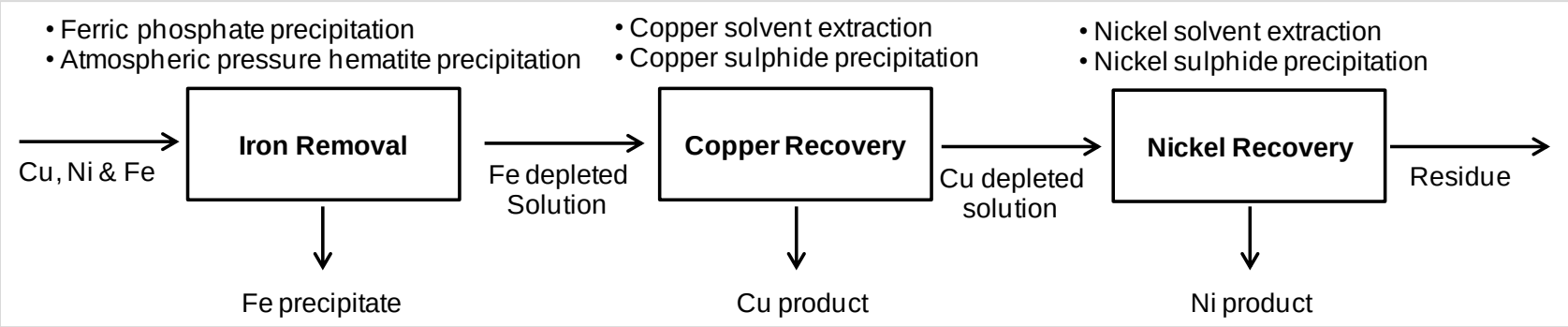

Figure G 1.General process options for iron removal, copper and nickel recovery

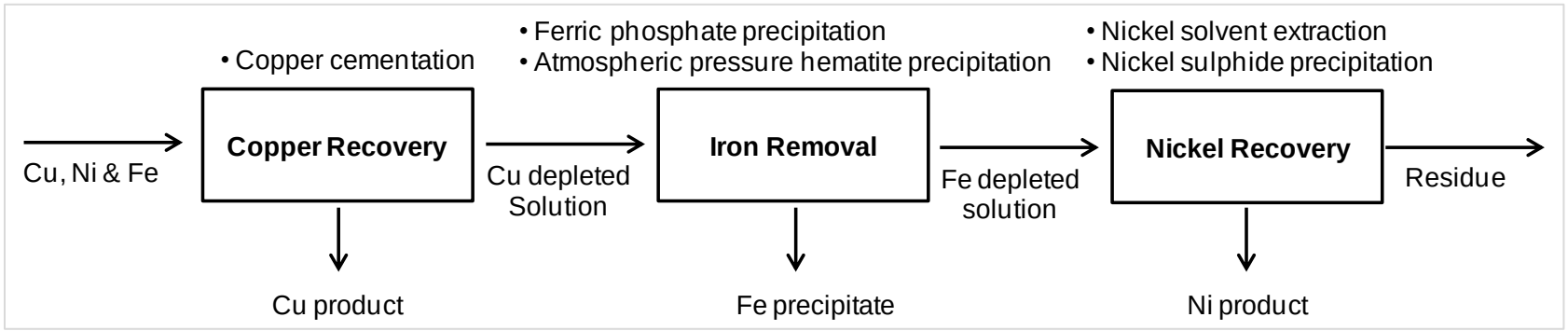

Figure G 2. General process options for copper recovery, iron removal and nickel recovery

APPENDIX H: [HCl] CALCULATIONS

Assuming a solution mainly containing Fe^{2+}, Fe^{3+}, Ni^{2+}, Cu^{2+}, Co^{2+} and Na^{+}, whose molarities are denoted by $M.Fe^{2+}$, $M.Fe^{3+}$, $M.Ni^{2+}$, $M.Cu^{2+}$, $M.Co^{2+}$ and $M.Na^{+}$ respectively, the molarity of HCl can be calculated using the analysed molarity of the total chloride ions ($M.Cl^{-}$) as shown in Equation H – 1.

$$M.HCl = M.Cl^{-} - \left(2M.Fe^{2+} + 3M.Fe^{3+} + 2M.Ni^{2+} + 2M.Cu^{2+} + 2M.Co^{2+} + M.Na\right) \qquad H - 1$$

The plant solution was analysed to contain mainly iron and nickel (see Table 5.1) as the significant cations. Titration analysis was used to obtain the split of iron(II) and iron(III) as about 100 g and 25.6 g respectively.

Mole of paired chloride ions = (2 x 100 / 55.85) + (3 x 25.6 / 55.85) + (2 x 12 / 58.7) = 5.338Therefore HCl concentration = (368 / 35.5) – 5.338 = 5.0 M free acid

Deficit acid therefore = 6.4 – 5 = 1.4 M

APPENDIX I: PARTICLE SIZE ANALYSIS DATA

Iron phosphate particle size

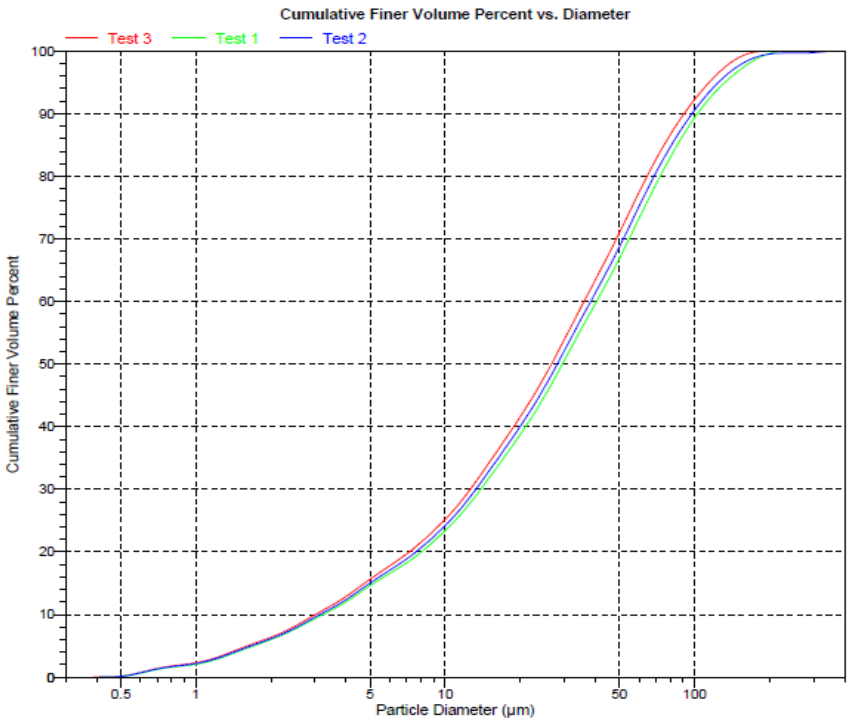

Figure I 1: Particle size distribution for seeded iron phosphate produced at pH 1 and 80°C

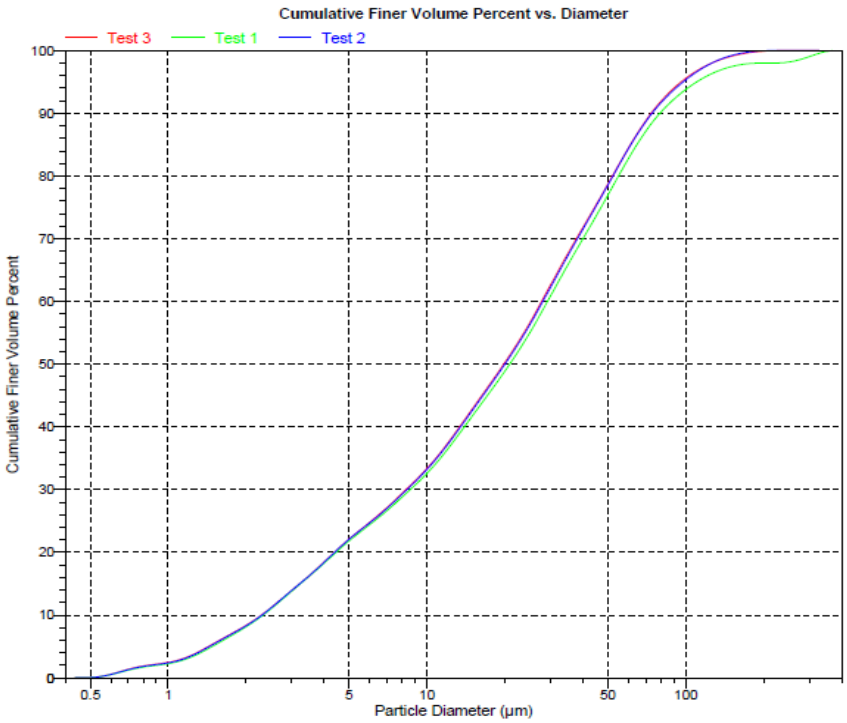

Figure I 2: Particle size distribution for seeded iron phosphate produced at pH 1 and 60°C

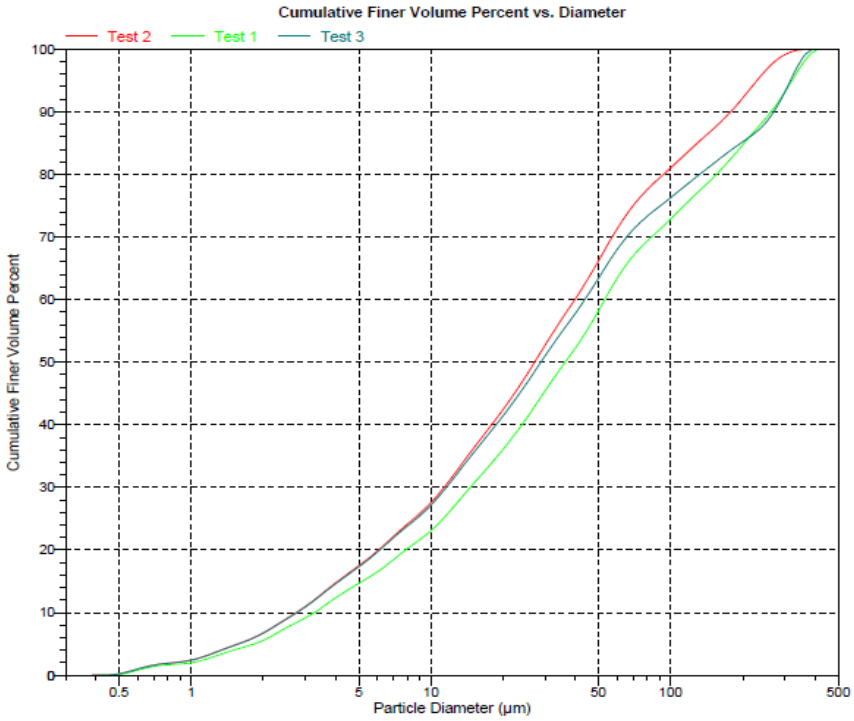

Figure I 3: Particle size distribution for seeded iron phosphate produced at pH 1 and 40°C

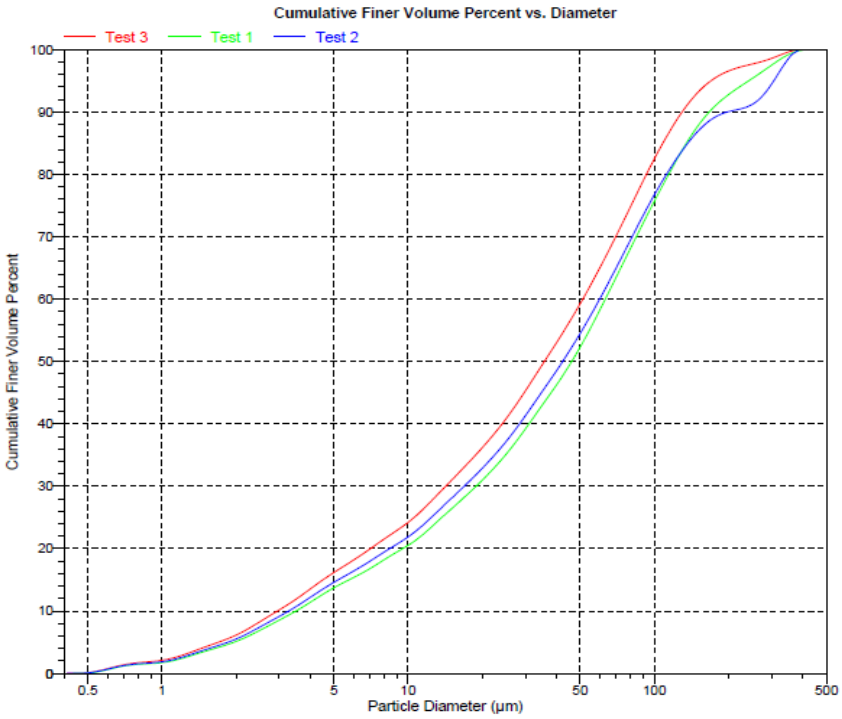

Figure I 4: Particle size distribution for seeded iron phosphate produced at pH 2 and 80°C

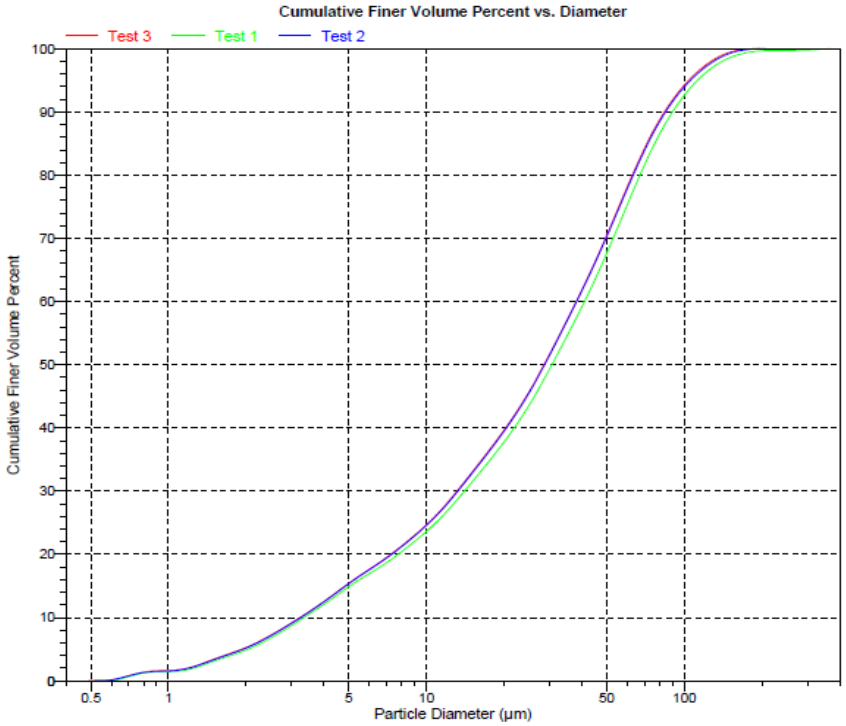

Figure I 5: Particle size distribution for seeded iron phosphate produced at pH 2 and 60°C

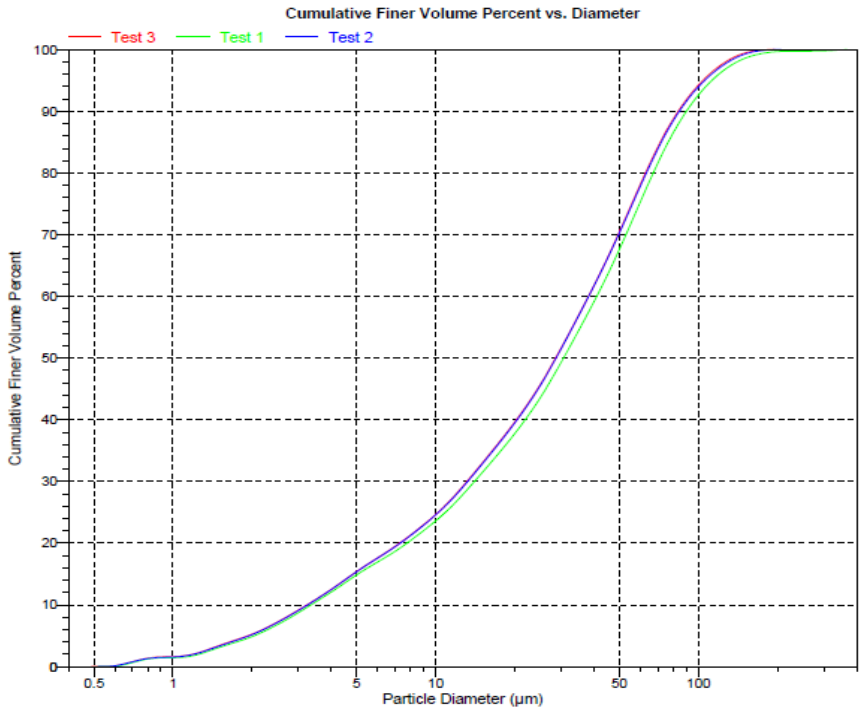

Figure I 6: Particle size distribution for seeded iron phosphate produced at pH 2 and 40°C

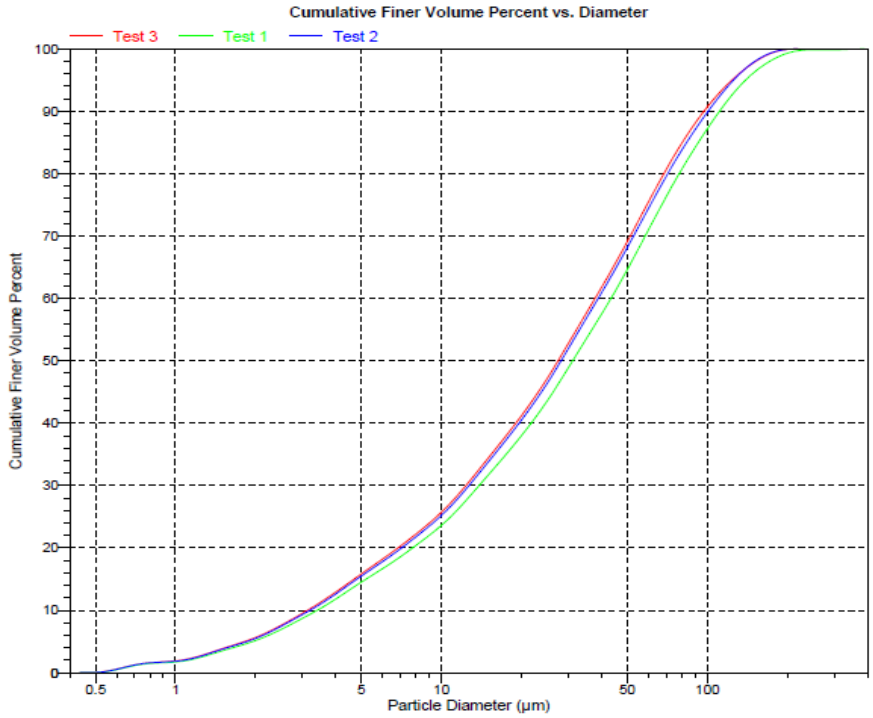

Figure I 7: Particle size distribution for seeded iron phosphate produced at pH 3 and 80°C

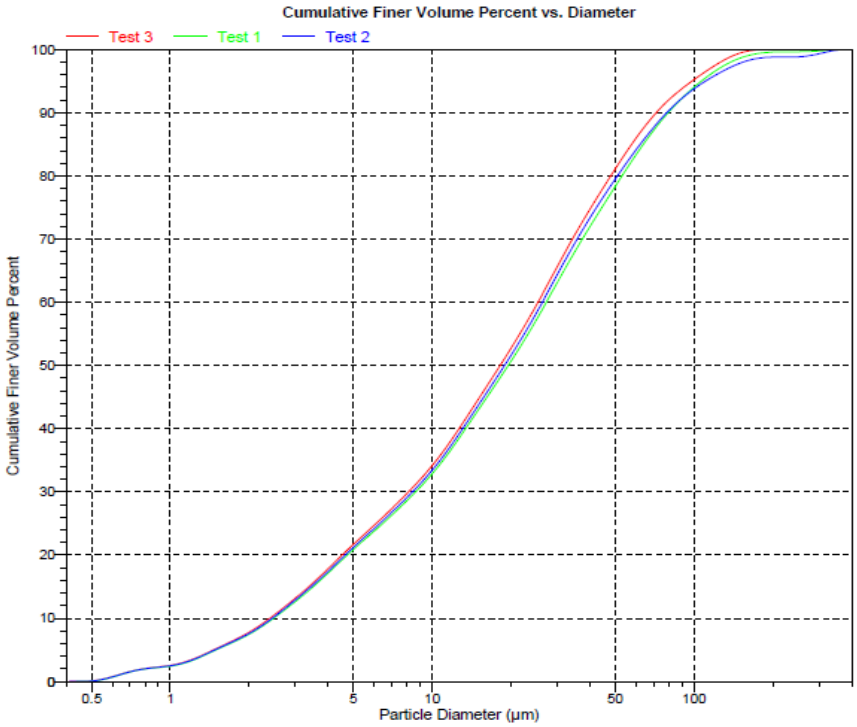

Figure I 8: Particle size distribution for seeded iron phosphate produced at pH 3 and 60°C

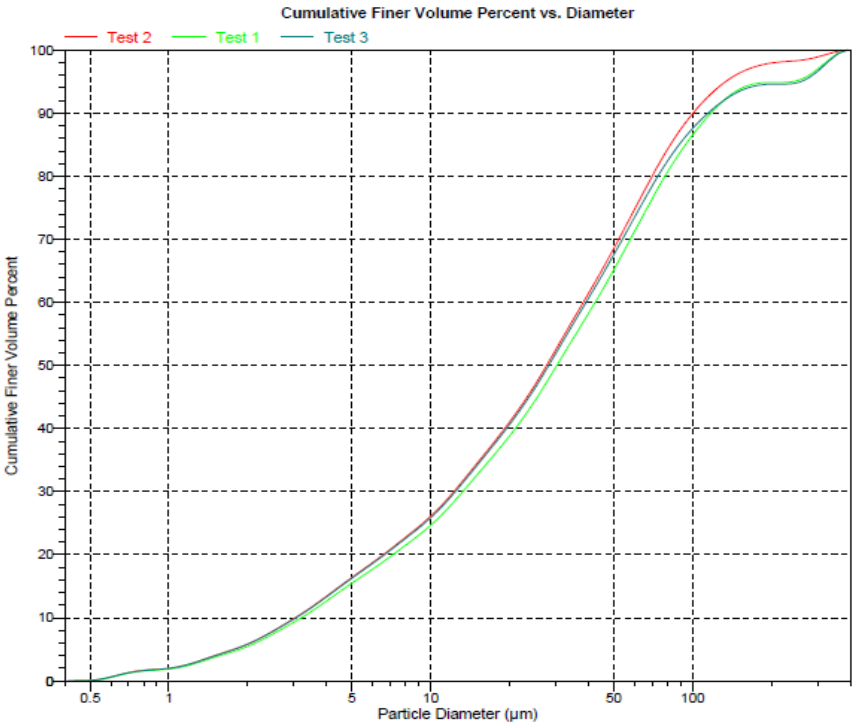

Figure I 9: Particle size distribution for seeded iron phosphate produced at pH 3 and 40°C

Hematite particle size

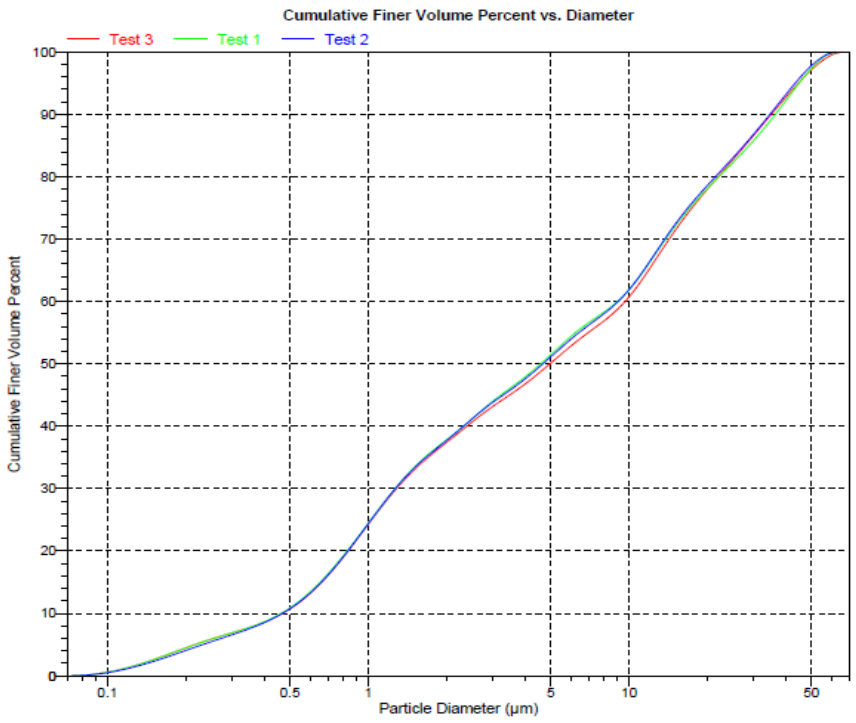

Figure I 10: Particle size distribution for seeded hematite produced at pH 1 and 90°C

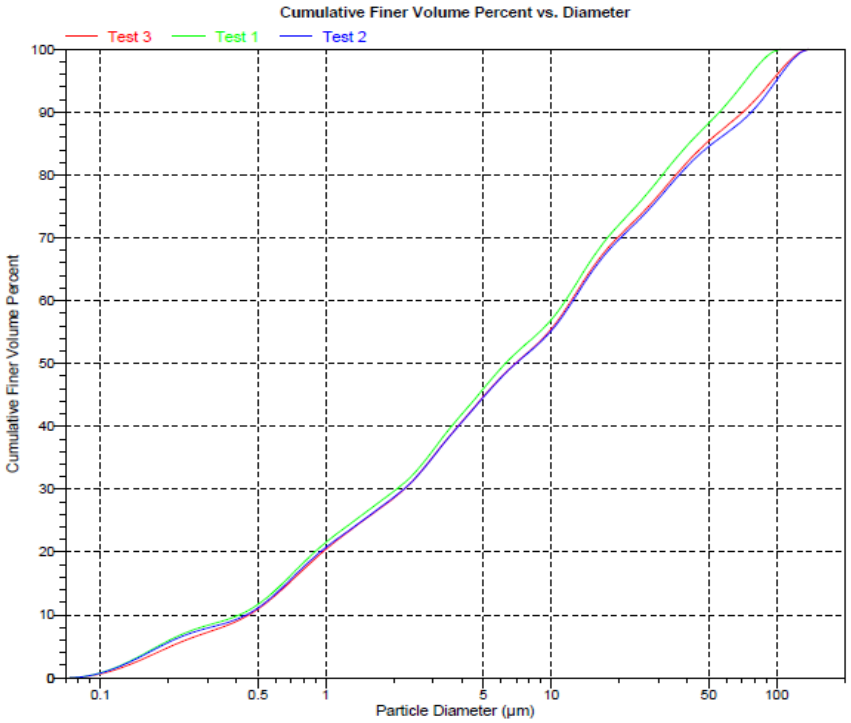

Figure I 11: Particle size distribution for seeded hematite produced at pH 1 and 80^{o}C

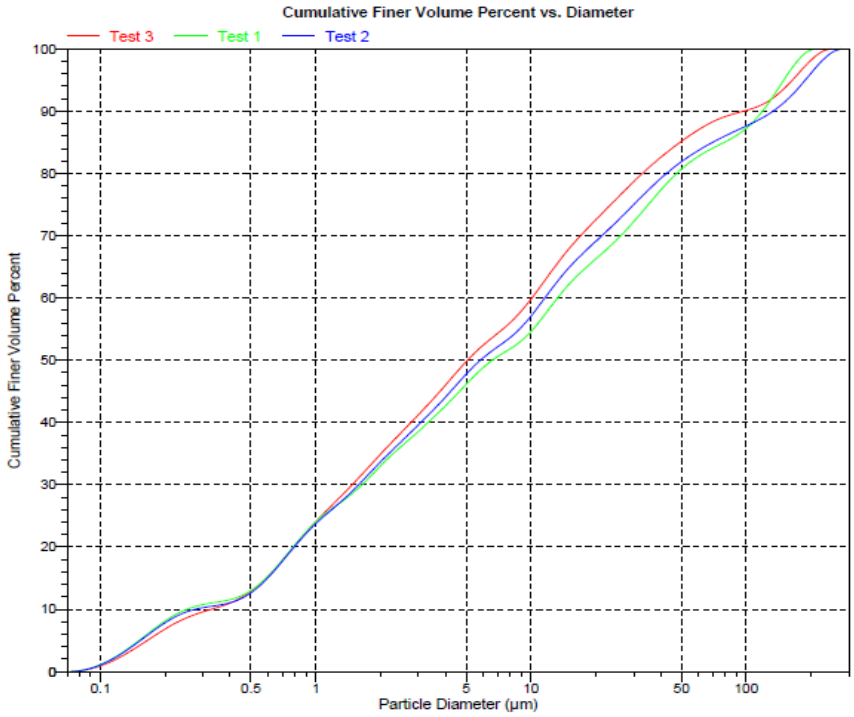

Figure I 12: Particle size distribution for seeded hematite produced at pH 1 and 60^{o}C

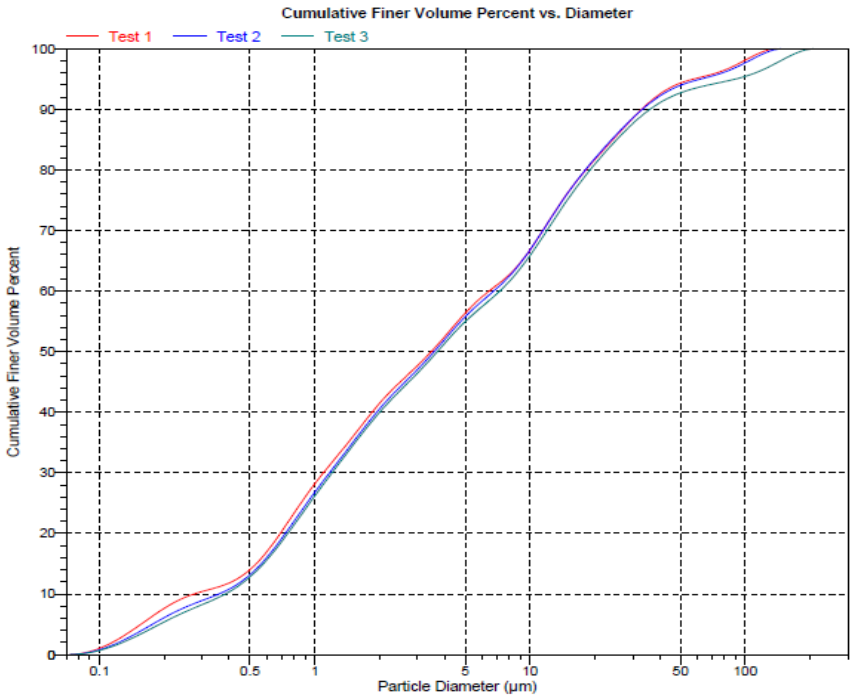

Figure I 13: Particle size distribution for seeded hematite produced at pH 2 and 90^{o}C

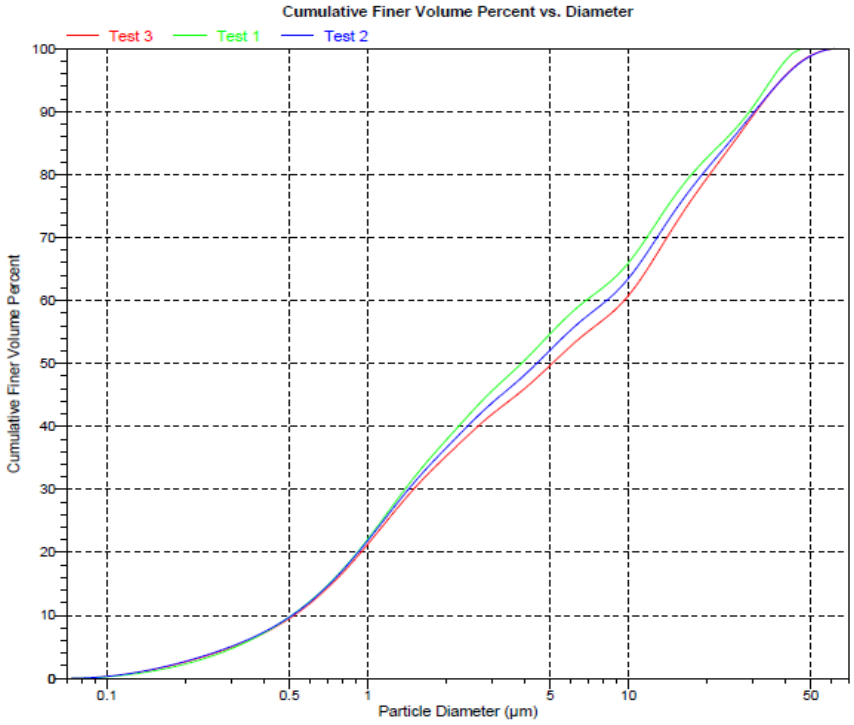

Figure I 14: Particle size distribution for seeded hematite produced at pH 2 and 80^{o}C

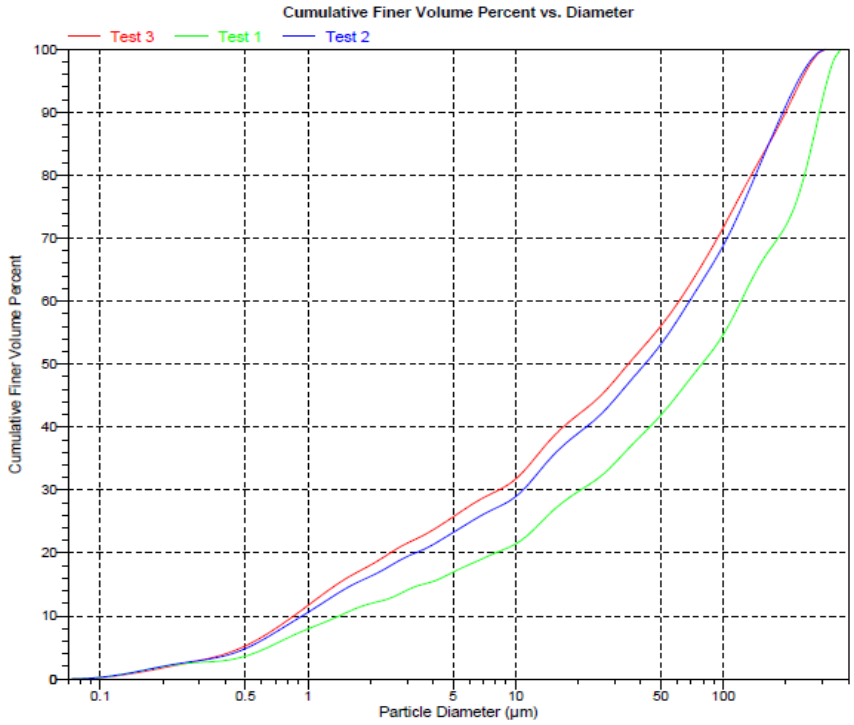

Figure I 15: Particle size distribution for seeded hematite produced at pH 2 and 60^{o}C

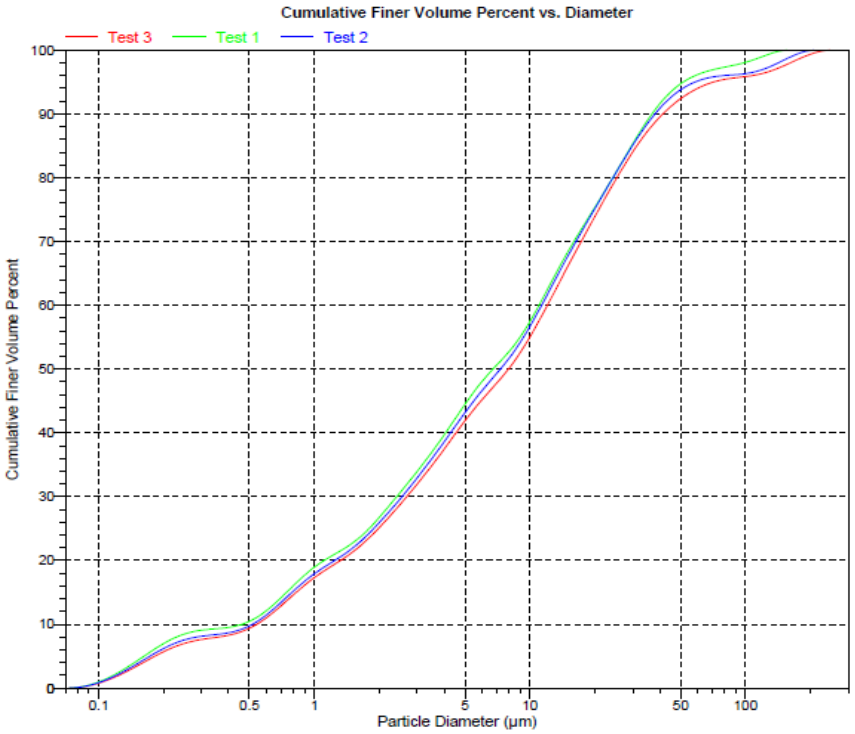

Figure I 16: Particle size distribution for seeded hematite produced at pH 3 and 90^{o}C

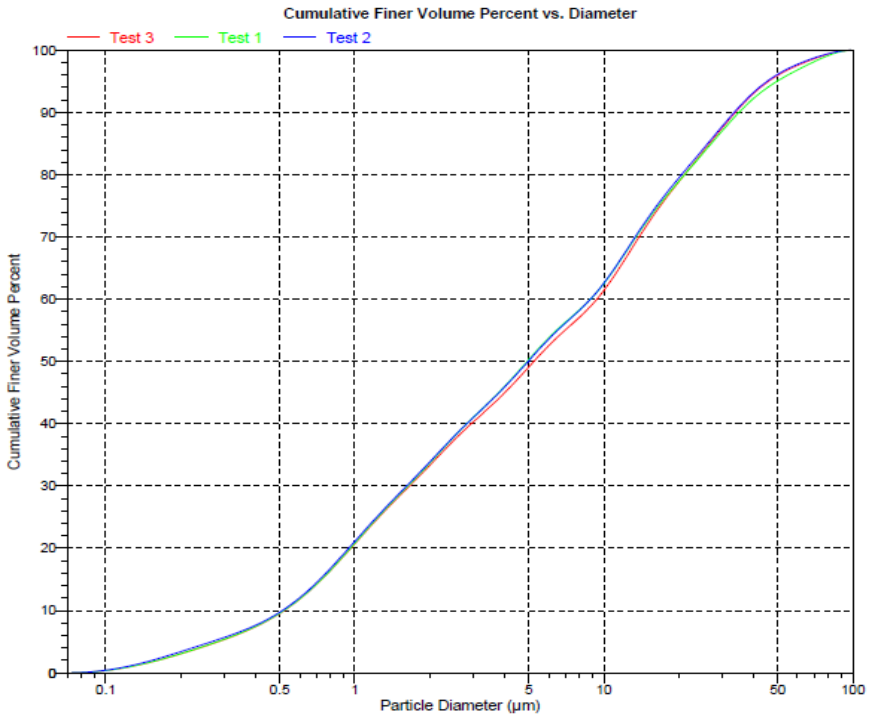

Figure I 17: Particle size distribution for seeded hematite produced at pH 3 and 80°C

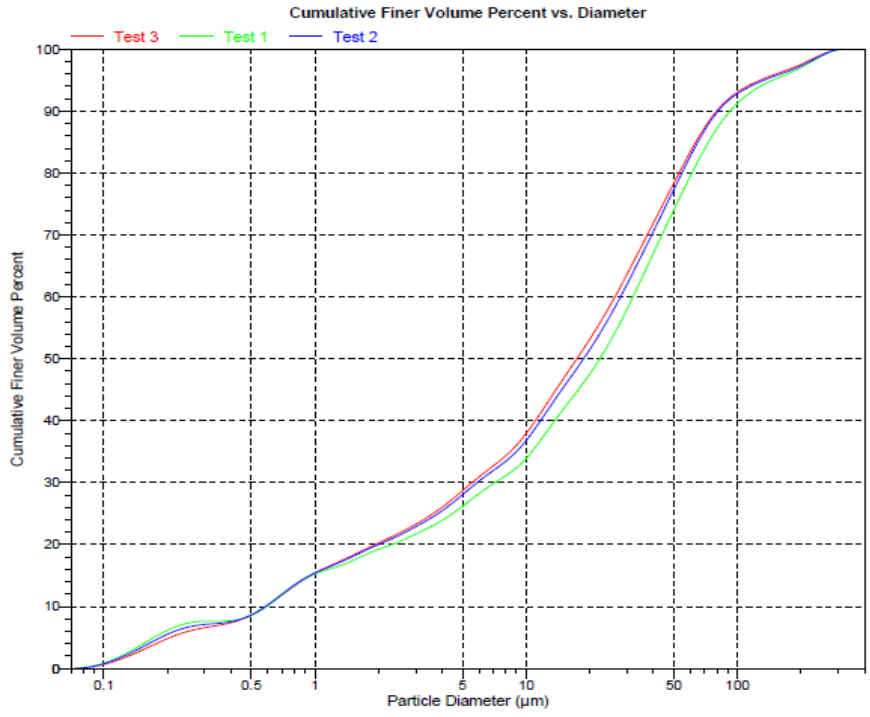

Figure I 18: Particle size distribution for seeded hematite produced at pH 3 and 60°C

APPENDIX J: SETUP HAZARD IDENTIFICATION

Table J 1. Experimental setup hazard identification summary

Hazard	Examples of hazard	Examples of activities	Preventive action
Hazardous chemicals			
Hydrochloric Acid	Spillage	Preparing synthetic solutions	Wear PPE
		Loading reaction vessel contents and sampling	Wear PPE
Sodium Hydroxide	Spillage	Loading the reaction vessel	Wash and rinse vessel and all components. Wear PPE
Sodium Hydroxide	Exothermic reaction	Loading of the reaction vessel	Wear PPE
Oxygen	Oxygen cylinder leaking	Fire hazard	Secure the oxygen cylinder. Ensure all valves are closed when not in use. Keep flammable substances away.
High temperatures			
Reaction vessel	High temperature of bottom of reactor	Moving of reactor at the end of experiment	Allow vessel to cool before handling
	Contact	Contact with the hot plate	Wear PPE
Physical hazards			
Moving parts	Fast rotating agitator	Stirring of open reactor	Be careful; increase the stirring speed gradually
	Unexpected rotation	Maintenance of stirrer	Ensure power is disconnected before conducting maintenance
Falling objects	Reactor vessel dropped on floor	Removal of vessel	Be careful and limit handling of vessel